RESILIENT GRID OPERATION BY INTEGRATING PHOTOVOLTAIC GENERATION, MOBILE ELECTRIC VEHICLE BATTERY ENERGY STORAGE, AND FIXED BATTERY ENERGY STORAGE

A Dissertation

by

BEI ZHANG

Submitted to the Office of Graduate and Professional Studies of
Texas A&M University
in partial fulfillment of the requirements for the degree of

DOCTOR OF PHILOSOPHY

Chair of Committee,	Mladen Kezunovic
Committee Members,	Alex Sprintson
	Le Xie
	Steven L. Puller
Head of Department,	Miroslav Begovic

December 2017

Major Subject: Electrical Engineering

ABSTRACT

The widespread utilization of photovoltaic (PV) generation, and battery energy storage (BES) in mobile (Electrical Vehicles-EVs) and fixed form is bringing opportunities, as well as challenges to the power grid operation.

To handle the uncertainties brought by EV BES, and PV generation, we propose to improve the system predictability through: 1) an analytical way to estimate the aggregated EVs BES power capacity for charging/discharging, considering factors such as EVs' mobility, drivers' stochastic behavior, energy need for future travel, etc.; and 2) an improved PV generation forecast based on Gaussian Conditional Random Fields (GCRF) method, which models both the spatial and temporal correlations in different graphs and works well even with missing or unavailable data.

One of the opportunities is to improve the system flexibility by utilizing the relatively high ramping capability of mobile (EV) and fixed BES given their quite adjustable operation modes (charging and discharging). This dissertation presents a model to integrate EVs and fixed BES into the ramp market with two types of participation: a) direct participation, and b) collaboration with conventional generators. By providing the ramp service in the electricity market, EVs and fixed BES can help the power grid better handle the short term net-load variability and uncertainty. On the other hand, EVs and fixed BES do not have to charge and discharge very frequently, while their fast ramping capability can still get rewarded. Also, the limitation on the energy capacity of EVs and fixed BES can be relieved to some extent.

As another opportunity, the integration of PV generation and fixed BES can also help the system in face of some unknowable uncertainties, such as the extreme event. The energy stored in the BES and generated by the PV panel can serve as the emergency power supply. Also, they are located in a more scattered manner than the conventional generators, which enables their capacity to be more accessible under the extreme conditions. This dissertation proposes an optimal allocation scheme of PV generation and fixed BES aiming at improving the system resilience, considering the unknowable nature of extreme events.

DEDICATION

To my beloved grandparents, father, husband Yingzhong, and those who have altruistically helped me.

ACKNOWLEDGEMENTS

First and foremost, I would like to express my deepest respect and gratitude to my advisor, Dr. Mladen Kezunovic, for his guidance, support and encouragement over the years. At the crossroad in my life, Dr. Kezunovic provided me an invaluable opportunity to continue my research and broaden my horizon. Thanks to his insightful guidance and persistent help through my Ph.D. process, I see myself growing to be a better researcher. It is truly a great honor to become his student.

Sincere thanks also go to my committee members: Dr. Alex Sprintson, Dr. Le Xie, and Dr. Steven L. Puller. I am grateful to them for their valuable discussion, suggestions, comments and time. Their encouragement and guidance also has helped me a lot in completing this dissertation.

Appreciation also goes to my friends and the staff in the Department of Electrical and Computer Engineering. I would like to particularly thank Payman Dehghanian, Yang Chen, Wenzong Wang, Meng Wu, Chen Yang, Anupam A. Thatte, and Omar A. Urquidez for their help and support along the way.

I wish to express my gratitude especially to my family for their endless love and support. I would like to thank my grandparents and my father for their endless and unconditional love, selfless dedication, persistent support, and their understanding. Also, I want to thank my uncle and untie for their encouragement and support. Moreover, I would like to express my gratitude to my dear husband, Yingzhong, for his love, company,

support and understanding. His being with me is the source of the power for me to complete my Ph.D. journey.

Moreover, I am profoundly grateful to those who have altruistically helped me during some critical moments. I wouldn’t become who I am today if it wasn’t for your support.

CONTRIBUTORS AND FUNDING SOURCES

Contributors

This work was supervised by a thesis (or) dissertation committee consisting of Dr. Mladen Kezunovic [Advisor], Dr. Alex Sprintson and Dr. Le Xie of the Department of Electrical and Computer Engineering, and Dr. Steven L. Puller of the Department of Economics.

All work for the thesis (or) dissertation was completed independently by the student.

Funding Sources

This work was made possible by the following founding sources:

- NSF I/UCRC: Electric Vehicle Transportation and Electricity Convergence (EV-TEC) under project titled “The Impact of PHEV/BEV Charging on Utility Distribution System”.
- NSF I/UCRC: Power System Engineering Research Center and Electric Vehicle Transportation and Electricity Convergence (EV-TEC) under project titled: “The Electricity and Transportation Infrastructure Convergence using EVs”.
- NPRP 8-241-2-095 award from the Qatar National Research Fund (a member of Qatar Foundation).
- Texas A&M Christa U. Pandey ‘84 Fellowship

TABLE OF CONTENTS

Page

LIST OF FIGURES

Page

LIST OF TABLES

Page

1. INTRODUCTION*

1.1 Background and Motivation

With the global climate change increasingly acknowledged, PV generation and EVs are catching more and more attention with a goal of reducing CO2 emissions. Around 2,051 megawatts (MW) of solar PV was installed in the U.S in the 2nd quarter of year 2016 to reach 31.6 gigawatts (GW) of total installed capacity, enough to power 6.2 million American homes [1]. New registrations of EVs (including both battery electric and plug-in hybrids) increased by 70% between 2014 and 2015, with over 550 000 vehicles being sold worldwide in 2015 [2]. As a result, the power grid is facing new challenges with such rapid development and integration of EVs BES and PV generation, e.g. the system's net-load is becoming more and more variable; the load is reaching its new peaks caused by the aggregated EV charging effect, etc. Those challenges are mainly attributed to the inherent uncertainties of PV generation and EV charging/ discharging resulting from weather and

* This section is in part a reprint of the material in the following papers: (1) Reprinted with permission from B. Zhang, M. Kezunovic, "Impact of Available Electric Vehicle Battery Power Capacity on Power System Reliability," *IEEE Power and Energy Society General Meeting*, Vancouver, Canada, July, 2013. Copyright 2013, IEEE. (2) Reprinted with permission from B. Zhang, P. Dehghanian, M. Kezunovic, "Spatial-Temporal Solar Power Forecast through Use of Gaussian Conditional Random Fields," *IEEE Power and Energy Society General Meeting*, Boston, MA, July 2016. Copyright 2016, IEEE. (3) Reprinted with permission from B. Zhang, M. Kezunovic, "Impact on Power System Flexibility by Electric Vehicle Participation in Ramp Market," *IEEE Transactions on Smart Grid*, Vol. 7, No. 3, pp. 1285-1294, May 2016. Copyright 2016, IEEE. (4) Reprinted with permission from B. Zhang, P. Dehghanian, M. Kezunovic, "Optimal Allocation of PV Generation and Battery Storage for Enhanced Resilience", *IEEE Transactions on Smart Grid*, accepted. (5) Reprinted with permission from M. Kezunovic, Z. Obradovic, T. Dokic, B. Zhang, J. Stojanovic, P. Dehghanian, and P. -C. Chen, "Predicating Spatiotemporal Impacts of Weather on Power Systems using Big Data Science," Springer Verlag, Data Science and Big Data: An Environment of Computational Intelligence, Pedrycz, Witold, Chen, Shyi-Ming (Eds.), ISBN 978-3-319-53474-9, 2017.

people's behavior, which can be alleviated by improving the predictability of those uncertainties.

Despite the challenges brought by the integration of EV, BES and PV generation, new opportunities are also emerging due to the controllability of EV charging/discharging and PV generation by integration of fixed BES. The collaboration among these three elements not only alleviates some of the negative impacts caused by the uncertainties, but also creates new capability and capacity to better control the grid operation. Compared with the conventional generator, EVs and fixed BES allow fast ramping rates, which makes them quite suitable for dealing with the short-term variation and uncertainty, resulting in the improvement of the system flexibility. Meanwhile, the capacity of the fixed BES to store energy produced by PVs and the grid, and doing it in a distributed fashion, helps especially during faults and some extreme events, leading to the enhancement of the grid resilience.

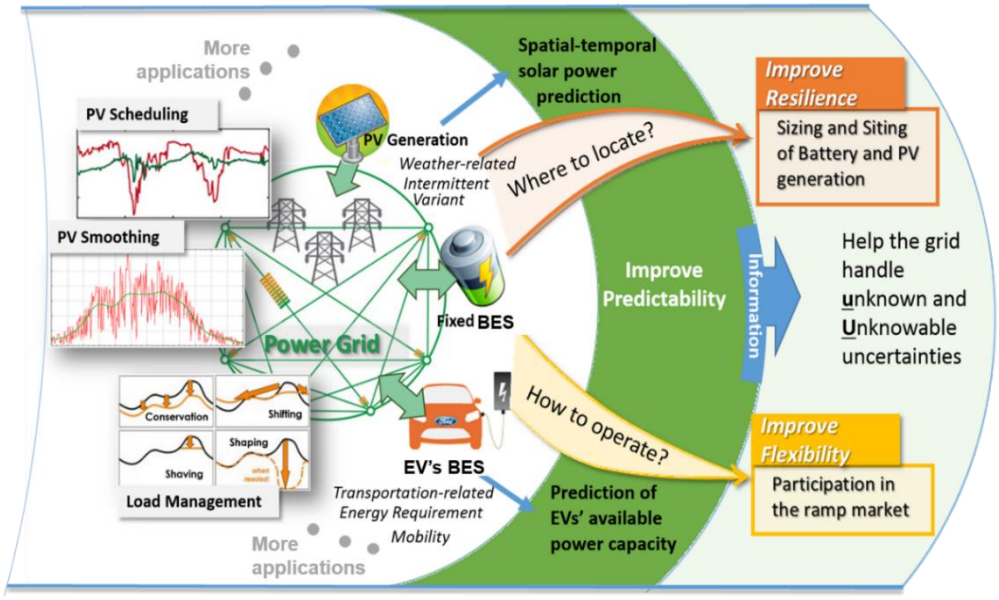

Figure 1.1 Integration of PV generation, mobile (EV) and fixed BES

Optimizing operation of all three elements (PV generation, EVs and fixed BES) integrated in a flexible way to enhance the grid resiliency is the main focus of this dissertation. Figure 1.1 illustrates the integration of these three elements: PV generation is adding to the power system some clean generation resources as well as more net-load variation and uncertainty; EVs and fixed BES are interacting bi-directionally with the power system, which provides more flexibility during the operation. When planned and operated properly, those three elements can be utilized to help the power system, e.g. more PV generation can be achieved while minimizing the variation and intermittence added to the system; the system load becomes smoother, and so on. The inherent uncertainties regarding PV generation and EVs BES are restraining their further utilization, which

requires improving performance predictability of these two elements. Two more questions arise afterward: where to locate the PV generation and fixed BES (EV BES is exempt from this question due to the mobility and private individual ownership of EVs); and how to operate EVs and fixed BES (the power generation of PV is dependent on the weather condition, and therefore not quite controllable). We are considering improvements in the system resilience when planning the placement of PV generation and fixed BES. The electricity market is adopted as a platform to integrate EVs and fixed BES during the system operation aiming at improving the system flexibility.

1.2 Related Work

Quite a few research efforts have been concerned with tackling the challenges caused by the uncertainties. Ref [3, 4, 5, 6, 7, 8] model the stochastic charging behavior of EVs: [3, 4, 5, 6] propose stochastic models which are based on the Monte Carlo approach. Fuzzy VPRS (Variable Precision Rough Set) Model, and non-homogeneous semi-Markov processes, to estimate the availability of EVs in the system considering drivers' behavior; Reference [7] describes a mathematical model for estimating the electric power capacity of a parking lot; reference [8] introduces an analytical way to derive the probability distribution of the available power capacity of EV BES taking into account drivers' plug-in duration probability. There are also a lot of reported studies focusing on improving the solar power prediction, and they can be mainly categorized into three groups: 1) the numerical weather prediction (NWP)-based forecast [9, 10, 11, 12]; 2) the data-driven methods [13, 14, 15, 16, 17, 18, 19, 20, 21, 22, 23] which are, nowadays, the most popular

methods; and 3) combinations of the NWP and the data-driven methods [24, 25, 26]. Among the aforementioned studies, [10, 13, 18, 19, 20] consider the spatial correlations of solar sites, while the rest are solely based on the local meteorological measurements.

Other than alleviating the challenges, more efforts are being devoting to making use of the opportunities brought about by integrating the new elements. References [27, 28, 29, 30, 31, 32, 33, 34, 35, 36] address the collaboration among EV BES, fixed BES and renewable generation to further reduce the variation caused by the renewables. EV and fixed BES are also suggested to participate in the electricity market by providing ancillary services to assist the system operation: [37, 38, 39, 40, 41, 42, 43, 44] discuss integrating EV and fixed BES into the frequency regulation service; [45, 46, 47, 48, 49, 50, 51] talk about enabling their participation in the reserve market; the combined bidding into the reserve market is discussed in [52, 53, 54]. The planning and placement of the fixed BES and renewable resources are also studied in [55, 56, 57, 58, 59, 56, 61, 61, 63, 64, 65, 66, 67, 68, 69], in which [55, 56, 57, 58, 59] mainly focus on the distribution system, while [60, 61, 62, 63, 64, 65, 66, 67, 68] on the transmission system, and [69] on both distribution and transmission systems. The integration of fixed BES in the transmission system can enable higher penetration of renewables [60, 61, 62, 63, 64] as well as facilitate the market operation to reduce the total cost [65, 66, 67, 68].

1.3 Problem Statement

The power system is facing a lot of uncertainties (Known, Unknown, Unknowable) [70], and how to deal with those uncertainties caused by integration of the PV generation,

mobile (EV) and fixed BES so as to improve the system resilience and flexibility is significantly important to system operators.

- Improving the **Predictability** of some **Known** uncertainties

First of all, the new elements (EV BES and PV generation) have added new uncertainties to the system operation due to the stochastic nature of people's charging behavior and weather change impacting the grid. Improving the predictability of those uncertainties by modeling the probability distribution is one of the ways to handle them, resulting in more information for system operators:

1) Previous studies have tried to address the modeling of EV charging behavior, as discussed in Section 1.2, however, most of them are based on the simulation method and none of them focuses on probabilistically model that represents the uncertainty. In order to better assist the operation, an analytical way to estimate the aggregated charging/discharging power capacity of EV BES needs to be formulated with more information taken into account;
2) The previous work on the PV generation prediction does not pay much attention to the probability distribution modeling, and most of them just focus on modeling the temporal correlations. We need a model that can not only incorporate both the spatial and temporal correlations among different solar stations, but also gives the probability distribution of the PV generation. GCRF model can meet both of those needs. GCRF model is a structured learning method which can well exploit the correlations among output variables, resulting in significant improvements in the prediction accuracy [71].

The collaboration among mobile (EV) BES, PV generation and fixed BES has created new opportunities in dealing with the uncertainties. The advantages and disadvantages of these three elements being integrated when compared with the conventional generators are briefly summarized in Table 1.1.

Table 1.1 Summary of (Dis)Advantages of Mobile (EV) and Fixed BES, and PV Generation

	Advantage	Disadvantage
Mobile (EV) BES, fixed BES	• More adjustable: can serve as both the load and generation • High ramping speed • Energy-storable • Located in a more scattered manner	• Energy capacity limitation • Battery degradation
PV generation	• Clean resources • Located in a more scattered manner	• Variant and uncontrollable output

- Improving the **Flexibility** to deal with some **Unknown** uncertainties

Nowadays, power system flexibility has received additional attention due to an increasing integration of the renewable energy. The variability of the renewable energy can lead to difficulties in energy balancing, thus compromising the power system's operation efficiency and reliability. Increasing the system flexibility requires high ramping capacity, which is one of the advantages that are enabled by mobile (EV) and fixed BES. A lot of ongoing research mainly focuses on integrating mobile (EV) and fixed BES into

the reserve market and frequency regulation, aiming at improving system reliability. The energy capacity limitation and battery degradation are not fully considered in this context: sustaining generation capacity for a long period of time is required by the reserve market, and frequent charging and discharging may happen during the frequency regulation. Finding a suitable service product to improve the system flexibility, in which mobile (EV) and fixed BES can get rewarded for their advantages while their disadvantages can be mitigated, is becoming an imperative.

- Improving the **Resilience** to deal with some **Unknowable** uncertainties

Power system resilience is gradually receiving more and more attention. It is defined as "the ability of a power system to recover quickly following a disaster or, more generally, to the ability of anticipating extraordinary and high-impact, low-probability events, rapidly recovering from these disruptive events, and absorbing lessons for adapting its operation and structure for preventing or mitigating the impact of similar events in the future" [72]. The concept of resilience is quite complicated and involves different aspects of the power system, one of which can be the accessibility to the capacity. The energy stored in the fixed BES can serve as the back-up capacity in the extreme event. Moreover, the distributed nature of the fixed BES and PV generation makes it easier for their energy to be accessed compared with the conventional generator during the extreme events in which transmission lines might be de-energized, resulting in the failure in energy delivery at a long distance. While there are disadvantages of the fixed BES and PV generation, their advantages shows significant value during the extreme event, which can be exploited to decrease the load-loss as much as possible and recover the system as soon as possible. The

focuses of the previous work related to the sizing and siting of the fixed BES and PV generation are mostly about facilitating the operation. No past research focusing on improving the system resilience through the placement of the fixed BES and PV generation has been found.

1.4 Dissertation Framework

The framework of the dissertation is illustrated in Figure 1.2.

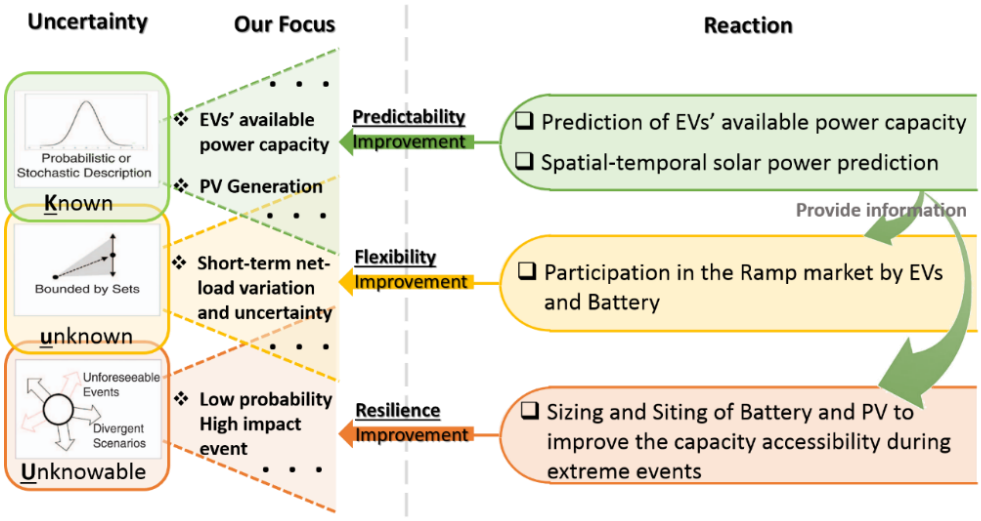

Figure 1.2 Illustration on dissertation framework

We intend *to improve the predictability* aiming at assisting the grid operation by: 1) modeling the probability distribution of the aggregated energy capacity of mobile (EV) BES and PV generation; 2) increasing the prediction accuracy of the PV generation by considering both the temporal and spatial correlations. With that intention in mind, our work focus is on: (a) a probabilistic analytical method to estimate the aggregated charging/discharging power capacity of EV BES based on the Markov model, with more information taken into account, e.g. drivers' connecting preference, traffic information, etc.; (b) spatial-temporal PV generation forecast by GCRF model, which is capable of modeling the probability distribution as well as providing more accurate forecast.

In order *to improve the system flexibility* in the operation planning, we propose to enable participation of mobile (EV) and fixed BES into the flexible ramp product, which is proposed to accommodate net-load variations and uncertainties to improve the grid flexibility. The ramp product can be integrated in RTD, which is applied on a 5–10 min time-scale, and therefore the limitation caused by the battery capacity can be relieved. No frequent charging and discharging will be required due to the infrequent appearance of large variations.

Also, a planning scheme is proposed to *improve the system resilience* by sizing and siting the fixed BES and PV generation so that their power and energy capacity is more accessible during extreme events. The capacity of the fixed BES and PV generation can not only help decrease the load loss, but also expedite the black-start process by providing energy to non-black-start (NB-S) generators.

The relationship among different blocks in Figure 1.2 is illustrated in Figure 1.3. The estimation on the available power capacity from EV BES provides the necessary information for EVs' participation in the ramp market. The forecast on the PV generation not only helps forming the net-load information in the ramp market, but also assists the planning of the placement of the PV panels. The sizing and siting information of the fixed BES exerts the limitation on the capacity in their bidding into the ramp market.

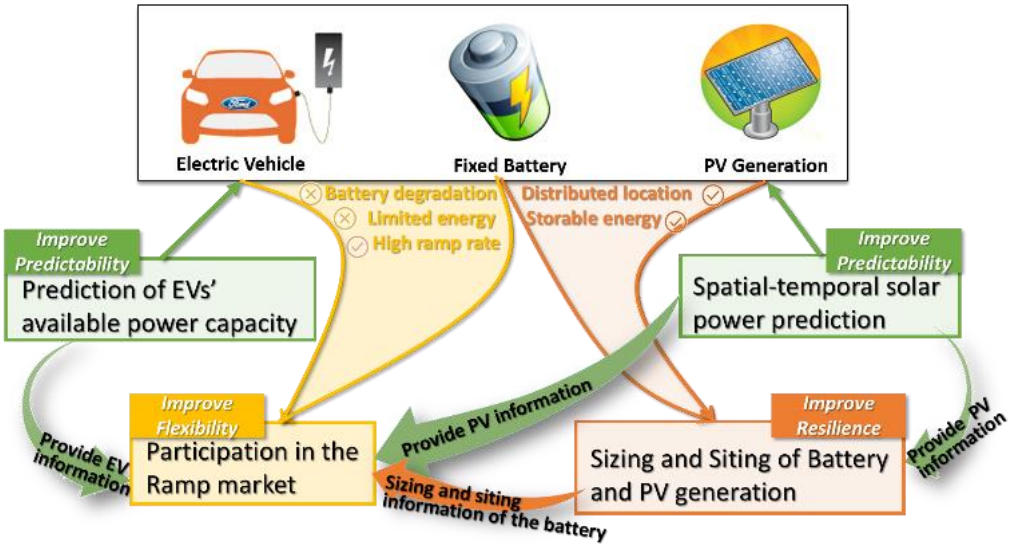

Figure 1.3 The relationship among different blocks in the proposed framework

1.5 Dissertation Outline

The rest of the dissertation is organized as follows:

Section 2 presents the methodology to estimate the aggregated available power capacity from EV BES for both charging and discharging in a probabilistic manner based on traffic conditions through Markov process. It aims at improving the system predictability, and takes into account several factors such as stochastic behavior of the EV drivers, charge depletion limit and the energy needed for transportation purposes, etc. Numerical experiments are conducted to estimate the aggregated power capacity of 30,000 EVs in a large area.

Section 3 focuses on another aspect of improving the system predictability, which is an application of the Gaussian Conditional Random Fields (GCRF) model for forecasting the PV power, with the consideration of both the spatial and temporal correlations among various PV stations. The numerical experiments conducted compare the forecast performance of the proposed method as well as some other existing methods. The results verify the advantage of the GCRF model over other models, especially under the situation with missing data.

Section 4 investigates the participation of mobile (EV) and fixed BES in the ramp market for the purpose of enhancing the system flexibility to deal with the short-term net-load uncertainty and variation. Since the modeling of integrating the EV BES into the ramp market is quite similar to that of integrating the fixed BES, EVs' bidding into the ramp market is studied in this section with two participation modes considered: 1) direct bidding into the ramp market; and 2) EVs' collaboration with the conventional generator. New

indices are also proposed in this section to evaluate the system flexibility. Numerical experiments are conducted to validate the proposed modeling and evaluate impact on the system flexibility by enabling EVs' participation in the ramp market.

Section 5 addresses the optimal sizing and siting scheme of the fixed BES and PV generation aiming at improving power system resilience in face of the extreme event, while facilitating the operation at the same time. New concept of capacity accessibility is proposed to evaluate the reachability to the power and energy capacity during extreme events for both electricity demand and NB-S generating units. Multi-objective optimization technique is adopted to find the optimal placement scheme of fixed BES and PV generation while considering the unknowable nature of the extreme event. Numerical experiments are conducted to validate the proposed approach and illustrate how the new planning approach can help improve the grid resilience.

Section 6 summarizes the conclusions and contributions of the research, and discusses some future research directions.

Section 7 lists my publications so far. References are given at the end.

2. ESTIMATION OF THE AGGREGATED POWER CAPACITY FROM EV BES FOR PREDICTABILITY IMPROVEMENT*

2.1 Introduction

With the price of oil rapidly peaking in the past and the threat of global climate change increasingly acknowledged, EVs are expected to become the economic and environmental friendly choice for transportation. Since the point source (smoke stack) pollution is easier to control than the mobile (tail-pipe) source pollution, the wide adoption of EV BES can greatly help reduce the carbon emission and hence meet the environmental challenges [73].

EVs can be quite adjustable in different operation modes: Grid-to-Vehicle (G2V), Vehicle-to-Grid (V2G) and Vehicle-to-Building (V2B) [74], and therefore are suggested to participate in the electricity market [75]. However, before EVs could be utilized to help the system operation, the widespread use of EV BES would bring about huge uncertainties to the power grid, due to the stochastic factors such as mobility, drivers' behavior, etc.

* This section is in part a reprint of the material in the following papers: (1) Reprinted with permission from B. Zhang, M. Kezunovic, "Impact of Available Electric Vehicle Battery Power Capacity on Power System Reliability," *IEEE Power and Energy Society General Meeting*, Vancouver, Canada, July, 2013. Copyright 2013, IEEE. (2) Reprinted with permission from B. Zhang, P. Dehghanian, M. Kezunovic, "Spatial-Temporal Solar Power Forecast through Use of Gaussian Conditional Random Fields," *IEEE Power and Energy Society General Meeting*, Boston, MA, July 2016. Copyright 2016, IEEE. (3) Reprinted with permission from B. Zhang, M. Kezunovic, "Impact on Power System Flexibility by Electric Vehicle Participation in Ramp Market," *IEEE Transactions on Smart Grid*, Vol. 7, No. 3, pp. 1285-1294, May 2016. Copyright 2016, IEEE. (4) Reprinted with permission from B. Zhang, P. Dehghanian, M. Kezunovic, "Optimal Allocation of PV Generation and Battery Storage for Enhanced Resilience", *IEEE Transactions on Smart Grid*, accepted. (5) Reprinted with permission from M. Kezunovic, Z. Obradovic, T. Dokic, B. Zhang, J. Stojanovic, P. Dehghanian, and P. -C. Chen, "Predicating Spatiotemporal Impacts of Weather on Power Systems using Big Data Science," Springer Verlag, Data Science and Big Data: An Environment of Computational Intelligence, Pedrycz, Witold, Chen, Shyi-Ming (Eds.), ISBN 978-3-319-53474-9, 2017.

Besides, it is quite impossible for hundreds of thousands of EVs to participate in the electricity market by themselves due to the limitation on the communication and coordination. Ref [8] points out that an intermediate service provider, called "*aggregator*", is necessary to manage the small-scale power capacity of vehicles to provide the ancillary service at the appropriate large-scale power system level. In order to further assist the "*aggregator*" to appropriately bid into the market, the aggregated power capacity from EV BES should be estimated with EVs' related uncertainties considered.

Different from the previous work discussed in Section 1, a probabilistic analytical method to estimate the aggregated power capacity from EV BES for both charging and discharging purposes is proposed, with several factors taken into account: EVs' mobility, EV drivers' behavior, EV battery depletion limitation, etc. Our method is based on data describing traffic condition, which are more accessible and can be monitored in real-time. The proposed method considers available energy from EV BES in parking lots as well as in other places (house garage, etc.) where charging services are provided. The aggregated power capacity from EV BES can be better estimated through our method, and thus leading to an improvement on the system predictability.

2.2 Mathematical Formulation

2.2.1 Estimation on EVs' Availability

Those EVs that are parked (home, office, street, etc.) might be available to provide the service back to the grid through charging or discharging. In order to estimate EVs' availability, we divide the total EVs into two groups: 1) those running in the traffic system;

and 2) those parked somewhere. By the estimation on the number of EVs in the traffic, we can then calculate the EVs parked assuming that the total number of EVs in a large area is relatively fixed.

In [8], Poisson distribution is adopted to deal with the traffic flow in highways, and the flow of vehicles coming into the highway traffic is assumed to be a Poisson process. We assume that the entrance to the whole traffic system is composed of multiple entrances that are similar to highway entrances, and the flow into every entrance is Poisson distribution, as depicted in the Figure 2.1. It can be proved that the equivalent distribution of the total flow into the traffic system also has a Poisson distribution with the equivalent arriving rate $\lambda = \lambda_1 + \lambda_2 + \cdots + \lambda_n$. (The detailed proof can be found in the appendix.)

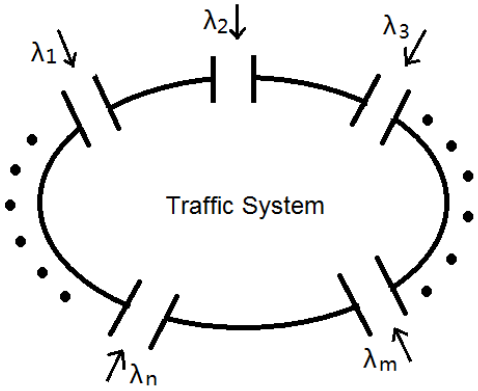

Figure 2.1 Illustration of entrances to the traffic system

A homogeneous Markov model with exponentially distributed inter-arrival and driving time is adopted to estimate the probability distribution of the EVs on the road, as depicted in Figure 2.2, where λ and μ are the vehicles' equivalent arriving and departure rates into/off the traffic system, which can be calibrated by the real time traffic data. *m* denotes the number of vehicles in the traffic system.

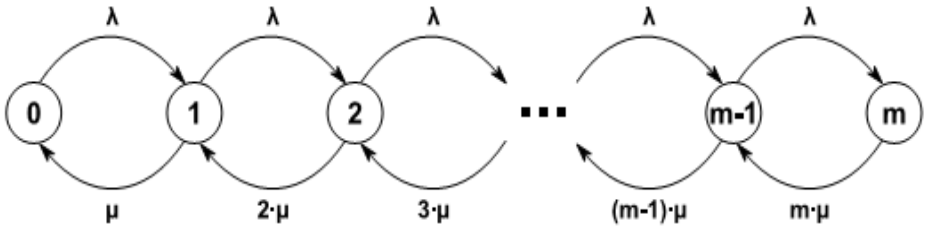

Figure 2.2 Markov chain describing the state of the traffic system

Therefore, the state-transition matrix is calculated in (2.1) and the corresponding Markov process is expressed in (2.2), where $\mathbf{P}(t) = \begin{pmatrix} P_0(t) & P_1(t) & \cdots & P_m(t) \end{pmatrix}^T$, and $P_k(t)$ stands for the probability that there are *k* vehicles in the traffic system.

$$A=\begin{pmatrix} -\lambda & \lambda & & & & & \\ \mu & -(\lambda+\mu) & \lambda & & & & \\ & 2\mu & -(\lambda+2\mu) & \lambda & & & \\ & \ddots & \ddots & \ddots & \ddots & & \\ & & (m-1)\mu & -(\lambda+(m-1)\mu) & \lambda & & \\ & & & m\mu & -m\mu & & \end{pmatrix} \tag{2.1}$$

$$\mathbf{P}(t)' = \mathbf{P}(t)A \tag{2.2}$$

Although the traffic condition is varying all the time, it is pointed out in [76] that traffic conditions do not vary too much in one unit of time (e.g., one hour). The final stable states can be calculated through (2.3) and (2.4), and expressed in (2.5) and (2.6), where $\rho = \frac{\lambda}{\mu}$.

$$0 = \mathbf{P}A \tag{2.3}$$

$$\sum_{i=0}^{m} P_i = 1 \tag{2.4}$$

$$P_k = \frac{\rho^k}{k!} P_0, k = 1, 2, \cdots m \tag{2.5}$$

$$P_0 = \left(\sum_{i=0}^{m} \frac{\rho^i}{i!} \right)^{-1} \tag{2.6}$$

When we assume that the number of vehicles in the traffic system is large, namely $m \to \infty$, the result can be approximated into (2.7) and (2.8), which is a Poisson distribution.

$$\lim_{m \to \infty} P_0 = e^{-\rho} \tag{2.7}$$

$$P_k = \frac{\rho^k}{k!} e^{-\rho}, k = 1, 2, \cdots m \tag{2.8}$$

Followed by the estimation on the number of vehicles on the road, the probability that there are *j* vehicles parked is calculated in (2.9), assuming that the total number of vehicles in a relatively large area is *N*.

$$P_j^{in} = \frac{\rho^{(N-j)}}{(N-j)!} e^{-\rho} \tag{2.9}$$

2.2.2 Estimation on the Available Energy from Mobile (EV) BES

As a flexible load, EVs can operate in different modes: G2V, V2G and V2B [74]. The aggregated available energy of mobile (EV) BES for charging/discharging is determined by: 1) EVs' availability; 2) EVs' connectivity to the grid; and 3) the available energy from EV BES.

The estimation on the average available energy from each EV considering the connectivity is conducted based on the Markov model illustrated in Figure 2.3. An individual EV is assigned with four states: S_1 - traveling on the road; S_2 – parked but not connected to the grid; S_3 – parked and plugged into the grid, but not fully charged; S_4 – parked, plugged into the grid and fully charged. In Figure 2.3, γ_{12} is calibrated based on the traffic data; γ_{23} is evaluated based on EVs' accessibility to charging infrastructures; γ_{34} is related to the charging time before fully charged; γ_{43} is affected by EVs' participation in the electricity market; γ_{31} and γ_{41} are correlated to drivers' charging behavior and

preference, i.e. whether they leave before the vehicle is fully charged. Such information can be obtained by conducting a survey with EV drivers.

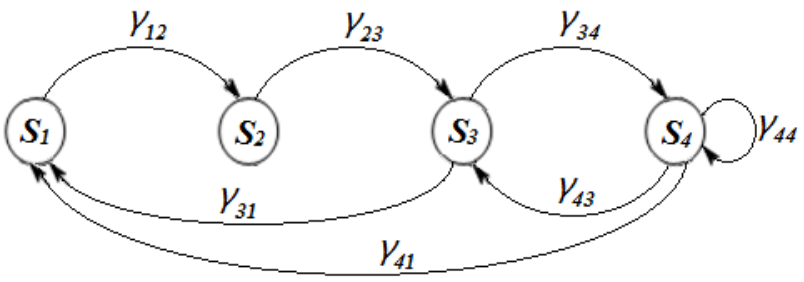

Figure 2.3 Markov chain describing the state of individual EV

The corresponding state-transition matrix is expressed in (2.10), and the probability of each state *i*, which is denoted as P_{si}, can be calculated in the similar way as in the Section 2.2.1 through (2.3) - (2.4).

$$\mathbf{B} = \begin{bmatrix} -\gamma_{12} & \gamma_{12} & 0 & 0 \\ 0 & -\gamma_{23} & \gamma_{23} & 0 \\ \gamma_{31} & 0 & -\gamma_{34}-\gamma_{31} & \gamma_{34} \\ \gamma_{41} & 0 & \gamma_{34} & -\gamma_{41}-\gamma_{43} \end{bmatrix} \tag{2.10}$$

By assuming that the average energy in each EV BES has a normal distribution, i.e. $E_{s23+} \sim N(\omega_{s23+}, \sigma^2_{s23+})$ and $E_{s4+} \sim N(\omega_{s4+}, \sigma^2_{s4+})$, where E_{s23+} denotes the available energy for discharging when an EV is in state S_2 or S_3; E_{s4+} denotes the available energy

for discharging when an EV is in state S_4; and the ω and σ are the corresponding mean and standard deviation for the corresponding normal distributions. Note that ω_{s23+} probably changes with the time while ω_{s4+} relatively remains the same. Besides, the value of σ^2_{s4+} can be small.

According to the properties of the normal distribution, the available energy of an individual EV for discharging when it is in the state of S3 or S4 is still in normal distribution, $E_{s34+} \sim N(\omega_{s34+}, \sigma^2_{s34+})$, where ω_{s34+}, σ^2_{s34+} is calculated in (2.11) and (2.12)

$$\omega_{34+} = \frac{P_{S3}}{P_{S2}+P_{S3}+P_{S4}} \times \omega_{S23+} + \frac{P_{S4}}{P_{S2}+P_{S3}+P_{S4}} \times \omega_{S4+} \tag{2.11}$$

$$\sigma^2_{S34+} = \left(\frac{P_{S3}}{P_{S2}+P_{S3}+P_{S4}}\right)^2 \times \sigma^2_{S23+} + \left(\frac{P_{S4}}{P_{S2}+P_{S3}+P_{S4}}\right)^2 \times \sigma^2_{S4+} \tag{2.12}$$

Therefore, with the calculation on EVs' availability in (2.9), the aggregated available energy from EV BES can be calculated in (2.13) and (2.14), where $F_{Z+}(z)$ and $f_{Z+}(z)$ are the cumulative probability distribution and its corresponding probability density function of the aggregated available energy from EV BES for discharging, respectively. The calculation on the cumulative probability distribution and probability density function of the aggregated available energy from EV BES for charging, $F_{Z-}(z)$ and $f_{Z-}(z)$, can be conducted following the similar procedures from (2.11) - (2.14).

$$F_{Z+}(z) = \int_{-\infty}^{z} \sum_{j=1}^{m} \frac{\rho^{(N-j)}}{(N-j)!} e^{-\rho} \frac{1}{j\sqrt{2\pi}\sigma_{S34+}} e^{-\frac{(\frac{u}{j}-\omega_{S34+})^2}{2\sigma^2_{S34+}}} du \tag{2.13}$$

$$f_{Z+}(z)=\sum_{j=1}^{m}\frac{\rho^{(N-j)}}{(N-j)!}e^{-\rho}\frac{1}{j\sqrt{2\pi}\sigma_{S34+}}e^{-\frac{(\frac{z}{j}-\omega_{S34+})^2}{2\sigma_{S34+}^2}} \quad (2.14)$$

After obtaining the probability estimation on the aggregated available energy from EV BES for both charging and discharging, we can apply F^{-1}_{Z+} (0.05) and F^{-1}_{Z-} (0.05) to serve as the exact quantity estimation on the available aggregated energy from EV BES, which indicates that the probability that the aggregated EVs can provide the energy no less than the amount of F^{-1}_{Z+} (0.05) and F^{-1}_{Z-} (0.05) is 95%. Meanwhile, two more factors should be further taken into account during the estimation on the discharging energy from EV BES, which are the battery depletion limit (in order not to damage the battery, the stage of charge (SOC) in the battery should not be lower than a certain limit) and the energy further needed for EVs to complete the travel. The quantity estimation on the aggregated energy from EV BES for both charging ($Energy^-$) and discharging ($Energy^+$) is described in (2.15) and (2.16), where $C_{EVtotal}$ is the total energy capacity of all EVs in one area; and q is average energy needed for an individual EV to finish its travel.

$$Energy^+ = F^{-1}_{Z}(0.05)\text{-}0.2\times C_{EVtotal}\times(N-\rho)/N - q\times\rho \quad (2.15)$$

$$Energy^- = F^{-1}_{Z-}(0.05) \quad (2.16)$$

2.2.3 Estimation on the Available Power Capacity from Mobile (EV) BES

The aggregated available power capacity from mobile (EV) BES is mainly limited by two aspects: 1) the available energy and the time duration; and 2) the limitation caused by EVs' maximum charging/discharging power. If we take the discharging as an example,

the first limitation can be expressed in (2.17), where $Power^+$ is the possible aggregated discharging power capacity from mobile (EV) BES; h is the assumed time duration. The second limitation is described in (2.18), where $r_{\max}^+$ is the assumed maximum discharging power of a single EV; and n_p is the estimation on the number of available EVs, as calculated in (2.19), indicating that the probability that the number of available EVs is no less than n_p is over 95%.

$$Power^+ = \frac{Energy^+}{h} \tag{2.17}$$

$$Limit^+ = r_{\max}^+ \times n_p \times P_{S3} / \left(P_{S2} + P_{S3} + P_{S4} \right) \tag{2.18}$$

$$\min \left| P_{rb}^{in}(n_p) - 0.05 \right| \text{ and } P_{rb}^{in}(n_p) \le 0.05 \tag{2.19}$$

The estimation on the aggregated discharging power capacity from mobile (EV) BES is determined by the minimum between these two factors, as shown in (2.20). Similar calculation as (2.17) - (2.20) can be conducted to finally estimate the aggregated charging power capacity from EV BES $p_{EV-}^{\max}$.

$$p_{EV+}^{\max} = \min(Power^+, Limit^+) \tag{2.20}$$

2.3 Numerical Experiments and Analysis

In this section, a numerical experiment is described based on the assumed scenario, listed in Table 2.1.

Table 2.1: Scenario Setup for EVs

Total number of EVs	30,000
Nissan Leaf (battery size 24 kWh)	15,000
Chevy Volt (battery size 16 kWh)	15,000
Number of Daily Vehicle Trips	3.02 [77]
Daily Vehicle Miles Traveled	28.97 miles [77]
Vehicles' average speed	40 miles/hour
Average energy needed per mile	0.35 kW [78]

The average time needed for an EV to complete its travel is about 14 min according to the calculation [(28.97/3.02/40)*60], which means that the average departure rate μ would be about 4 times/hour. Besides, the parameter q in (2.15) is about 3.36kW (0.35*28.97/3.02).

The probability density function $f_{Z+}(z)$ for the aggregated discharging energy from mobile (EV) BES in two different hours are illustrated in Figure 2.4 and Figure 2.5 respectively. One can observe from these two figures that: 1) the aggregated discharging energy from mobile (EV) BES behave quite like normal distribution, and this result is consistent with the Central Limit Theorem (CTD). This is based on the assumption that although people's behavior sometimes tend to have some regular patterns, EV charging and discharging is not necessarily tied to people's behavior, particularly when an optimized algorithm for decisions when to charge/discharge is used.; and 2) the standard deviation of the result during 3:00-4:00 am is smaller than that of the result during 4:00-

5:00 pm. This is because EVs tend more to be parked and fully charged during the early morning.

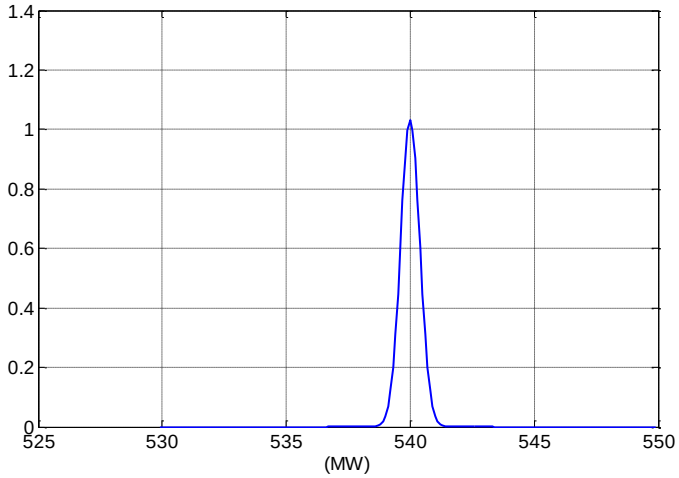

Figure 2.4 Probability density of the energy in mobile (EV) BES during 3:00 – 4:00 am

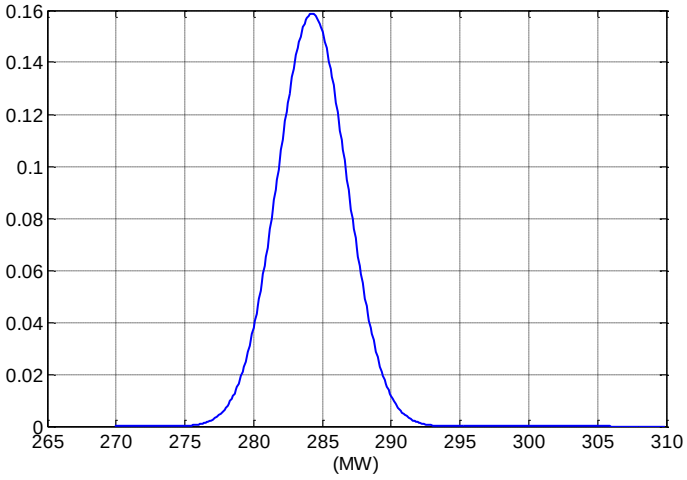

Figure 2.5 Probability density of the energy in mobile (EV) BES during 4:00 –5:00 pm

Meanwhile, the aggregated discharging power from mobile (EV) BES during the two hours in Figure 2.4 and Figure 2.5 under different considerations are listed in Table 2.2, in which A stands for the consideration on the battery depletion limit (20%) and B stands for the consideration on the energy needed for transportation purpose. It can be observed from the result that the battery depletion limit causes much more decrease on the aggregated power capacity from EV BES for discharging, compared to that of the travel need. This limitation can be hopefully alleviated with the potential improvement on the battery technology in the future.

Table 2.2 Quantity Estimation on the Aggregated Discharging Power Capacity from mobile (EV) BES

Time period	Aggregated power from EV BES (MW)		
	Without A or B	With A	With A and B
3:00 – 4:00 am	489.36	369.53	369.39
4:00 – 5:00 pm	243.10	130.59	124.30

The estimation on the aggregated power capacity from mobile (EV) BES for both charging and discharging during one day are depicted in Figure 2.6.

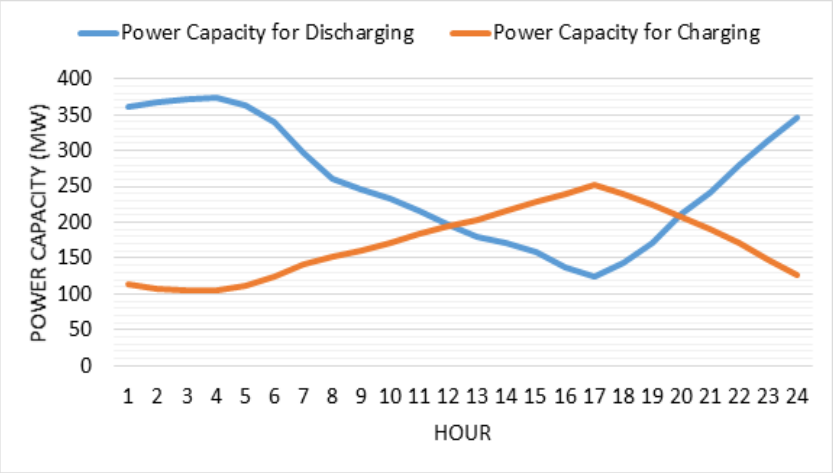

Figure 2.6 Aggregated power capacity from EV BES during one day

2.4 Summary

This section presents a method to estimate the aggregated power capacity from mobile (EV) BES for both charging and discharging purposes in a probabilistic way. The proposed method aims at assisting the EV aggregator to better provide service to the power grid, while improving the system predictability through better handling the uncertainties caused by EVs. The mobility of the EVs is captured through the traffic data, and the EV-related uncertainties are modeled through Markov model. The battery depletion limit and the energy for travel are also considered. Our proposed method is able to model the probability distribution of the aggregated energy from EV BES, which makes the results more compatible with other power system applications such as stochastic modeling, risk modeling, probabilistic optimal power flow, etc. The numerical experiments illustrate the

estimation results of the method and point out that the battery depletion limitation greatly limits the aggregated discharging power from mobile (EV) BES.

3. SPATIAL-TEMPORAL SOLAR POWER FORECAST THROUGH GCRF MODEL FOR PREDICTABILITY IMPROVEMENT*

3.1 Introduction

With the rapid growth of the solar industry, the variability and intermittency of this renewable source becomes another major source of uncertainty to the power grid, which brings about major challenges in energy balancing which may jeopardize the system reliability and flexibility [13]. Therefore, it is very critical to have an accurate real-time forecast of the solar generation so that both higher system operation efficiency and maximum solar utilization can be achieved.

Some of the previous studies show that the prediction accuracy can be significantly improved when spatial in addition to temporal correlation is considered [10], [13], [18, 19, 20]. The GCRF method provides a probabilistic framework for exploiting complex dependence structure among output variables [80], [81], which can help model the spatial correlations among different solar generation stations more effectively.

* This section is in part a reprint of the material in the following papers: (1) Reprinted with permission from B. Zhang, M. Kezunovic, "Impact of Available Electric Vehicle Battery Power Capacity on Power System Reliability," *IEEE Power and Energy Society General Meeting*, Vancouver, Canada, July, 2013. Copyright 2013, IEEE. (2) Reprinted with permission from B. Zhang, P. Dehghanian, M. Kezunovic, "Spatial-Temporal Solar Power Forecast through Use of Gaussian Conditional Random Fields," *IEEE Power and Energy Society General Meeting*, Boston, MA, July 2016. Copyright 2016, IEEE. (3) Reprinted with permission from B. Zhang, M. Kezunovic, "Impact on Power System Flexibility by Electric Vehicle Participation in Ramp Market," *IEEE Transactions on Smart Grid*, Vol. 7, No. 3, pp. 1285-1294, May 2016. Copyright 2016, IEEE. (4) Reprinted with permission from B. Zhang, P. Dehghanian, M. Kezunovic, "Optimal Allocation of PV Generation and Battery Storage for Enhanced Resilience", *IEEE Transactions on Smart Grid*, accepted. (5) Reprinted with permission from M. Kezunovic, Z. Obradovic, T. Dokic, B. Zhang, J. Stojanovic, P. Dehghanian, and P. -C. Chen, "Predicating Spatiotemporal Impacts of Weather on Power Systems using Big Data Science," Springer Verlag, Data Science and Big Data: An Environment of Computational Intelligence, Pedrycz, Witold, Chen, Shyi-Ming (Eds.), ISBN 978-3-319-53474-9, 2017.

Based on the literature survey, no studies have been devoted to the solar power forecast through application of the GCRF model before. It is a structured learning method which allows modeling different correlations among output variables, resulting in significant improvements of the prediction accuracy. Besides, its Gaussian nature facilitates the inference as well as the learning efficiency [71]. In this section, the GCRF model is introduced to forecast the solar power considering both the spatial and temporal correlations. Different from the previous works, the proposed methodology captures the probabilistic nature of the GCRF model which will further help modeling the inherent uncertainties of the solar generation, and thus possibly leading to a further improvement on the system predictability.

It should be noted that we are mainly targeting at exploring the possible outcome of adopting the GCRF into the solar forecast, instead of improving this method itself. This is typically the case with some other approaches adopted to power system studies such as many different optimization methods: robust optimization, stochastic optimization, etc. They are introduced into the power grid studies with a goal to adopt and adapt them to solve our problems rather than to improve the approaches themselves in the fundamental sense.

3.2 Mathematical Formulation

3.2.1 Solar Generation vs Solar Irradiance

Solar generation is mainly determined by the solar irradiance, although also affected by other factors. By modeling the relationship between the solar power generation

and the solar irradiance, the solar generation can also be predicted once the forecast on the solar irradiance is obtained. A linear relationship is assumed to model the aforementioned relationship in [19], as described in (3.1), where P_{solar} is the solar generation (kW); I_{solar} is the solar irradiance (kWh/m^2); and S and η are the area (m^2) and generation efficiency of the solar panel, respectively.

$$P_{solar} = I_{solar} \times S \times \eta \tag{3.1}$$

3.2.2 Solar Irradiance Forecast Models

3.2.2.1 Persistent (PSS) Model

The PSS model is usually adopted as a benchmark model to evaluate the performance of other forecast methods, i.e. the method is considered to be exceptional if its forecast accuracy outperforms that of the PSS model, and vice versa. The basic assumption of the PSS model is that the solar irradiance won't deviate too much in the next time step from the value at the current time step, and therefore the current solar irradiance is adopted as the forecast value for the next time step, as described in (3.2). This forecast scheme is working well for the very short term forecast, however, its forecast error grows largely with the increase of the forecast interval.

$$y_k^t = y_k^{t-1} \tag{3.2}$$

where y_k^t stands for the forecasted value of the k^{th} solar station at time t, and y_k^{t-1} is the measured value at time t-1.

3.2.2.2 Autoregressive with Exogenous Input (ARX) Model

The ARX model is a data-driven regression model, and can be formulated in (3.3) , where z_j^{t-l} is the historical measurement of station *j* at time *t-l*; y_k^{t-i} is the historical measurement of the target station *k* at time *t-i*; ε_t is the white noise; β_{jl}, φ_i are the coefficients obtained after regression; and *c* is the constant to be determined.

$$y_k^t = c + \sum_{i=1}^{p} \varphi_i y_k^{t-i} + \sum_{j=1, j\neq k}^{m} \sum_{l=1}^{n_j} \beta_{jl} z_j^{t-l} + \varepsilon_t \tag{3.3}$$

By considering the exogenous input z_j^{t-l}, which does not belong to the targeted solar station *k*, the spatial besides the temporal correlation is also considered.

3.2.2.3 GCRF Model

The GCRF model is a structured learning method, in which both the temporal correlations and spatial correlations can be taken into account and modeled in different graphs. It is a data-driven method, and a huge amount of historical data would be utilized to find the conditional distribution $P(\mathbf{y}|\mathbf{x})$, based on which the forecast on the future output would be conducted. $\mathbf{y}=[y^t{}_1, y^t{}_2, \ldots, y^t{}_N]^{\mathrm{T}}$ stand for the forecast solar irradiance at different solar stations; *N* is the number of the solar stations; vector **x** is the historical measurements on the solar irradiance in different solar stations, as described in detail in (3.4).

$$\mathbf{x} = [x_1^{t-1}, x_1^{t-2}, \ldots, x_1^{t-m_1}, x_2^{t-1}, x_2^{t-2}, \ldots, x_2^{t-m_2}, \ldots, x_N^{t-1}, x_N^{t-2}, \ldots, x_N^{t-m_N}] \tag{3.4}$$

The conditional distribution $P(\mathbf{y}|\mathbf{x})$ can be expressed in (3.5), where $A(\boldsymbol{\alpha}, y_i, \mathbf{x})$ is the association potential which models the relationship between the output y_i and input vector

x; $I(\boldsymbol{\beta}, y_i, y_j, \mathbf{x})$ is the interaction potential which relates different sets of output variables y_i and y_j [81].

$$P(\mathbf{y}|\mathbf{x}) = \frac{1}{Z(\mathbf{x}, \boldsymbol{\alpha}, \boldsymbol{\beta})} \exp\left(\sum_{i=1}^{N} A(\boldsymbol{\alpha}, \mathrm{y}_i, \mathbf{x}) + \sum_{j \sim i} I(\boldsymbol{\beta}, \mathrm{y}_i, \mathrm{y}_j, \mathbf{x}) \right) \tag{3.5}$$

We can approximate the A and I through the linear combinations of some pre-determined feature functions, as shown in (3.6) and (3.7), where $\boldsymbol{\alpha}$ and $\boldsymbol{\beta}$ are the corresponding parameters to be determined through training.

$$A(\boldsymbol{\alpha}, \mathrm{y}_i, \mathbf{x}) = \sum_{k=1}^{K_i} \alpha_k f_k(y_i, \mathbf{x}) \tag{3.6}$$

$$I(\boldsymbol{\beta}, \mathrm{y}_i, \mathrm{y}_j, \mathbf{x}) = \sum_{l=1}^{L_i} \beta_l g_l\left(y_i, y_j, \mathbf{x}\right) \tag{3.7}$$

The A and I become quadratic functions of **y** if we defined the feature functions f_k and g_l in quadratic forms also, as described in (3.8) - (3.10).

$$f_k\left(y_i, \mathbf{x}\right) = -\left(y_i - R_k\left(\mathbf{x}\right)\right)^2, \qquad k = 1, ..., K \tag{3.8}$$

$$g_l\left(y_i, y_j, \mathbf{x}\right) = -e_{ij}^{(l)} S_{ij}^{(l)}\left(\mathbf{x}\right)\left(y_i - y_j\right)^2 \tag{3.9}$$

$$e_{ij}^{(l)} = \begin{cases} 1 & (i, j) \in G_l \\ 0 & \text{otherwise} \end{cases} \tag{3.10}$$

where $R_k(\mathbf{x})$ is the prediction of y_i based on the input variables **x;** G_l is the graph modeling a certain correlation between y_i and y_j. $S_{ij}^{(l)}(\mathbf{x})$ is the similarity function between y_i and y_j.

Under this circumstance, $P(\mathbf{y}|\mathbf{x})$ then becomes a multivariate Gaussian distribution, namely $P(\mathbf{y}|\mathbf{x}) \sim N(\boldsymbol{\mu}, \boldsymbol{\Sigma})$, and can be re-formed in (3.11) and (3.12), where $\boldsymbol{\mu}$ is the mean

vector and $\boldsymbol{\Sigma}$ is the covariance matrix. $\boldsymbol{\Sigma}^{-1}=2(\mathbf{Q}_1+\mathbf{Q}_2)$, and $\mathbf{Q}_1$, $\mathbf{Q}_2$ are calculated in (3.13) and (3.14), respectively; while $\boldsymbol{\mu}=\boldsymbol{\Sigma}\mathbf{b}$, where $\mathbf{b}$ can be calculated in (3.15).

$$P(\mathbf{y}|\mathbf{x})=\frac{\exp\left(-\sum_{i=1}^{N}\sum_{k=1}^{K_i}\alpha_k\left(y_i-R_k(\mathbf{x})\right)^2-\sum_{i,j}\sum_{l=1}^{L_i}\beta_l e_{ij}^{(l)}(\mathbf{x})\left(y_i-y_j\right)^2\right)}{Z(\mathbf{x},\boldsymbol{\alpha},\boldsymbol{\beta})} \tag{3.11}$$

$$P(\mathbf{y}|\mathbf{x})=\frac{1}{(2\pi)^{N/2}|\boldsymbol{\Sigma}|^{1/2}}\exp\left(-\frac{1}{2}(\mathbf{y}-\boldsymbol{\mu})^{\mathbf{T}}\boldsymbol{\Sigma}^{-1}(\mathbf{y}-\boldsymbol{\mu})\right) \tag{3.12}$$

$$Q_{1ij}=\begin{cases}\sum_{k=1}^{K_i}\alpha_k & i=j\\ 0 & i\neq j\end{cases} \tag{3.13}$$

$$Q_{2ij}=\begin{cases}\sum_{k}\sum_{l=1}^{L_i}\beta_l e_{ik}^{(l)}S_{ik}^{(l)}(\mathbf{x}) & i=j\\ -\sum_{l=1}^{L_i}\beta_l e_{ij}^{(l)}S_{ij}^{(l)}(\mathbf{x}) & i\neq j\end{cases} \tag{3.14}$$

$$b_i=2\left(\sum_{k=1}^{K}\alpha_k R_k(\mathbf{x})\right) \tag{3.15}$$

To obtain the final conditional distribution $P(\mathbf{y}|\mathbf{x})$, the parameter vectors $\boldsymbol{\alpha}$ and $\boldsymbol{\beta}$ need to be calculated through the training based on the historical data, considering that the feature functions are pre-determined. The parameter vectors can be learnt through maximizing the conditional log-likelihood based on the training sets, as denoted in (3.16) and (3.17). Gradient decent algorithm can be adopted to solve this problem and obtain the final parameter vectors $\boldsymbol{\alpha}$ and $\boldsymbol{\beta}$.

$$L(\alpha,\beta)=\sum\log P\left(\mathbf{y}|\mathbf{x}\right) \tag{3.16}$$

$$\left(\boldsymbol{\alpha},\boldsymbol{\beta}\right)=\arg\max_{\boldsymbol{\alpha},\boldsymbol{\beta}}\left(L(\boldsymbol{\alpha},\boldsymbol{\beta})\right) \tag{3.17}$$

Due to its Gaussian nature, the mean vector $\boldsymbol{\mu}$ can be adopted as the forecast outputs of the solar irradiance for different solar stations. Moreover, owning to the property of the multivariate Gaussian distribution (for multivariate Gaussian distribution, the marginal distribution over a subset of its random variables is also a Gaussian distribution), the probability distribution of a single output y_i can be calculated in (3.18).

$$P\left(y_i \middle| \mathbf{x}\right) \sim N\left(\mu_i, \Sigma_{ii}\right) \tag{3.18}$$

Since the real solar irradiance is the sum of the forecast value and the forecast error, as show in in (3.19), where e_i is the forecast error for the i^{th} solar station, the probability distribution of the forecast error e_i can be expressed in (3.20).

$$y_i = \mu_i + e_i \tag{3.19}$$

$$e_i \sim N\left(0, \Sigma_{ii}\right) \tag{3.20}$$

With such probability distributions, the forecast result can be more compatible with other system applications such as stochastic modeling, risk modeling, etc.

3.2.3 Forecast Performance Evaluation

There are couples of indices aiming at evaluating the forecast performance. Here, we select two of them to assess the forecast accuracy, which are the mean absolute errors (MAE) and the root mean square error (RMSE), as shown in (3.21) and (3.22), respectively.

$$\text{MAE} = \frac{1}{Z}\sum_{t=1}^{Z}\left|y_t - y_t\right| \tag{3.21}$$

$$\text{RMSE} = \sqrt{\frac{1}{Z}\sum_{t=1}^{Z}\left(y_t - y_t\right)^2} \tag{3.22}$$

3.3 Numerical Experiments and Analysis

3.3.1 System Description

The hourly solar irradiance data (8 solar stations, year 2010) are collected from the California Irrigation Management Information System (CIMIS) [82] and utilized for our simulation. Figure 3.1 shows the graphical location of the studied solar stations. For more information, please refer to [82]. Marked in green in Figure 3.1, station No. 1 is selected as the target station, and we will pay particular attention on the forecast results of it.

Besides, two artificial solar stations (No. 9 & No. 10) are added very close to the target station in the interest of enhancing the spatial correlations, and resulting in potentially more clear impact of modeling the spatial correlations on the forecast results. (With the popularization of solar generation, the solar stations could be very close with each other.) Therefore, it is reasonable to assume that the hourly solar irradiance measurement of the added artificial stations should be very similar to that of the target station. We adopt the data from station No. 1 plus some low noises as the measurements of the artificial stations No. 9 and No. 10.

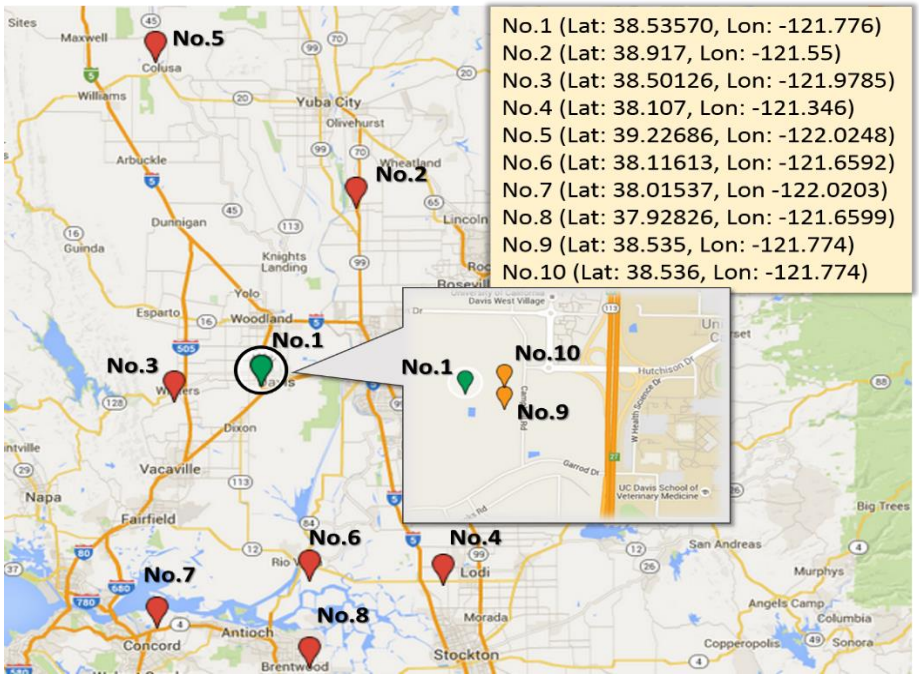

Figure 3.1 Illustration on the location of the studied solar station

3.3.2 Parameter Configuration

We are planning to compare the forecast performance of the aforementioned three forecast methods using different models: PSS, ARX and GCRF. The configuration of the parameters is needed before we utilize those models.

For the PSS model, no parameter configuration is needed, and we just use the previous data as the forecast value for the next time step.

In the ARX model, described in (3.3), parameter m is selected to be 9 to consider 9 historical measurements from the target solar station; the parameter p and n_j (j=1,2,…,9)

are all selected to be 10 in order to take into account 10 historical measurements from other solar stations.

Regarding the GCRF model, the focus would be to properly model both the temporal and spatial correlations among different solar stations, which is depicted in Figure 3.2.

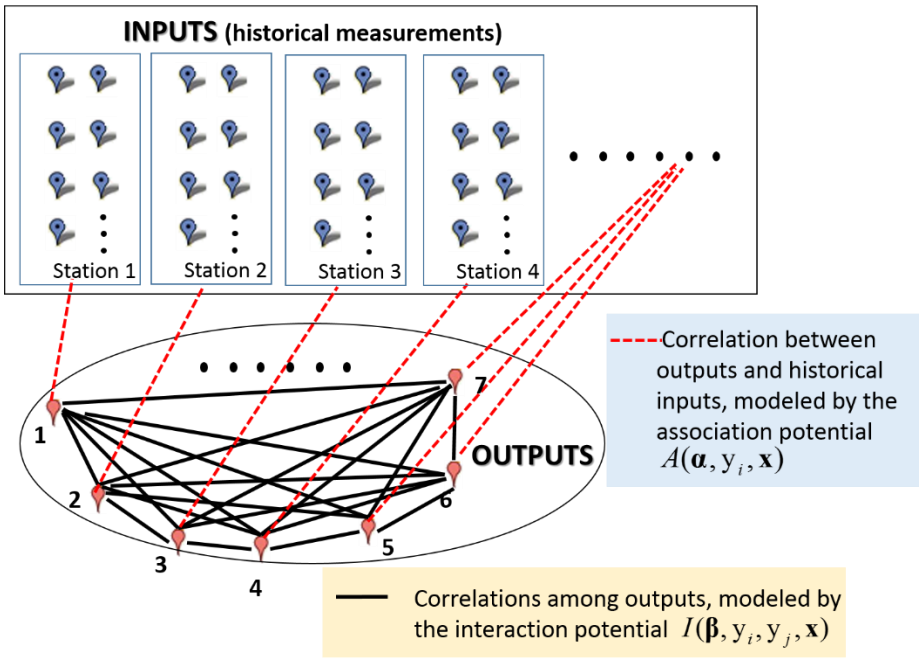

Figure 3.2 Modeling both the spatial and temporal correlations in GCRF model

As marked in the red dotted lines in Figure 3.2, the temporal correlations are modeled through the association potential $A(\boldsymbol{\alpha},y_i,\mathbf{x})$. In (3.6), where the association potential is defined, the parameter K_i is selected to be 1. Also, $R(x)$ in the feature function f_k, defined in (3.8) is selected to be an Autoregressive (AR) model, as described in (3.23), where the parameter p_i is set to be 10 to enable 10 historical measurements be considered.

$$R_i(x) = c + \sum_{m=1}^{p_i} \varphi_m y_i^{t-m} \tag{3.23}$$

We plan to model the spatial correlations among different solar stations through the interaction potential $I(\boldsymbol{\beta},y_i,y_j,\mathbf{x})$, as marked in the black solid lines in Figure 3.2. The geographical graph with all the solar stations is selected to be the one to model the spatial correlations, and therefore, L_i is selected to be 1 in (3.7); S_{ij} in (3.9) can be modeled in (3.24), where D_{ij} is the distance between station No. i and No. j. The reason to take the reciprocal is that the similarity between the outputs of two solar stations are in inversely proportional to the distance between these two stations.

$$S_{ij} = \frac{1}{D_{ij}^{\ 2}} \tag{3.24}$$

3.3.3 Simulation Cases and Scenarios

Four cases are generated out of the collected data in terms of different training and validation periods, as listed in Table 3.1. The reason behind is that the patterns of the solar irradiance vary among different seasons, and the forecast could be improved by separately model those patterns.

Table 3.1: Case Setup

Case	1	2	3	4
Training Period	January, March	May	July, September	November
Validation Period	February, April	April, June	August, October	October, December

The different scenarios are established based on the different cases:

- *Scenario1*: there is no missing data;
- *Scenario2*: there exist some missing data:
    a) *Scenario 2-1*: only one hourly data is missing in the target solar station;
    b) *Scenario 2-2*: two successive hourly data are missing in the target solar station;
    c) *Scenario 2-3*: only one hourly data is missing in several solar stations;
    d) *Scenario 2-4*: one solar station is totally excluded from the training process, since we assumed that no data is available at that station.

Scenario 2 is tested here to further see the performance of different forecast models in case of missing data. In the real life, the measurements of the solar station may not be available or accurate all the time (communication issue, equipment failure, etc.). Also, very few data would be available for training when a solar station is just established.

3.3.4 Simulation Results

The forecast performance of PSS, ARX and GCRF models under Scenario 1, evaluated through indices MAE and RMSE, is tabulated in Table 3.2. Besides, the detailed forecast performance of the studied models are illustrated in Figure 3.3 and Figure 3.4, in which the green line denotes ideal forecast result (the closer to this line means the better performance it is). From the results, one can observe that the GCRF model has the best forecast performance among the three models in all four cases under Scenario 1.

Table 3.2: Performance of Different Models under Scenario 1

Index	Cases	Forecast Model		
		PSS	ARX	GCRF
MAE	Case 1	90.3676	56.5334	55.1527
	Case 2	98.1372	51.8562	40.4062
	Case 3	96.6623	35.5478	25.5906
	Case 4	92.8664	51.6816	29.6195
RMSE	Case 1	111.9337	76.7457	74.4007
	Case 2	116.5823	81.9164	60.6969
	Case 3	111.6060	55.8073	40.6566
	Case 4	108.1498	67.8648	43.7008

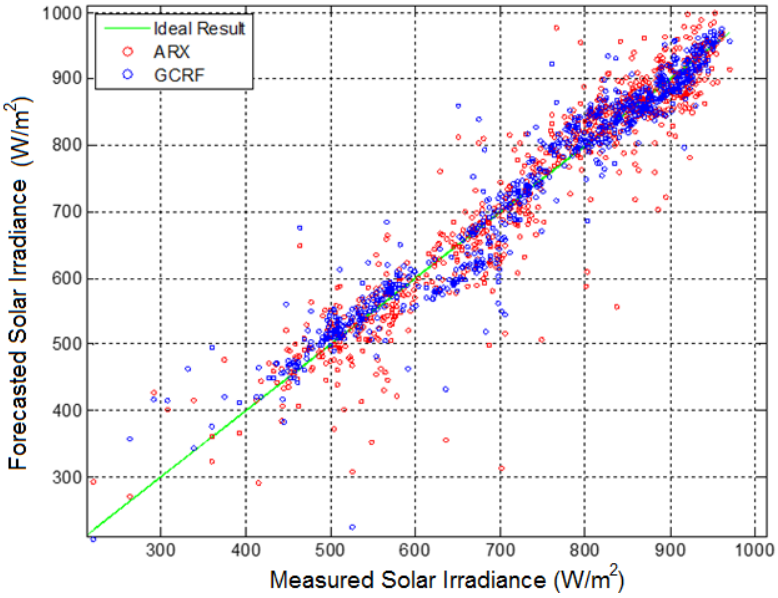

Figure 3.3 Illustration on the forecast performance of ARX and GCRF models (Scenario 1, case 3)

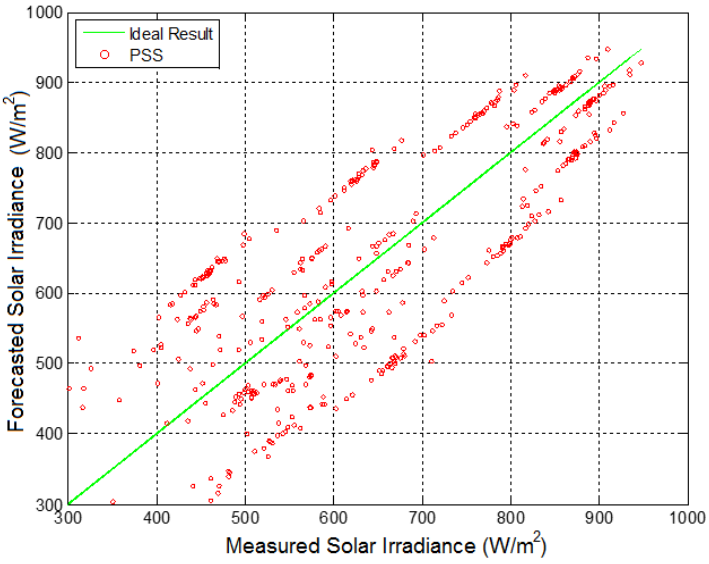

Figure 3.4 Illustration on the forecast performance of PSS model (Scenario 1, case 3)

Figure 3.5 and Figure 3.6 show the forecast performance of the PSS, ARX as well as the GCRF model under Scenario 2 and case 3. When one hourly data is missing, we simply use the measurement from the previous hour to approximate the missing one. From the results in Figure 3.5 and Figure 3.6, one can observe that the GCRF model shows the best forecast performance among the studied three models. The ARX model, however, may compromise a lot and become even worse than the PSS model, especially when more data is missing.

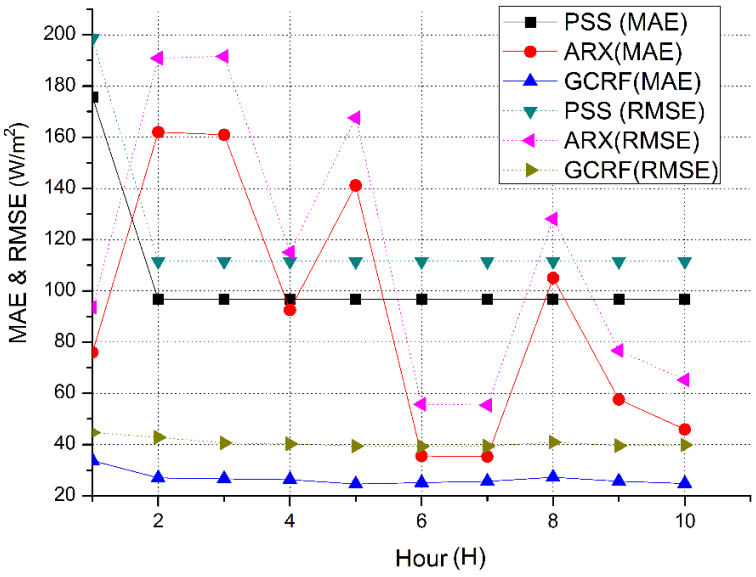

Figure 3.5 Illustration on the forecast performance of three models (Scenario 2-1, case 3)

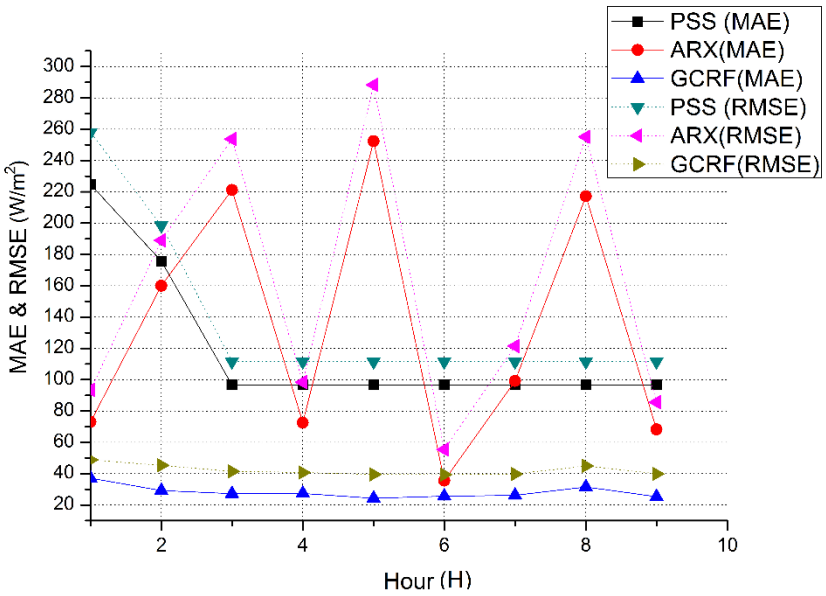

Figure 3.6 Illustration on the forecast performance of three models (Scenario 2-2, case 3)

Figure 3.7 shows the forecast performance of the studied three models in terms of the index MAE in Scenario 2-4, case 3, when missing data exist in multiple stations. It can be observed that: 1) the GCRF models still outperforms the other two models; 2) from the two sub-figures in the first row, one can see that the GCRF model is performing very well when there is no missing data in the station No. 9 or No.10, which have strong spatial correlation with the target solar station, and less missing data lead to better forecast performance; and 3) from the two sub-figures in the second row, it can be observed that the forecast performance of the GCRF model may compromise a little bit when missing data also appear in the station No. 9 or No. 10, however, it still outperforms the other two models most of the time.

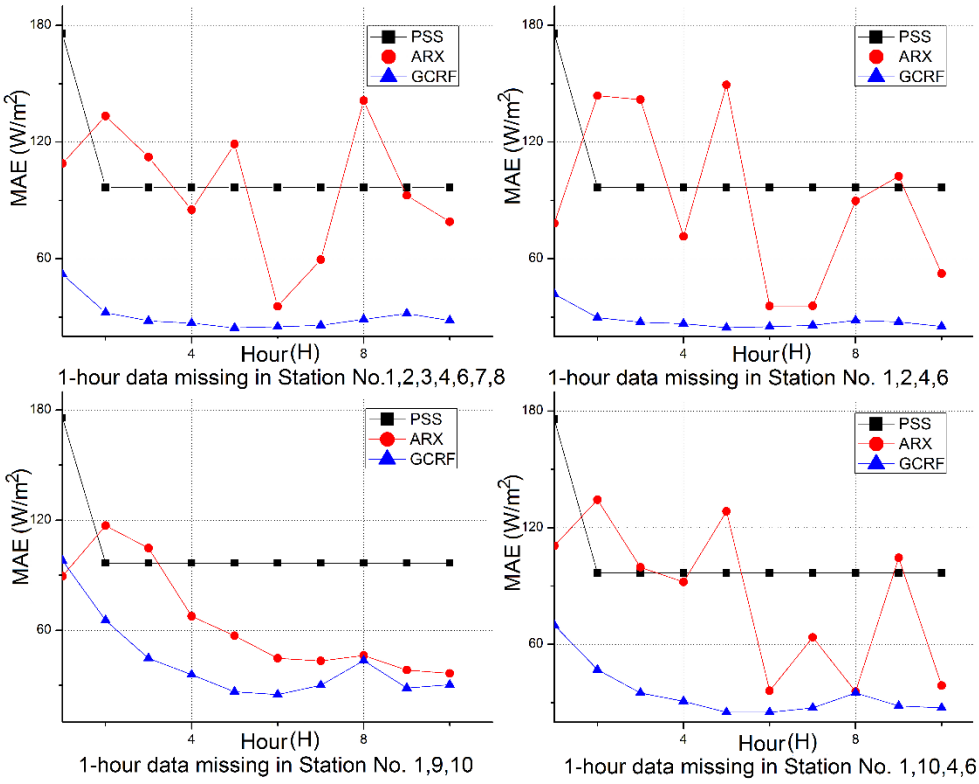

Figure 3.7 Illustration on the forecast performance of three models (Scenario 2-3, case 3)

The reason for the better performance of the GCRF model is due to its modeling of the spatial correlations: station No. 1, No. 9 and No. 10 have strong spatial correlations among each other, due to that fact that they are physically located very near to each other. Such strong spatial correlations are modeled and considered in the GCRF model, and utilized to adjust the deviated forecast results caused by the appearance of the missing data. One of the advantages of GCRF model is that different correlations can be modeled

separately and differently in various graphs. The spatial correlation is modeled specifically in one graph here in this numerical example, which is correlated to the distance between each two solar stations, and is quite logical in accordance to the reality.

Table 3.3 tabulates the forecast performance of the three models under Scenario 2-4, when the data from station No. 5 are assumed to be unavailable, and therefore, the data from that station is not taken into account during the training process. From the result, one can observe that the GCRF model still outperforms the other two models, although the performance worsens a bit compared with that in Scenario 1. Meanwhile the performance of the ARX model is quite unpredictable, and it deteriorates a lot in case 3.

Table 3.3: Performance of Different Models under Scenario 2-4

Index	Cases	Forecast Model		
		PSS	ARX	GCRF
MAE	Case 1	90.3676	58.2602	55.9011
	Case 2	98.1372	47.7145	43.0316
	Case 3	96.6623	50.2712	26.8112
	Case 4	92.8664	56.3702	30.7201
RMSE	Case 1	111.9337	79.2030	75.6125
	Case 2	116.5823	76.5143	63.7870
	Case 3	111.6060	68.0714	41.8258
	Case 4	108.1498	72.0233	44.8699

Table 3.4 illustrates the probability distribution modeling of the forecast error according to the property of multivariate Gaussian distribution (under Scenario 1), as modeled in (3.18) to (3.20). The results list the percentage that the forecast errors fall within the $\pm m\,\sigma$ (m=0.5, 1, 1.5, 2, 2.5, 3, 3.5) range of the forecast value. Compared with the standard percentages of the normal distribution, which is also listed in the table for comparison, one can observe that the forecast error basically fits the normal distribution, although not that perfect. Future work is to improve the performance of GCRF technique for modeling the forecast error.

Table 3.4: Distribution of the Forecast Error under Scenario 1

	Normal distribution	Case1	Case2	Case3	Case4	Combined
±0.5σ	0.383	0.4042	0.5263	0.3225	0.4462	0.4045
±1σ	0.6826	0.5556	0.8352	0.7089	0.7652	0.729
±1.5σ	0.7062	0.7203	0.9048	0.8031	0.8423	0.8258
±2σ	0.9544	0.818	0.9548	0.9167	0.9427	0.9146
±2.5σ	0.9596	0.9023	0.9756	0.9469	0.9695	0.9567
±3σ	0.9973	0.9349	0.9951	0.9589	0.9857	0.9707
±3.5σ	0.99772	0.9713	0.9963	0.9698	0.9892	0.982

3.4 Summary

This section mainly presents the forecast of solar power generation through GCRF model so as to improve the system predictability. In the GCRF model, both temporal and

spatial correlations among various solar stations are considered and modeled in different graphs, which can greatly improve the forecast accuracy and illustrated in the numerical experiments. The forecast performance of three models is compared: PSS model, ARX model as well as the GCRF model. It is shown in the results that the forecast performance of the GCRF model outperforms the other two models under most of the scenarios, and it has obvious advantage over the other two methods under the situation with the missing or unavailable data. The reason lies behind is the modeling of the spatial correlations in GCRF model can be utilized to adjust the deviation caused by the missing or unavailable data. Besides, the property of multivariate Gaussian distribution can help modeling the distribution of the forecast error, which makes the results more compatible with other system applications.

4. PARTICIPATION OF MOBILE (EV) AND FIXED BES IN THE RAMP MARKET FOR IMPROVED FLEXIBILITY*

4.1 Introduction

The flexibility issue has drawn increasing attention ever since the growing penetration of renewable energy sources aiming at reducing power systems' carbon emission. Though being clean and relatively inexpensive, renewable energy sources are making it quite challenging to predict or control their outputs. Integration of renewable energy demands improving power system flexibility, since its variability can lead to difficulties in energy balancing, thus compromising the power system operation efficiency and reliability [83], [84].

In order to better handle the uncertainty brought by the renewable energy sources, a new market product, the flexible ramping product, has been recently proposed by different independent system operators (ISOs) to accommodate net-load variations and

* This section is in part a reprint of the material in the following papers: (1) Reprinted with permission from B. Zhang, M. Kezunovic, "Impact of Available Electric Vehicle Battery Power Capacity on Power System Reliability," *IEEE Power and Energy Society General Meeting*, Vancouver, Canada, July, 2013. Copyright 2013, IEEE. (2) Reprinted with permission from B. Zhang, P. Dehghanian, M. Kezunovic, "Spatial-Temporal Solar Power Forecast through Use of Gaussian Conditional Random Fields," *IEEE Power and Energy Society General Meeting*, Boston, MA, July 2016. Copyright 2016, IEEE. (3) Reprinted with permission from B. Zhang, M. Kezunovic, "Impact on Power System Flexibility by Electric Vehicle Participation in Ramp Market," *IEEE Transactions on Smart Grid*, Vol. 7, No. 3, pp. 1285-1294, May 2016. Copyright 2016, IEEE. (4) Reprinted with permission from B. Zhang, P. Dehghanian, M. Kezunovic, "Optimal Allocation of PV Generation and Battery Storage for Enhanced Resilience", *IEEE Transactions on Smart Grid*, accepted. (5) Reprinted with permission from M. Kezunovic, Z. Obradovic, T. Dokic, B. Zhang, J. Stojanovic, P. Dehghanian, and P. -C. Chen, "Predicating Spatiotemporal Impacts of Weather on Power Systems using Big Data Science," Springer Verlag, Data Science and Big Data: An Environment of Computational Intelligence, Pedrycz, Witold, Chen, Shyi-Ming (Eds.), ISBN 978-3-319-53474-9, 2017.

uncertainties, [85, 86, 87]. The objective of this product is to build dispatch flexibility in terms of ramp capability in RTD to meet energy imbalances that may arise in the future.

There are many valuable studies of the flexible ramping product. Papers [88, 89, 90, 91] discuss the impact of the flexible ramping product on operation as well as power system reliability & flexibility; paper [92] proposes a new principle to determine the amount of ramp capacity needed; papers [93, 94] compare the performances of the flexible ramping product model, traditional dispatch model, stochastic model and robust model. However, few efforts have been devoted to discussing the provision of the flexible ramping product from mobile (EV) or fixed BES.

Mobile (EV) and fixed BES have been suggested to participate in the electricity market by providing ancillary services such as reserve and regulation in a lot of studies, such as [3, 8, 37, 39, 40 ,42, 47, 48, 75, 95]. However, the constraints on the battery capacity and battery cost related to frequent charging/discharging are the core problems restricting the flexible performance of mobile (EV) and fixed BES in the electricity market.

Different from the operating reserve, the ramp product can be integrated in RTD, which is applied on a 5-10 min time scale, and therefore the limitation caused by the battery capacity can be relieved. The ramp capacity is usually dispatched in just several short intervals due to the infrequent appearance of large variations. Mobile (EV) and fixed BES, if participating, won't have to charge or discharge frequently, compared with the frequency regulation while their fast ramping capability can still be rewarded. What is more important is that by bidding into the ramp market, mobile (EV) and fixed BES can more effectively improve the ISO's dispatch flexibility in RTD compared with their involvement in reserve

or regulation. This is due to the fact that the ramp product can be dispatched in RTD on a regular basis, whereas regulations are dispatched by automatic generation controls (AGC) and operating reserves only after major contingency happens.

This section aims at integrating mobile (EV) and fixed BES into the ramp market in order to improve the system flexibility to deal with the short time variability and uncertainty. Since the integration of EV BES will be quite similar with that of fixed BES, this section mainly focuses on addressing EVs' participation in the ramp market and their corresponding impact from system operators' point of view. The estimation on the aggregated power capacity from EV BES discussed in Section 2 can provide the necessary information for aggregators to conduct the bidding. Two types of participation will be modeled and compared: 1) EVs' direct provision of the ramp product; 2) EVs' cooperation with conventional generators.

4.2 Background Information on the Ramp Market

The concept of the ramp product is proposed by California ISO and Midwest ISO to deal with the energy imbalance in RTD caused by the increasing penetration of renewables, which leads to a more variable and uncertain net-load (the difference between the forecasted load and the expected electricity production from variable generation resources such as wind, solar, etc.). Such variation and uncertainty in the net-load, which is with a 5-min or 10-min time scale, might hardly be dispatched among generators due to the lack of ramp capability, though the generation capacity is enough.

The basic idea of the ramp market is to reserve the ramp capacity at this moment to handle the potential load variation and uncertainty in the future. In order to integrate the ramp product in the wholesale market, the system's ramp need is evaluated and merged into the existing RTD model, as denoted by (4.10) and (4.11). The evaluation of the ramping need is based on the variation and uncertainty of the net-load, and a certain confidence level (e.g. 95%) shall be chosen to achieve the cost effectiveness.

For the sake of ensuring the ramp product's being dispatched in RTD, a resource is required to have an energy bidding while participating in the ramp market. Separate bids on the ramp product, both upward and downward, are accepted. The ramp products are priced at the marginal values of the requirements. The capacity will receive flexible ramping payment once awarded and also the energy payment if dispatched.

4.3 Mathematical Formulation

4.3.1 Direct Participation in the Ramp Market

The participation in the ramp market can reward the fast ramping capability of mobile (EV) and the fixed BES, while at the same time avoid their disadvantage of the limited energy capacity. As mentioned earlier, the modeling of EVs' participation in the ramp market would be quite similar to that of the fixed BES, and this section focuses on modeling EVs' involvement in the ramp market.

We are planning to apply the look-ahead technique here to model the participation of EV BES in the ramp market, so that: 1) the uncertainty caused by the net-load can be better handled; 2) the energy requirement from the EVs can be also considered. The look-

ahead economic dispatch model (5-10 min base) with the participation in the ramp market of EV BES is described as follows:

$$Min \sum_{t=t_0}^{t_n} \begin{Bmatrix} \sum_{i\in G}\left[C_{Gi} p_{Gi}^t + C_{FRUi} FRU_i^t + C_{FRDi} FRD_i^t \right] \\ + C_{EVG} p_{EVG+}^t + C_{EVFRU} FRU_{EV}^t + C_{EVFRD} FRD_{EV}^t \end{Bmatrix} \tag{4.1}$$

$$\sum_{i\in G} p_{Gi}^t + p_{EVG+}^t = P_L^t + p_{EVG-}^t \quad t = t_0, t_1, ..., t_n \tag{4.2}$$

$$p_{Gi}^{\min} \le p_{Gi}^t \le p_{Gi}^{\max} \quad i \in G, t = t_0, t_1, ..., t_n \tag{4.3}$$

$$0 \le FRU_i^t \le R_i \times \Delta t \quad i \in G, t = t_0, t_1, ..., t_n \tag{4.4}$$

$$0 \le FRD_i^t \le R_i \times \Delta t \quad i \in G, t = t_0, t_1, ..., t_n \tag{4.5}$$

$$p_{Gi}^t + FRU_i^t \le p_{Gi}^{\max} \quad i \in G, t = t_0, t_1, ..., t_n \tag{4.6}$$

$$p_{Gi}^t - FRD_i^t \ge p_{Gi}^{\min} \quad i \in G, t = t_0, t_1, ..., t_n \tag{4.7}$$

$$p_{Gi}^t - p_{Gi}^{t-1} \le R_i \times \Delta t \quad i \in G, t = t_0, t_1, ..., t_n \tag{4.8}$$

$$p_{Gi}^{t-1} - p_{Gi}^t \le R_i \times \Delta t \quad i \in G, t = t_0, t_1, ..., t_n \tag{4.9}$$

$$\sum_{i\in G} FRU_i^t + FRU_{EV}^t \ge D_{FRU}^t \quad t = t_0, t_1, ..., t_n \tag{4.10}$$

$$\sum_{i\in G} FRD_i^t + FRD_{EV}^t \ge D_{FRD}^t \quad t = t_0, t_1, ..., t_n \tag{4.11}$$

$$0 \le p_{EVG+}^t \le p_{EV+}^{\max,t} \quad t = t_0, t_1, ..., t_n \tag{4.12}$$

$$0 \le p_{EVG-}^t \le p_{EV-}^{\max,t} \quad t = t_0, t_1, ..., t_n \tag{4.13}$$

$$E_{EV}^{t-1} - E_{EV}^t = \left(\frac{1}{\eta^+} p_{EVG+}^t - \eta^- p_{EVG-}^t \right) \times \Delta t \quad t = t_0, t_1, ..., t_n \tag{4.14}$$

$$E_{EV}^{t}\Big|_{t=t_k} \geq C_{req} \tag{4.15}$$

$$p_{EVG+}^{t} - p_{EVG-}^{t} + FRU_{EV}^{t} \leq p_{EV+}^{\max,t} \quad t = t_0, t_1, ..., t_n \tag{4.16}$$

$$p_{EVG+}^{t} - p_{EVG-}^{t} - FRD_{EV}^{t} \geq -p_{EV-}^{\max,t} \quad t = t_0, t_1, ..., t_n \tag{4.17}$$

$$0 \leq FRU_{EV}^{t} \leq p_{EV+}^{\max,t} \quad t = t_0, t_1, ..., t_n \tag{4.18}$$

$$0 \leq FRD_{EV}^{t} \leq p_{EV-}^{\max,t} \quad t = t_0, t_1, ..., t_n \tag{4.19}$$

where p_{EVG+} and p_{EVG-} are the discharging power and charging power from EV BES; FRU_{EV} and FRD_{EV} are the ramp up service and ramp down service from EV BES. Their upper limits are the aggregated charging/discharging power capacity evaluated in Section 2.2 based on the traffic information and EV owners' driving habits. The reason why EV BES should also bid into the energy market, characterized by p_{EVG+} and p_{EVG-}, is to ensure the timely release of the ramp capacity from EV BES when needed. By bidding into the ramp market, EV BES get rewarded by providing the ramp service for their fast ramp capacity. Once called upon, they will be paid additionally based on the energy provided.

The set G includes all on-line operating generators; p^t_{Gi} is the generation of generator i at time t; FRU^t_i and FRD^t_i are the ramp up and ramp down service provided by generator i at time t; C_{FRUi} and C_{FRDi} stand for the marginal cost of generator i to provide the ramp-up and ramp-down service, respectively; C_{EVG}, C_{EVFRU} and C_{EVFRD} represent the cost of EV BES to provide the energy service, ramp-up and ramp-down service, accordingly; P^t_L denotes the net-load of time t; p^{min}_{Gi} and p^{max}_{Gi} stand for the minimum and maximum operating limit of the generator i; R_i is the ramp rate of generator i; $\triangle t$ is the time interval of the clearance of the market; D^t_{FRU} and D^t_{FRD} denote the system requirement

for the ramp-up and ramp-down service at time t; $p_{EV+}^{max,t}$ and $p_{EV-}^{max,t}$ represent the aggregated discharging and charging power capacity from EV BES calculated through Section 2.2; E^t_{EV} is the aggregated energy from EV BES at time t; η^+ and η^- are the discharging efficiency and charging efficiency (between 0 and 1) of EV BES; C_{req} is the energy requirement of the aggregated EVs.

Equation (4.1) is the objective function aiming at minimizing the system cost; (4.2) describes the power balance in the system at all the time intervals; (4.3) to (4.9) set the operation limits (max/min generation limit, ramp limit) on the generators; (4.10) and (4.11) enforce the system ramp requirement; (4.12) and (4.13) represent the power capacity limits of the aggregated EV BES; (4.14) is the battery dynamic equation, which models the relationship between the battery energy and (dis)charging power of EV BES; (4.15) denotes the energy requirement by the aggregated EVs, which should be greater than or equal to C_{req} at time t_k; (4.16) to (4.19) set constraints on the bidding into the ramp market and energy market of EV BES.

4.3.2 Collaboration with the Conventional Generator

Both mobile (EV) and fixed BES have the limitation on the energy capacity, they may not be able to provide sustainable power like the conventional generator. Through the collaboration with the conventional generator, mobile (EV) and fixed BES can help improve the equivalent ramping capability of the conventional generator with relatively low ramp rates, owning to their fast ramping capacity. Here, we take EV BES as an

example to see how they can collaborate with the conventional generator and participate in the ramp market accordingly. It would be quite similar for the case of fixed BES.

4.3.2.1 Calculation of the Equivalent Ramp Rate

The basic idea for EV BES to collaborate with the conventional generator is to utilize the capacity of EV BES until the output of the conventional generator can catch up with the new generator point. Figure 4.1 illustrates two scenarios on EVs' collaboration with the conventional generators (in ramp-up case), where T denotes the time interval for the ramp market to get cleared; the red shaded area is the energy provided by EV BES under each scenarios; the black line is the output power of the conventional generator.

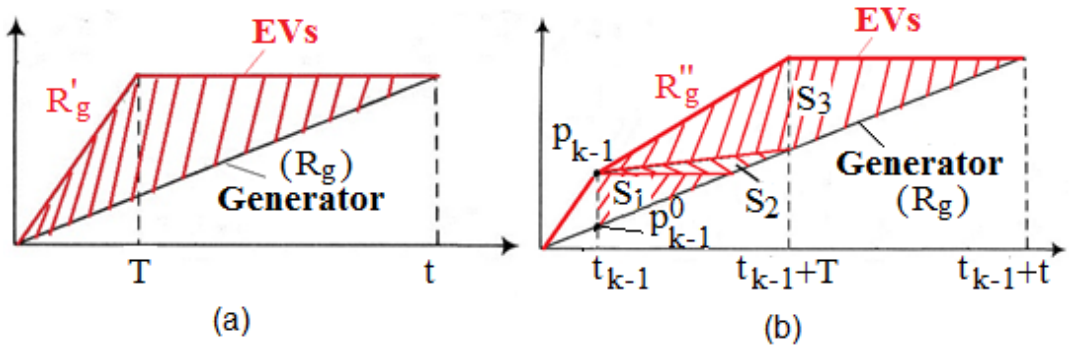

Figure 4.1: Two scenarios on EVs' collaboration with the conventional generator

The equivalent ramp rate to be achieved depends on how much aggregated energy that EV BES can provide to or extract from the grid. Just like what is shown in Figure 4.1 (a), the energy provided by EV BES should be enough for the generator to catch up at one moment t. Besides, the new ramp rate will also be limited by the maximum power that can be provided by EV BES. The generation limit can also exert the limitation on the equivalent ramp rate.

If we take the ramp-up for illustration, the first scenario shown in Figure 4.1 (a) illustrates the situation when EV BES do not provide energy or EV BES is charging at the very beginning. When the decision is made to improve the generator's ramp rate, EV BES will start discharge. The energy limitation caused by EV BES can be expressed in (4.20), where $Energy^+$ denotes the aggregated discharging energy capacity from EV BES obtained in Section 2.2.

$$\frac{1}{2}\times(t-T)\times R_g \times t \le Energy^+ \tag{4.20}$$

Equation (4.20) will always have solutions, and the solution that makes sense is shown in (4.21).

$$t \le \frac{T+\sqrt{T^2+\frac{8\times Energy^+}{R_g}}}{2} \tag{4.21}$$

Hence, the corresponding new equivalent ramp rate limited by the available energy capacity from EV BES R_{g1} can be obtained through (4.22).

$$R_{g1} = \frac{T+\sqrt{T^2+\frac{8\times Energy^+}{R_g}}}{2}\times R_g / T \tag{4.22}$$

The limitation caused by the maximum power output from EV BES should also be considered, as shown in (4.23), and the corresponding equivalent ramp rate R_{g2} is calculated in (4.24).

$$R_{g2} \times T - R_g \times T \le P_{EV}^{+} \tag{4.23}$$

$$R_{g2} = \frac{P_{EV}^{+}}{T} + R_g \tag{4.24}$$

The limitation caused by the maximum generation point can be expressed in (4.25) , where P_{gmax} is the maximum generation point of the generator.

$$R_{g3} = \frac{P_{g\max}}{T} \tag{4.25}$$

The final equivalent ramp rate should be the minimum of these three results, as denoted in (4.26).

$$R_g^{'} = \min(R_{g1}, R_{g2}, R_{g3}) \tag{4.26}$$

The second scenarios, as shown in Figure 4.1 (b), appears when EV BES is providing some energy at the very beginning, which means the aggregated output of both EV BES and generator is actually higher than the output of generator itself. Under this situation, the equivalent ramp rate may not be higher than that of the generator depending on the available energy from EV BES.

As is shown in Figure 4.1 (b), $P_{k\text{-}1}$ denotes the aggregated output from both EV BES and the conventional generator; $P^{0}_{k\text{-}1}$ is the original output from the generator. According to the previous calculation on the ramp rate, the difference between these two

generation outputs, which is the output from EV BES, must be within the output capability from EV BES. Moreover, the energy in EV BES must be greater than the area S_1.

Then, the available energy from EV BES should be compared with the area S_1+ S_2. If the energy available from EV BES is less than that, the equivalent ramp rate caused by the limitation of the aggregated energy capacity from EV BES is expressed in (4.27).

$$R_{g1}^{*} = \frac{P_{k-1}^{0} + R_g \times T - P_{k-1}}{T} \tag{4.27}$$

Otherwise, the energy limitation can be expressed in (4.28).

$$\begin{aligned} &\frac{1}{2} \times (P_{k-1} - P_{k-1}^{0} + P_{k-1}^{0} + R_g \times t - P_{k-1}^{0} - R_g \times T) \times T \\ &+ \frac{1}{2} \times (t - T) \times \left(P_{k-1}^{0} + R_g \times t - P_{k-1}^{0} - R_g \times T \right) \le Energy^{+} \end{aligned} \tag{4.28}$$

If the energy available from EV BES is larger than S_1+ S_2, there should be solution to (4.28), and the maximum ramp rate can be calculated through (4.29) and (4.30).

$$R_{g1}^{*} = \frac{P_{k-1}^{0} + R_g \times t_{\max} - P_{k-1}}{T} \tag{4.29}$$

$$t_{\max} = \frac{T + \sqrt{T^2 - \frac{4 \times \left(P_{k-1} - P_{k-1}^{0} \right) \times T - 8 \times Energy^{+}}{R_g}}}{2} \tag{4.30}$$

Similarly, the limit caused by the power output from EV BES should also be checked, as shown in (4.31). The corresponding equivalent ramp rate is expressed in (4.32).

$$P_{k-1} + R_{g2}^{*} \times T - P_{k-1}^{0} - R_g \times T \le P_{EV}^{+} \tag{4.31}$$

$$R_{g2}^{*} = \frac{P_{EV}^{+} + R_g \times T + P_{k-1}^{0} - P_{k-1}}{T} \tag{4.32}$$

Moreover, the limitation caused by the maximum generation point of the conventional generator is expressed in (4.33).

$$R_{g3}^{*} = \frac{P_{g\max} - P_{k-1}}{T} \tag{4.33}$$

The final equivalent ramp rate can be calculated in (4.34).

$$R_g^{"} = \min\left(R_{g1}^{*}, R_{g2}^{*}, R_{g3}^{*}\right) \tag{4.34}$$

Similar scenarios and calculation procedures, as (4.20) to (4.34), can be taken to calculate the equivalent ramp rate for the ramp down service.

4.3.2.2 Collaboration Strategy

The cooperation strategy we apply here is first to let mobile (EV) BES help improving the ramp rate of the designated generator as much as possible. If there is any capacity left for EV BES, they will be able to bid into the ramp market alone with those capacities. This is because once the generator is operating on its upper limit, it then loses the ramp up capacity even with the help of EV BES, since EV BES cannot provide stable power for a long time. This may limit EVs' participation into the ramp market. Therefore, the spare capacity from EV BES will be allowed to provide the ramp product on their own.

As a result, the model of EVs' participation in the ramp market proposed in Section 4.3.1 needs to be modified according to this new cooperation scheme. Two parameters,

which are $p^{g,t}{}_{EVG+}$ and $p^{g,t}{}_{EVG-}$, are added to denote the portion of power that EV BES cooperate with the generator. Suppose the k^{th} generator cooperates with EV BES.

Among equations (4.6) and (4.7), all equations related with generator k have to be modified as (4.35) and (4.36).

$$p_{Gk}^{t} + FRU_{k}^{t} + p_{EVG+}^{g,t} - p_{EVG-}^{g,t} \le p_{Gk}^{\max} \quad t = t_0, t_1, ..., t_n \tag{4.35}$$

$$-p_{Gk}^{t} + FRU_{k}^{t} - p_{EVG+}^{g,t} + p_{EVG-}^{g,t} \le -p_{Gk}^{\min} \quad t = t_0, t_1, ..., t_n \tag{4.36}$$

The limitation related to EV BES denoted in (4.16) and (4.17) should be modified into (4.37) and (4.38).

$$p_{EVG+}^{t} - p_{EVG-}^{t} + FRU_{EV}^{t} + p_{EVG+}^{g,t} - p_{EVG-}^{g,t} \le p_{EV+}^{\max} \quad t = t_0, t_1, ..., t_n \tag{4.37}$$

$$-p_{EVG+}^{t} + p_{EVG-}^{t} + FRU_{EV}^{t} - p_{EVG+}^{g,t} + p_{EVG-}^{g,t} \le p_{EV-}^{\max} \quad t = t_0, t_1, ..., t_n \tag{4.38}$$

Meanwhile, the power balance equation denoted in (4.2) should be updated into (4.39).

$$\sum_{i \in G} p_{Gi}^{t} + p_{EVG+}^{t} + p_{EVG+}^{g,t} = P_{L}^{t} + p_{EVG-}^{t} + p_{EVG-}^{g,t} \quad t = t_0, t_1, ..., t_n \tag{4.39}$$

And the energy dynamic equation of EV BES in (4.14) should be modified as (4.40).

$$E_{EV}^{t-1} - E_{EV}^{t} = \left(\frac{1}{\eta^{+}} p_{EVG+}^{t} - \eta^{-} p_{EVG-}^{t} + \frac{1}{\eta^{+}} p_{EVG+}^{g,t} - \eta^{-} p_{EVG-}^{g,t} \right) \times \Delta t \quad t = t_0, t_1, ..., t_n \tag{4.40}$$

Last but not least, the equivalent ramp rate of generator *k* should be calculated and modified according to the method proposed in Section 4.3.2. And the up and down limit of the two newly added variable should also be set properly.

4.3.3 Power System Flexibility

Ever since the flexible ramping product was proposed, the North American Electric Reliability Corporation (NERC) has established a task force to examine the integration of variable generation. Several researches have been working on evaluating system flexibility [96, 97, 98]. It is pointed out that the difference between the evaluation of system reliability and system flexibility is because generators ramp up or down capacity, which is the source of system flexibility is not independent of each other. How much ramp capacity one generator has is correlated with all other generating position.

The indices proposed here are based on the market commitment result, under which circumstance the correlation among generations can be greatly reduced. Different from the indices proposed in the previous references, they just reflect system flexibility under certain commitment result.

We propose to use the probability that the system can meet the ramping requirement, Fail to Ramp Probability (FTRP-up and FTRP-down), to assess system flexibility under a certain market commitment result. There are mainly two steps to calculate the FTRP-up and FTRP-down indices. The first step is to calculate the ramp capacities for generators according to (4.41) and (4.42), where x_i is the state of the generator to indicate whether it is on or off.

$$RC_{Gi,+}^{t} = x_i \times \min\left(R_i \times \Delta t,\, p_{Gi}^{\max} - p_{Gi}^{t}\right) \tag{4.41}$$

$$RC_{Gi,-}^{t} = x_i \times \min\left(R_i \times \Delta t,\, p_{Gi}^{t} - p_{Gi}^{\min}\right) \tag{4.42}$$

Similar steps can be taken to form a table, like the capacity outage probability table, with the ramp capacity as well as the corresponding probabilities.

The second step is to obtain the desired probability for the combined system with the participation of EV BES. Assume that the ramp up and down capacity for the generators in the whole system at time t is denoted as $RC^t_{G,+}$ and $RC^t_{G,-}$ respectively, the ramp requirement at time t are D^t_{FRU} and D^t_{FRD}, and the probability that generators have x MW ramp capacity loss can be denoted as $p_{rbU}(x)$ and $p_{rbD}(x)$. The FTRP-up can be expressed in (4.43) and FTRP-down can be written in the similar way.

$$FTRP-up\left(D^t_{FRU}\right)=\sum_{x=0}^{RC^t_{G,+}} p_{rbU}\left(x\right)F_{Zp+}\left(D^t_{FRU}-RC^t_{G,+}+x\right) \tag{4.43}$$

Sometimes, the results of the index FTRP-up are so close to compare. In order to tackle that, another index, which is more direct, is proposed to help evaluate the system flexibility – Ramp Up Room (RUR) and Ramp Down Room (RDR) which denote how much the system will be able to ramp up or ramp down under a certain probability p_{rb}. *RUR* and *RDR* can be calculated through the inverse function of FTRP-up and FTRP-down. RUR is expressed in (4.44), and RDR can be obtained in similar way. Illustration on the detailed steps and the relationship among different indices is shown in Figure 4.2.

$$RUR=FTRP-up^{-1}(p_{rb}) \tag{4.44}$$

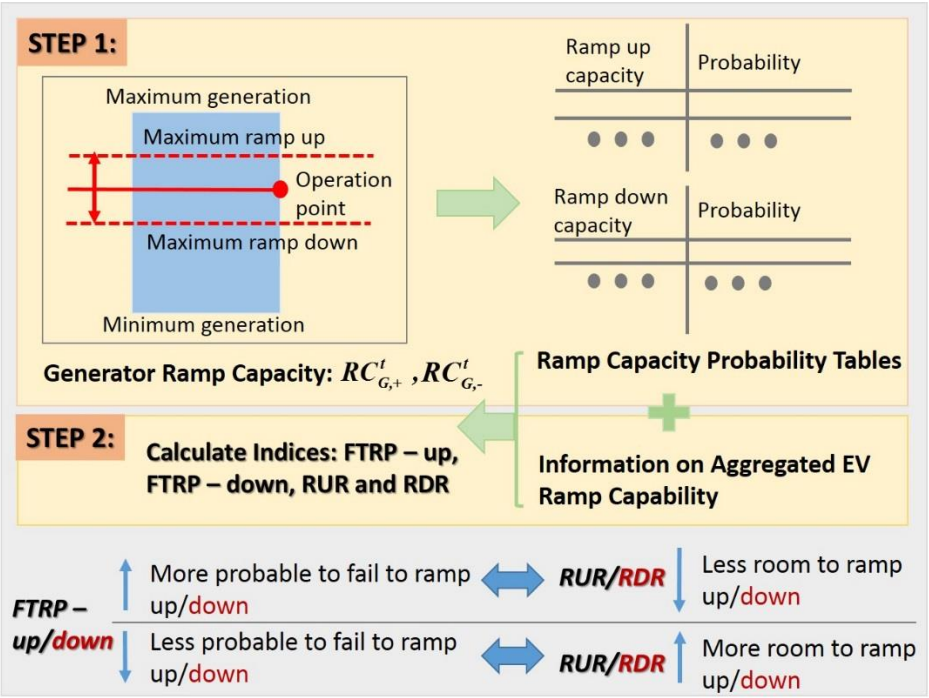

Figure 4.2: Illustration on the detailed steps and the relationship among different indices

4.4 Numerical Experiments and Analysis

4.4.1 System Description

The scenario setup on the EVs is similar to that in the Section 2.3. The aggregated charging and discharging power capacity from EV BES is illustrated in Figure 4.3, which serves as the upper limit of the ramp capacity of EV BES.

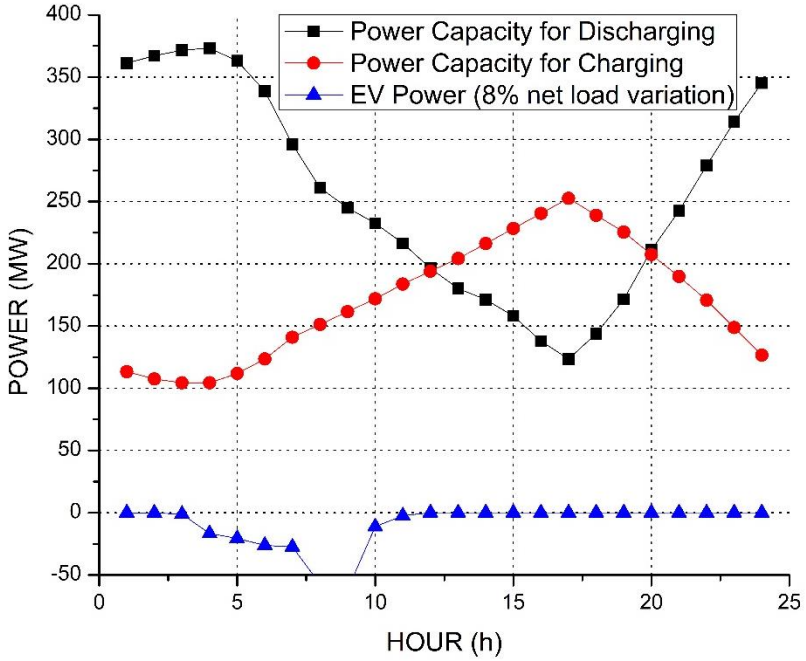

Figure 4.3: Illustration on the aggregated power capacity and the power from EV BES during one day (8% net-load variation)

We conducted the simulation on EVs' participation in the ramp market on a modified IEEE-RTS 96 test case system. The detailed configuration on the system connection and various parameters can be found in [99]. Load profiles are collected from the ERCOT System [100]. EVs are assumed to be located at Bus 114 (9,000 EVs), 115 (18,000), and 116 (3,000). It is required that the state of charge (SOC) of EV BES should be higher than 80% of the total battery capacity at the beginning of the next day. Meanwhile, an EV aggregator, as in [47], is selected to coordinate all the EVs to participate in the ramp market, and EVs' cost of providing the ramp service is assumed to be 5.44

$/MWh. EVs cost in providing the ramp service should not be high, because: 1) unlike the energy market, EVs do not have to physically increase/decrease its generation/consumption unless called. Therefore, there is no physical cost for the mobile (EV) battery or fixed battery to just sit somewhere and provide that service. The mobile (EV) battery or fixed battery may also be rewarded energy price other than the ramp price, and in that case the energy cost will have relationship with the physical cost. For traditional generators, it might be different, since some generators at least still need the fuel to keep running; 2) there is no opportunity cost for the mobile (EV) battery or fixed battery to provide the ramp service. This may not be the case for the conventional generators.

Four scenarios are considered: 1) a market with the provision of the ramp product from EV BES; 2) a market with the ramp product, but EV BES just act as loads; 3) a market without the ramp product and EV BES act as loads; and 4) a market with the provision of the ramp product from EV BES and EVs cooperate with one conventional generator (U155 at Bus115).

4.4.2 Impact of the Direct Participation

First, an illustrative numerical experiment is conducted based on the net-load forecast shown in Table 2.1 to see the impact of the ramp market and EVs' bidding into the ramp market. Accordingly, the energy price of the one-interval market clearance results are tabulated in Table 4.2, where the symbol "-" means that the market cannot be cleared at this moment. When this happens, other products (frequency regulation, reserve, etc.) in

the electricity market need to be called on with a higher cost. In MISO, the value of lost load (VOLL) is assumed to be $3500/MWh when the market cannot be cleared [93].

Table 4.1: Net-load Forecast

Forecast (MW)	T1	T2	T3	T4
T1	2531	2503		
T2		2600	2700	
T3-Case 1			2850	2600
T3-Case 2			2900	2600

Table 4.2: Results of the Energy Price under Four Scenarios

Energy Price ($)	Scenario 1	Scenario 2	Scenario 3	Scenario 4
T1	27.5688	27.5688	27.5688	26.7796
T2	27.5688	27.7537	27.5688	27.5688
T3-Case 1	211.1405	58.6814	-	211.141
T3-Case 2	211.1405	-	-	211.141

One can observe from this simple experiment that: 1) the involvement of the ramp market can improve the system flexibility to handle the uncertainty (Scenario 3 vs. Scenario 1, 2 & 4: with the introduction of the ramp market, it becomes feasible to clear the market in case1); and 2) the further involvement of EV BES into the ramp market can further improve the system flexibility, since more ramp capacity is available to handle the

net-load variation and uncertainty (Scenario 2 & 3 vs. Scenario 1 & 4: with the participation from EV BES in the ramp market, the market can be cleared in both case 1 & 2). Although the energy price becomes higher with the introduction of the ramp market and the involvement of EV BES, the price spikes, due to the lack of capacity to handle the highly variable net-load, can be prevented to some extent.

Then, the simulation on the look-ahead energy dispatch with the ramp market involved is conducted for 24 hours with dispatch interval of 10 minutes, under various net-load variations ranging from 1% to 8%. Figure 4.4 shows the result of the energy prices under different scenarios with 6% net-load variation. It can be easily observed that there is one extremely high price spike under Scenario 2, circled in black. The reason lies behind is that the system requirement on the ramp capacity also increases with the growth of the net-load variation. As a result, the system may lack the capacity to meet such requirement on the ramp capacity, although the net-load can still be met. The further involvement of EV BES in the ramp market can enhance the system flexibility and mitigate the price spikes under this circumstance.

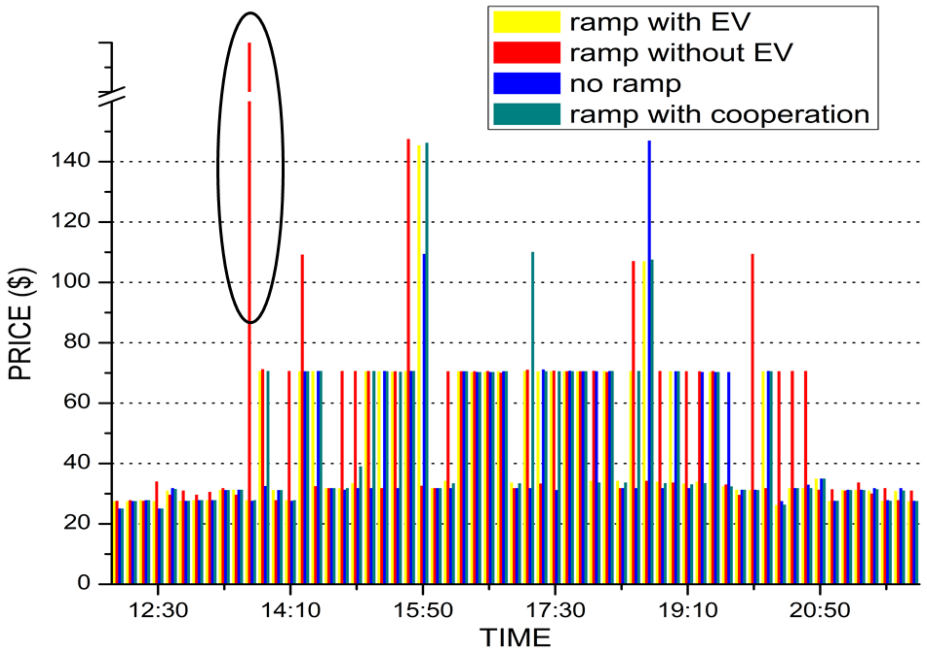

Figure 4.4: Results of energy prices under different scenarios (6% net-load variation)

Figure 4.5 illustrates the price for the ramp-down service when the markets get cleared. What can be observed from the result is that the participation of EV BES in the ramp market lowers down the price of the ramp service (Scenario 1 &4). The reason behind is the relatively low cost of the ramp services provided by EV BES.

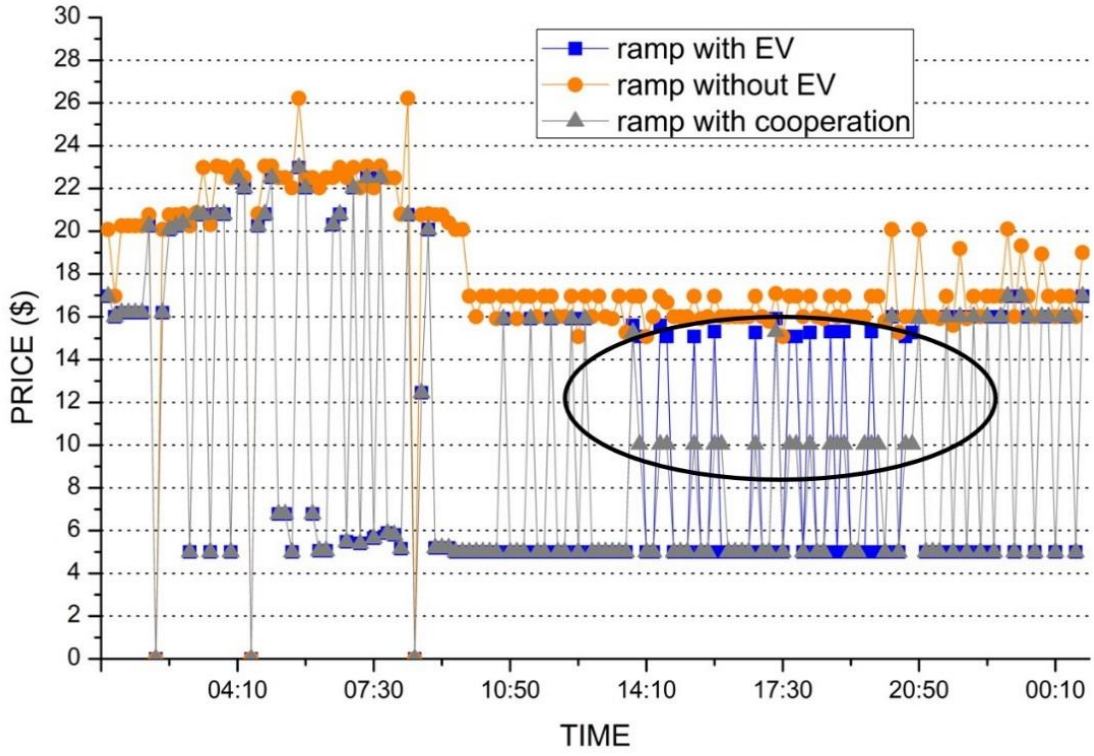

Figure 4.5: Results of the price for the ramp-down service (6% net-load variation)

Table 4.3 tabulates the results of the system cost under various scenarios and different net-load variations. One can observe that the introduction of the ramp market leads to an increase on the system cost (Scenario 2 vs. Scenario 3). With further involvement of EV BES into the ramp market, an improvement in cost saving can be observed (Scenarios 2, 3 vs. Scenarios 1, 4). The main reasons are: 1) the relatively low cost in providing the ramp service from EV BES; and 2) EV BES are enabled to charge smartly in our proposed model, and thus leading to a reduction in cost compared with the

dumb charging in Scenarios 2 & 3. The charging cost of EV BES under different scenarios is listed in Table 4.4.

Table 4.3: List of System Cost under Various Scenarios

System Cost ($)		Scenarios			
		No. 1	No. 2	No. 3	No. 4
Net-Load Variation	1%	1110358	1135591	1111111	1110097
	2%	1119107	1160420	1113580	1119039
	3%	1126841	1185118	1113264	1126505
	4%	1136544	1213335	1113212	1135015
	5%	1146267	1281181	1115552	1163985
	6%	1165168	1281181	1115552	1163985
	7%	1187228	1323758	1117879	1183974
	8%	1206859	1357614	1114052	1203468

Table 4.4: List of the Charging Cost of EV BES under Various Scenarios

Charging Cost ($)		Scenarios			
		No. 1	No. 2	No. 3	No. 4
Net-Load Variation	1%	1615	48801	48606	1596
	2%	1609	47965	47617	1605
	3%	1623	48902	48583	1624
	4%	1631	54548	47408	1632
	5%	1861	53517	48622	1863
	6%	2036	53562	48448	2016
	7%	1935	61609	45819	1935
	8%	2223	62023	49673	2532

Figure 4.6 shows the result of Loss of Load Probability (LOLP) (under 5% net-load variation) calculated according to [101], which reflects EVs' reliability impact on the system. One can observe that the reliability gets improved with the involvement of EV BES into the ramp market.

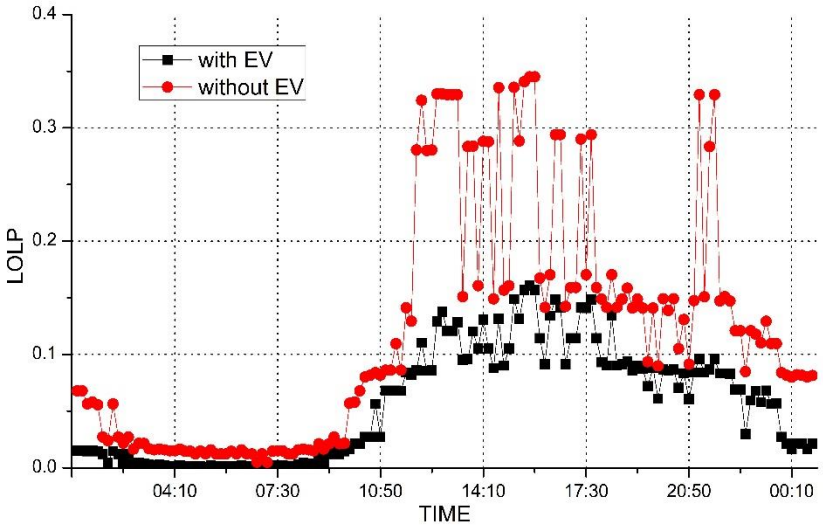

Figure 4.6: Illustration of the LOLP result (5% net-load variation)

Figure 4.7 and Figure 4.8 shows the impact on the system flexibility of the ramp service (under 8% of net-load variation) provided by EV BES, assessed through our proposed indices. One can observe from the results that: 1) the introduction of the ramp market improves the system flexibility since the system has higher probability to meet the

ramp requirement and more ramp room is observed (P_{rb} in (4.44) is set to be 0.001 in Figure 4.8); and 2) the system flexibility is further improved with the involvement of EV BES into the ramp market (the results of FTRP-up and RUR get further improved in Scenarios 1 and 4).

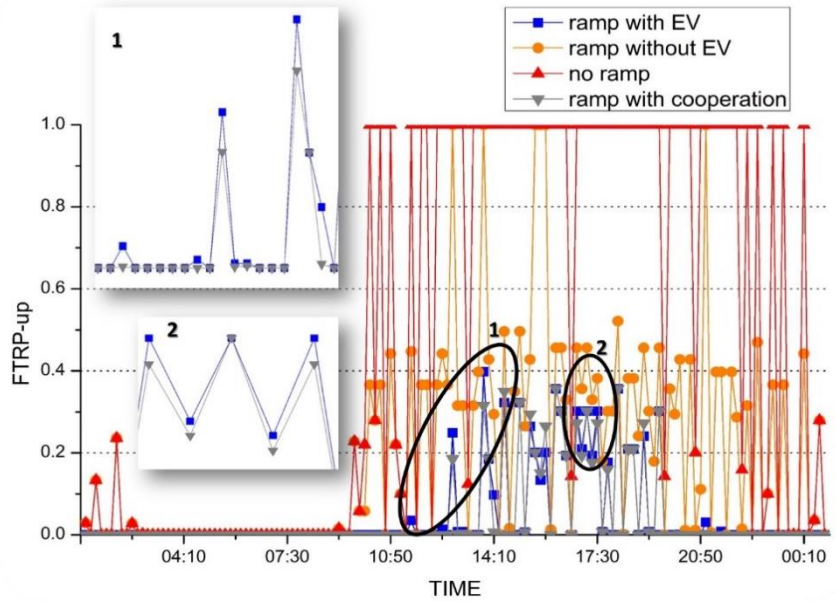

Figure 4.7: Illustration of FTRP-up result (8% net-load variation).

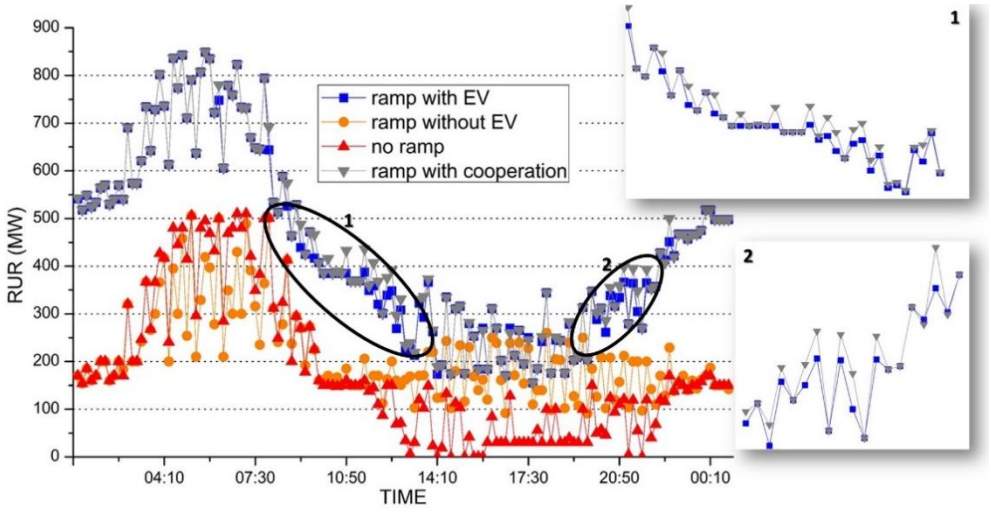

Figure 4.8: Illustration of RUR result (8% net-load variation)

4.4.3 Impact of the Collaboration with the Conventional Generator

The impact of EVs' collaboration with the conventional generator can be observed from the black circles in Figure 4.5, Figure 4.7, and Figure 4.8. One can observe that the prices of the ramp down service get further lowered down with EVs' cooperation with the conventional generator. Besides, the system flexibility result also gets further improved. The improvement will get more obvious with the increase in the net-load uncertainty and variation.

The Table 4.5 lists the benefits for both EV BES and the generator with and without the collaboration (with an assumption of 3% profit rate for both sides). It can be observed from the result that the collaboration can potentially increase the benefit for both EV BES

and the designated generator. Such increase in the profit can encourage the widespread use and development of EVs and EV infrastructure.

Table 4.5: Total Benefit for EV BES and the Generator (U155 at Bus115)

Benefit ($)	Net-load Uncertainty and Variation			
	1%	2%	3%	4%
No cooperation	15263	15642	22717	25106
With cooperation	15311	15646	22748	25992
Benefit ($)	Net-load Uncertainty and Variation			
	5%	6%	7%	8%
No cooperation	47340	60839	74016	100474
With cooperation	47465	61086	77840	111070

Two factors contribute to the difference between EVs direct bidding into the ramp market and their collaboration with the conventional generator. Firstly, less ramp capacity from EV BES will participate in the market under the case of EVs' collaboration with the conventional generator, which could lead to more reserve on the ramp capacity for the other generators. The second factor is that the collaboration with the conventional generator results in a more efficient utilization of the ramp capability from EV BES, which is exhibited in Figure 4.9. The upper part of Figure 4.9 is similar to that of Figure 4.1 (a), and energy equal to S_1 is needed from EV BES to achieve the equivalent ramp rate R'_g when collaborating with the conventional generator. However, energy equal to S_1+S_2 will

be needed from EV BES to achieve the same ramp rate during their direct participation in the ramp market (the down part of Figure 4.9). Less energy is needed from EV BES to achieve the same ramp rate when EVs and the conventional generators are collaborating with each other. This might not be the case when the situation in Figure 4.1 (b) happens. Such situation rarely happens due to the fact that the ramp capacity from EV BES is rarely called since a high uncertainty event does not happen that often.

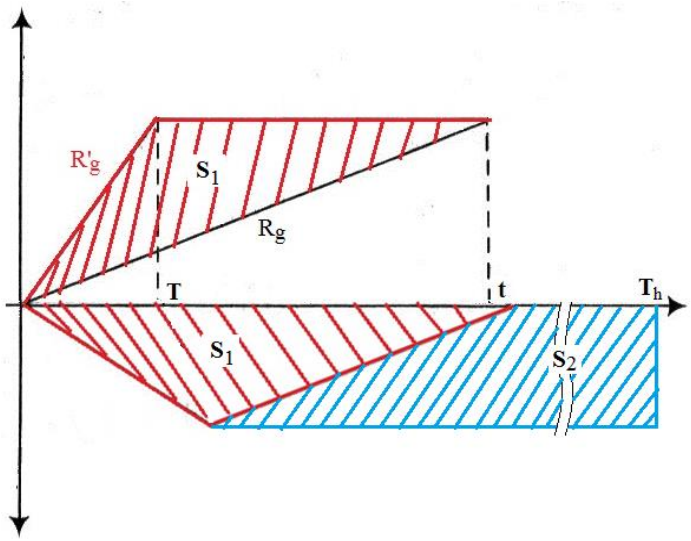

Figure 4.9: The difference in energy needed between EVs' collaboration with the conventional generator and EVs' direct participation

Last but not least, we found during the simulation that EV BES seldom gets called to discharge, although they take the majority in the ramp market, as illustrated in Figure 4.3. This indicates that EV BES, in most cases, is serving as backup for dealing with the net-load uncertainty and variation. This attribute is quite beneficial for EV BES, since their fast ramp capacity can get rewarded without frequent charging and discharging. Besides, their charging can also be optimized and thus leading to a reduction in the charging cost accordingly.

4.5 Summary

Nowadays, the battery is encouraged to participate in the ramp market as described in the white papers of some ISOs [86, 87]. The challenges regarding enabling the battery participate in the ramp market incudes but not limited to: the battery technology, the systems' protection scheme, (dis)charging infrastructure, design of a proper incentive, the division of the profit among different parties, etc. This section addresses the integration of the mobile (EV) and fixed BES into the ramp market, especially the EVs' participation in the ramp market, so as to improve the system flexibility in face of the increasing variation and uncertainty of the net-load. Two ways of participation are discussed: 1) their direct bidding into the ramp market; and 2) their collaboration with the conventional generator. Also, new indices to evaluate the system flexibility based on the market clearance results are proposed to further assess the impact of the mobile (EV) and fixed BES participation in the ramp market. Numerical experiments illustrate the impact of the ramp product provided by EV BES in two ways on the market clearance as well as the system flexibility.

It is shown that: 1) the provision of the ramp product by EV BES can facilitate the market clearance; 2) the system flexibility is improved with the participation of mobile (EV) and fixed BES in ramp market; 3) EVs' collaboration with the conventional generators can further improve the system flexibility compared with their direct bidding into the ramp market; and 4) the cooperation can potentially bring more benefit for both EV owners and the generators, which can provide incentives for the widespread use of EVs. The same results can also apply to the provision of the ramp service by the fixed BES.

5. OPTIMAL ALLOCATION OF PV GENERATION AND FIXED BES FOR ENHANCED RESILIENCE [*]

5.1 Introduction

Power grids are traditionally designed and planned to operate reliably under normal operating conditions and withstand the expected contingencies. Due to the recent years' severe events in power industry (2011 Fukushima Daiichi nuclear disaster, 2012 Superstorm Sandy, and 2016 Hurricane Hermine with approximately 8.5 million customer power outages and direct damage amounted to $71.4 billion in United States [102]), it became apparent that further considerations beyond the traditional reliability analysis is needed for keeping the lights on at all times. New NERC power system planning performance standard TPL-0014/0040a enforced in 2016 states that "studies shall be performed to assess the impact of the extreme events [103]." The resilience is becoming

[*] This section is in part a reprint of the material in the following papers: (1) Reprinted with permission from B. Zhang, M. Kezunovic, "Impact of Available Electric Vehicle Battery Power Capacity on Power System Reliability," *IEEE Power and Energy Society General Meeting*, Vancouver, Canada, July, 2013. Copyright 2013, IEEE. (2) Reprinted with permission from B. Zhang, P. Dehghanian, M. Kezunovic, "Spatial-Temporal Solar Power Forecast through Use of Gaussian Conditional Random Fields," *IEEE Power and Energy Society General Meeting*, Boston, MA, July 2016. Copyright 2016, IEEE. (3) Reprinted with permission from B. Zhang, M. Kezunovic, "Impact on Power System Flexibility by Electric Vehicle Participation in Ramp Market," *IEEE Transactions on Smart Grid*, Vol. 7, No. 3, pp. 1285-1294, May 2016. Copyright 2016, IEEE. (4) Reprinted with permission from B. Zhang, P. Dehghanian, M. Kezunovic, "Optimal Allocation of PV Generation and Battery Storage for Enhanced Resilience", *IEEE Transactions on Smart Grid*, accepted. (5) Reprinted with permission from M. Kezunovic, Z. Obradovic, T. Dokic, B. Zhang, J. Stojanovic, P. Dehghanian, and P. -C. Chen, "Predicating Spatiotemporal Impacts of Weather on Power Systems using Big Data Science," Springer Verlag, Data Science and Big Data: An Environment of Computational Intelligence, Pedrycz, Witold, Chen, Shyi-Ming (Eds.), ISBN 978-3-319-53474-9, 2017.

an emerging topic since how the electricity grid can withstand and react to unexpected extreme events has rendered more and more criticality to people's lives and every aspect of our economy.

Recent research on power system resilience framework is elaborated in references [72] and [104]. In [105], the grid resilience is quantified by assessing the vulnerability of transmission lines under different loading and weather conditions. Power system resilience is quite a complicated concept with many driving factors such as generator governor actions [106], transient stability [107], physical degradation [108], etc. Resource adequacy, as another important factor influencing the grid resilience, as discussed in [109] where a deterministic approach based on the extent of the resource adequacy is adopted to examine the system resilience in face of an extreme event similar to the 2014 Polar Vortex Event.

As an evolving and promising resource, the PV generation and fixed BES are rapidly being deployed in the grid. Compared with conventional generators, fixed BES is able to store the energy for use during emergencies. Besides, both the PV generation and fixed BES devices can be distributed, and thus leading to a potentially higher accessibility during extreme events. Despite some disadvantages of the fixed BES (e.g., limited energy capacity) and the PV generation (e.g., variable power output), their advantages still exhibit promising features during extreme events. References [110], [111] investigate the energy not supplied (ENS) reduction through batteries. How the black start (B-S) process can be expedited by the additional battery capacity is investigated in [112]. Hence, optimal allocation of the fixed BES and PV generation aiming at improving the system resilience in face of extreme events is an emerging planning problem to be solved.

Quite a few researchers have been studying the sizing and siting problem of the fixed BES and the renewable resources [55, 57, 59, 62, 63, 64, 65, 66, 67, 68, 69, 113] and facilitating the grid operation is the main goal of the aforementioned research: [55] focuses on the risk-based operation of distribution companies; [57] reduces the real power loss; [59] enhances the system reliability; [63] and [64] improve the grid-scale integration of renewables; [66] alleviates the transmission congestion; and [62, 65, 67, 68, 69, 113] minimize the total operation cost. The impact of such resources on enhancing the grid resilience requires further research. This section presents an optimal allocation scheme for the fixed BES and the PV generation in the transmission network. The suggested allocation scheme extends the conventional sizing and siting paradigm for accommodating the fixed BES and the PV generation to further improve the grid resilience in face of extreme events.

5.2 Mathematical Formulation

Capacity adequacy is one of the key factors playing a critical role on system resilience [109]. Higher capacity adequacy during the extreme events leads to a higher accessibility to the capacity (conventional generation, PV generation, battery energy, etc.), which renders a reduced energy not supplied (ENS), expedited B-S process, etc. during the extreme events. With rapid advancements in the control by power electronics, battery storage and PV generation are also able to provide the required reactive power [114, 115]. Coordinated with the conventional generators, their effectiveness in speeding up the system restoration is studied and proved in the past research [112, 116].

In this section, a new metric of capacity accessibility during extreme events is proposed to describe the capacity adequacy status during extreme events. The capacity accessibility determines the extent of power and energy the grid would be able to utilize during the extreme events. The difficulty in assessing the capacity accessibility lies in the unknowable nature of the extreme events [70], i.e., those with low occurrence probability but high impact [72, 104]. It is almost impossible and not realistic to enumerate all the possible cases and scenarios of different extreme events. Besides, referring the extreme event to several particular kinds of contingencies may cause an inappropriate disregard of others. Differentiated from the conventional "N-m" contingency principle, we propose to emulate the extreme event based on its common impact, which is the sharp decrease in the availability of system elements, instead of specifically defining the contingency set. Extreme events under various severity levels are considered to take into account their unknowable nature.

Generally, the capacity accessibility depends on: (1) the size of available capacity, and (2) the reachability to the capacity during extreme events.

5.2.1 Reachability during the Extreme Event

We quantify the reachability based on the common impact of the extreme events, i.e., the sharp decrease in the availability of system elements. An availability index is first assigned to each element during an extreme event, as presented in (5.1).

$$A_i^s = A_{event,s} \times \zeta_i^s \tag{5.1}$$

where $A_{event,s}$ is a designated system availability reflecting the general availability of all system elements under an extreme event of severity level s (it can also be viewed as a probability that an element would still remain available if encountered some extreme condition, i.e. the more severe the extreme event is, the less likely that the device would "survive" the extreme event.). In this way, extreme events of different severity levels can be emulated by altering the system availability $A_{event,s}$ (the lower $A_{event,s}$, the more severe the event is). ζ^s_i is an adjusting coefficient for the element i under the severity level s. This coefficient reflects the element's reaction during the extreme event and differentiates the availability of different elements during the extreme event of the same severity level. This coefficient is statistically correlated to the factors such as the equipment reliability, its size/capacity, its vulnerability in some extreme conditions, etc. Combining $A_{event,s}$ and ζ^s_i, A^s_i is the final availability index of the element i during an extreme event of level s.

The reachability $R^s_{i\text{-}j}$ between node i and j under $A_{event,s}$ is defined as the probability that node i and j are within the same island and, therefore, reachable to each other. Monte Carlo simulations can be conducted to obtain such kind of probability for a complex system, which can be calculated in (5.2).

$$R^s_{i-j} = \frac{\text{Number of scenarios where } i \text{ and } j \text{ are within the same island}}{\text{Total number of simulated senarios}} \tag{5.2}$$

System availability $A_{event,s}$ can be altered to simulate the extreme events of different severity levels. Under each $A_{event,s}$, the system reachability $\mathbf{R}^s$ can be evaluated by calculating the reachability among each two nodes, as presented in (5.3), where M is the total number of nodes in the system.

$$\begin{array}{c} \begin{matrix} 1 & 2 & \cdots & i & \cdots & j & \cdots & M \end{matrix} \\ \begin{bmatrix} R^s_{1-1} & R^s_{1-2} & \cdots & R^s_{1-i} & \cdots & R^s_{1-j} & \cdots & R^s_{1-M} \\ & R^s_{2-2} & \cdots & R^s_{2-i} & \cdots & R^s_{2-j} & \cdots & R^s_{2-M} \\ & & \ddots & & & & & \vdots \\ & & & R^s_{i-i} & \cdots & R^s_{i-j} & \cdots & R^s_{i-M} \\ & & & & \ddots & & & \vdots \\ & & & & & R^s_{j-j} & \cdots & R^s_{j-M} \\ & & & & & & \ddots & \vdots \\ & & & & & & & R^s_{M-M} \end{bmatrix} \begin{matrix} 1 \\ 2 \\ \vdots \\ i \\ \vdots \\ j \\ \vdots \\ M \end{matrix} \end{array} \tag{5.3}$$

Meanwhile, under each extreme event level $A_{event,s}$, demand reachability of bus k, $Reach^{k,s}_{load}$, can be defined as the total reachability of the unit capacity on bus k to the entire distributed load, as presented in (5.4).

$$Reach^{k,s}_{load} = \frac{\sum_{l \in L} \left(R^s_{l-k} \times \overline{D_l} \right)}{\sum_{l \in L} \overline{D_l}} \tag{5.4}$$

where L is the set for all the buses with load connected; $\overline{D_l}$ is the demand prioritizing factor at bus l. It can also be written in a matrix form, as described in (5.5), where $\mathbf{Reach}^s_{load} = [\, Reach^{1,s}_{load}, Reach^{2,s}_{load}, \ldots, Reach^{M,s}_{load}]^{\mathrm{T}}$, is the vector of all demand reachability of all buses; $\overline{\mathbf{D}_l} = \left[\overline{D_1}, \overline{D_2}, \cdots, \overline{D_M} \right]^T$ is the vector of the demand prioritizing factor for different buses ($\overline{D_l}$ is 0 if there is no load connected to the bus l); sum($\overline{\mathbf{D}_l}$) is the sum of all the elements in the vector $\overline{\mathbf{D}_l}$.

$$\mathbf{Reach}^s_{load} = \frac{\mathbf{R}^s \times \overline{\mathbf{D}_l}}{\mathrm{sum}\left(\overline{\mathbf{D}_l} \right)} \tag{5.5}$$

Following the similar procedure, we can define the generating unit reachability of bus k under each extreme event level $A_{event,s}$, denoted as $Reach^{k,s}{}_{gen}$, to reflect the total reachability of the unit capacity at bus k to all the NB-S units, calculated in (5.6). In the B-S process, generators can be categorized into B-S units and NB-S units. No external energy is needed for B-S units to start up, while cranking power is needed for NB-S units to initiate the start up.

$$Reach_{gen}^{k,s} = \frac{\sum_{g \in NBS_G} \left(R_{g-k}^{s} \times Q_g \right)}{\sum_{g \in NBS_G} Q_g} \tag{5.6}$$

where NBS_G stands for the set of all NB-S generating units; Q_g is the prioritizing factor for different NB-S generating units. Equation (5.7) shows the matrix form to calculate the generating unit reachability, where $\mathbf{Reach}^{s}{}_{gen}=[\, Reach^{1,s}{}_{gen}, Reach^{2,s}{}_{gen}, \ldots, Reach^{M,s}{}_{gen}]^{\mathrm{T}}$, is the vector of all generating unit reachability of all buses; $\mathbf{Q}_g=[Q_1, Q_2, \ldots, Q_M]$ is the vector of the prioritizing factors of the NB-S generating units on different buses (Q_g=0 if there is no NB-S unit on bus g); sum($\mathbf{Q}_g$) is the sum of all elements in the vector $\mathbf{Q}_g$.

$$\mathbf{Reach}_{gen}^{s} = \frac{\mathbf{R}^{s} \times \mathbf{Q}_g}{\mathrm{sum}\left(\mathbf{Q}_g\right)} \tag{5.7}$$

5.2.2 Capacity Accessibility for Electricity Demand

The concept of capacity accessibility for the electricity demand is proposed here to reflect how much capacity would be accessible for continuing supporting the electricity demand during the extreme event. Higher capacity accessibility at least signifies that more

capacity will be reachable to restore the demand during the unexpected situation. Both the power capacity and the energy capacity are taken into account. The consideration on the energy capacity particularly aims at quantifying the energy in the fixed BES and how long the power from the battery can last.

Meanwhile, the demand should also be treated differently according to the various consequence of loss of the load. For example, the load of a hospital should be quite important since the loss of load may mean loss of human lives. Here, the magnitude of the load is considered as the prioritizing factor, and it can be easily modified according to other practical considerations. Equations (5.8) and (5.9) define the system-wide capacity accessibility for the electricity demand regarding to both power capacity (PCA_load^s) and energy capacity (ECA_load^s) respectively, under the extreme event of severity level s. In (5.8), the capacity availability factors θ_{pow}, θ_{pv} and θ_G are introduced to consider the uncertainty associated with the availability of the battery power, PV power and the power from the conventional generators, respectively. Due to the dependence on the solar irradiance, PV generation may not be able to always generate at its rated maximum capability. Such capacity availability factor can be calculated as the ratio of the potential maximum generation, which is constrained by the weather conditions (PV generation), available energy (fixed BES) and equipment reliability (conventional generator), to the rated maximum generation within a period of time.

$$\text{PCA\_load}^s = \frac{\sum_{k\in K}\left(\theta_{pow}B_{pow}^k + \theta_{pv}B_{pv}^k + \theta_G p_{G\max}^k\right)\sum_{l\in L}\left(R_{l-k}^s \times \overline{D_l}\right)}{\sum_{l\in L}\overline{D_l}} \tag{5.8}$$

$$\text{ECA\_load}^s = \frac{\sum_{t=t_0}^{t_n} \sum_{k \in K} S_{k,t} \sum_{l \in L} \left(R_{l-k}^s \times \overline{D_l} \right)}{T \times \sum_{l \in L} \overline{D_l}} \tag{5.9}$$

where K stands for the set including all the system buses; B^k_{pow}, B^k_{PV}, P^k_{Gmax} are the power capacities of the fixed BES, the PV generation, and the conventional generating units at bus k; $\overline{D_l}$ here is set as the average load at bus l; $S_{k,t}$ is the energy remained in the fixed BES at bus k and time t; T is the total time duration.

With the demand reachability defined in (5.4) and (5.5), PCA_load^s and ECA_load^s can be rewritten into (5.10) and (5.11) respectively, where $\mathbf{B}_{pow}$=[B^1_{pow}, B^2_{pow}, … , B^M_{pow}] is the vector of the power capacity of the fixed BES on each bus; $\mathbf{B}_{pv}$=[B^1_{pv}, B^2_{pv}, … , B^M_{pv}] is the vector of the power capacity of the PV generation on each bus; $\mathbf{p}_{G\max}$=[$p^1_{G\max}$, $p^2_{G\max}$, …, $p^M_{G\max}$] is the vector of the power capacity of the conventional generator on each bus; $\mathbf{S}_t$=[$S_{1,t}$, $S_{2,t}$, …, $S_{M,t}$] is the vector of the energy remained in the battery on each bus.

$$\begin{aligned} \text{PCA\_load}^s &= \sum_{k \in K} \left(\theta_{pow} B^k_{pow} + \theta_{pv} B^k_{pv} + \theta_G p^k_{G\max} \right) \times Reach^{k,s}_{load} \\ &= [\theta_{pow} \mathbf{B}_{pow} + \theta_{pv} \mathbf{B}_{pv} + \theta_G \mathbf{p}_{G\max}] \times \mathbf{Reach}^s_{load} \end{aligned} \tag{5.10}$$

$$\text{ECA\_load}^s = \frac{\sum_{t=t_0}^{t_n} \sum_{k \in K} S_{k,t} \times Reach^{k,s}_{load}}{T} = \frac{\sum_{t=t_0}^{t_n} \mathbf{S}_t \times \mathbf{Reach}^s_{load}}{T} \tag{5.11}$$

5.2.3 Capacity Accessibility for NB-S Generating Units

Other than reducing the ENS at load points, expediting the system B-S process can also help improving the system resilience. Conventional generating units can be categorized into B-S and NB-S units. For those NB-S units, cranking power is needed to initiate the first start, while a B-S unit (e.g. hydro unit, combustion turbine) can start on its own. At the very beginning of the B-S process, the cranking power can be supplied from the B-S units, the energy stored in the battery storage, and possibly the power from the installed PV generation. Previous research demonstrated that increasing the system capability to provide the required cranking power can rapidly speed up the B-S process [112].

The concept of the system-wide capacity accessibility for NB-S units is proposed here to reflect how much power and energy capacity would be available to provide the cranking power for the NB-S units to start up during the B-S process. The power and energy capacity accessibility for NB-S units during an extreme event of level *s*, denoted as PCA_Gen^s and ECA_Gen^s, are defined in (5.12) and (5.13), where BS_G stand for the set of all B-S units.

$$\text{PCA\_Gen}^s = \frac{\sum_{k\in K}\left(\theta_{pow}B^k_{pow}+\theta_{pv}B^k_{pv}\right)\sum_{g\in NBS_G}\left(R^s_{g-k}\times Q_g\right)+\sum_{h\in BS_G}\theta_G p^h_{G\max}\sum_{g\in NBS_G}\left(R^s_{g-h}\times Q_g\right)}{\sum_{g\in NBS_G}Q_g} \tag{5.12}$$

$$\text{ECA\_Gen}^s = \frac{\sum_{t=t_0}^{t_n}\sum_{k\in K}S_{k,t}\sum_{g\in NBS_G}\left(R^s_{g-k}\times Q_g\right)}{T\times\sum_{g\in NBS_G}Q_g} \tag{5.13}$$

Similarly, with the generating unit reachability defined in (5.6) and (5.7), PCA_Gen^s and ECA_Gen^s can be re-written in (5.14) and (5.15) respectively, where $\mathbf{p}^{BS_G}{}_{G\max}=[\, p^{1,BS_G}{}_{G\max}, p^{2,BS_G}{}_{G\max}, \ldots, p^{M,BS_G}{}_{G\max}]$ is the vector of power capacity of the B-S units at each bus ($p^{i,BS_G}{}_{G\max}=0$, if there is no B-S units on bus i). Figure 5.1 illustratively summarizes the concepts proposed so far: system availability, (generating unit/demand) reachability (node-based, illustratively for node i), and the capacity accessibility (system-wide). Three illustrative scenarios in terms of the extreme events of different severity levels (reflected by different system availability indices $A_{event,s}$) are presented. In a more severe extreme event (scenarios 2 and 3), the availability of the elements tends to be lower and the reachability indices also decline. However, the reachability and accessibility indices are higher (reflected by longer-dotted lines) in a less severe extreme event (scenario 1).

$$\begin{aligned}\text{PCA\_Gen}^s &= \sum_{k\in K}\left(\theta_{pow}B^k_{pow}+\theta_{pv}B^k_{pv}\right)\times Reach^{k,s}_{gen}+\sum_{h\in BS_G}\theta_G\, p^h_{G\max}\times Reach^{h,s}_{gen}\\ &=\left[\theta_{pow}\mathbf{B}_{pow}+\theta_{pv}\mathbf{B}_{pv}+\theta_G\mathbf{p}^{BS_G}_{G\max}\right]\times\mathbf{Reach}^s_{gen}\end{aligned} \tag{5.14}$$

$$\text{ECA\_Gen}^s=\frac{\sum_{t=t_0}^{t_n}\sum_{k\in K}S_{k,t}\times Reach^{k,s}_{gen}}{T}=\frac{\sum_{t=t_0}^{t_n}\mathbf{S}_t\times\mathbf{Reach}^s_{gen}}{T} \tag{5.15}$$

Meanwhile, the prioritizing index Q_g of each NB-S units is defined as its importance in the B-S process, i.e. how much less the pick-up energy would be, if this given NB-S unit does not participate in the B-S process, which can be calculated in (5.16)

.

$$Q_g=E^0_{bl-start}-E^g_{bl-start} \tag{5.16}$$

where $E^{0}_{bl\text{-}start}$ is the energy that can be picked up within a certain period of time in the B-S process with the participation of all the generators; $E^{g}_{bl\text{-}start}$ is the energy picked up without the participation of unit *g*.

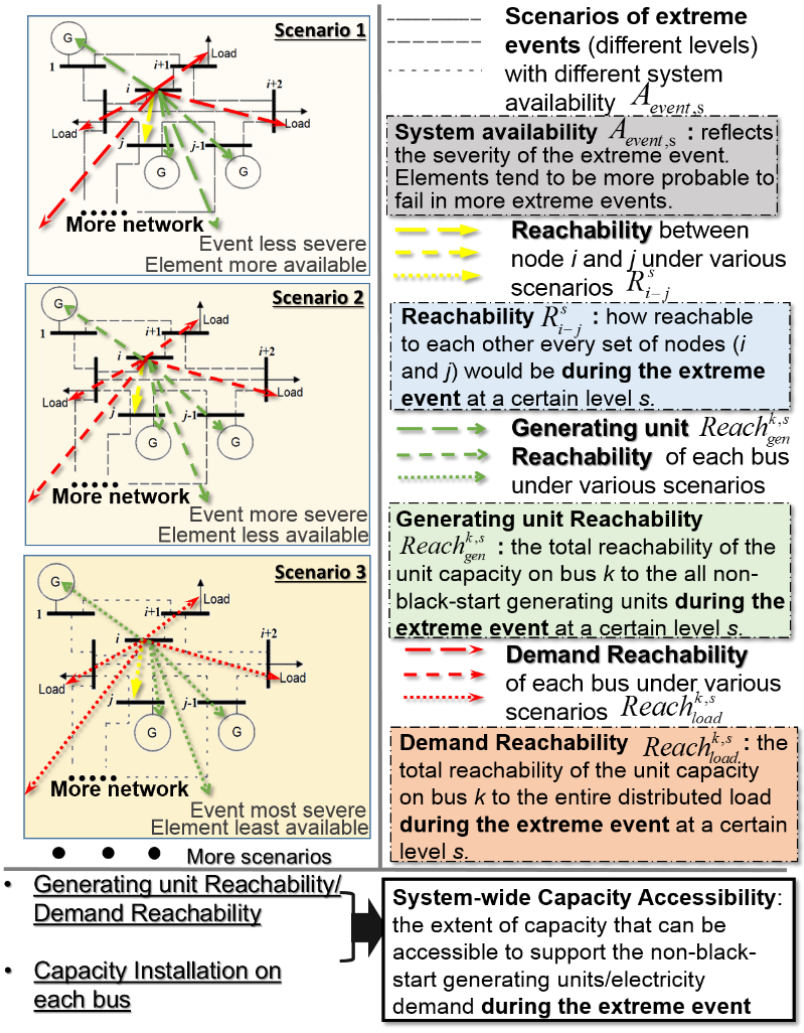

Figure 5.1: Illustration on different concepts: system availability, reachability, and capacity accessibility.

The calculation of $E^0_{bl\text{-}start}$ and $E^g_{bl\text{-}start}$ is related to the start-up process of each NB-S generating units, i.e. the start-up order of each NB-S units, which is reflected via variable t_{jstart}. In order to calculate that, the model proposed in [117] is adopted, with some modifications to further improve the calculation performance. The order of the start-up process of the NB-S units is calculated in the following optimization model from (5.17) to (5.35).

$$obj. \quad \max \sum_{j \in NBS_G,\, j \neq g} \left(P_{j\max} - P_{jstart} \right) \times t_{jstart} \tag{5.17}$$

$$s.t. \qquad t_{jstart} \le T_{jc\max}, \quad j \in NBS_G,\, j \neq g \tag{5.18}$$

$$t_{jstart} \ge T_{jc\min}, \quad j \in NBS_G,\, j \neq g \tag{5.19}$$

$$\sum_{\substack{i \in ALL \\ ,i \neq g}} Rr_i \left(t - t^t_{i1} - t^t_{i3} \right) - \sum_{\substack{j \in NBS_G \\ ,j \neq g}} w^t_{j3} P_{jstart} \ge 0, t = 1, 2, ..., T_{bl\_start} \tag{5.20}$$

$$w^t_{l1} T_{lctp} \le t^t_{l1} \le T_{lctp}, \; t = 1, 2, ..., T_{bl\_start}, \; l \in BS_G \tag{5.21}$$

$$\begin{aligned} &\left(T_{bl\_start} + 1 + T_{jctp} \right) w^t_{j1} - \sum_{t=1}^{T_{bl\_start}} u_{jt} \le t^t_{j1} \le t_{jstart} + T_{jctp} \\ &, \quad t = 1, 2, ..., T_{bl\_start}, \; j \in NBS_G, \; j \neq g \end{aligned} \tag{5.22}$$

$$t^t_{j1} \ge 0, \quad t = 1, 2, ..., T_{bl\_start}, \; j \in NBS_G, \; j \neq g \tag{5.23}$$

$$w^t_{i2} \cdot P_{i\max} / Rr_i \le t - t^t_{i1} - t^t_{i3} \le w^t_{i1} \cdot P_{i\max} / Rr_i, t = 1, 2, ..., T_{bl\_start}, \; i \in ALL, i \neq g \tag{5.24}$$

$$t^t_{l3} \le w^t_{l2} \left(T - T_{lctp} - P_{l\max} / Rr_l \right), \quad t = 1, 2, ...T_{bl\_start}, \; l \in BS_G \tag{5.25}$$

$$\begin{aligned} &t^t_{j3} \le \sum_{t=1}^{T_{bl\_start}} u_{jt} - \left(T_{jctp} + P_{j\max} / Rr_j + 1 \right) w^t_{j2} \\ &, \quad t = 1, 2, ..., T_{bl\_start}, \; j \in NBS_G, \; j \neq g \end{aligned} \tag{5.26}$$

$$t_{j3}^{t} \le w_{j2}^{t} T_{bl\_start}\ ,\quad t = 1,2,...,T_{bl\_start},\ j \in NBS_G,\ j \ne g \tag{5.27}$$

$$w_{j3}^{t} T_{bl\_start} - \sum_{t=1}^{T_{bl\_start}} u_{jt} \le t_{j4}^{t} \le t_{jstart} - 1,\quad t = 1,2,...,T_{bl\_start},\ j \in NBS_G,\ j \ne g \tag{5.28}$$

$$t_{j4}^{t} \ge 0,\quad t = 1,2,...,T_{bl\_start},\ j \in NBS_G,\ j \ne g \tag{5.29}$$

$$w_{j3}^{t} \le t - t_{j4}^{t} \le \sum_{t=1}^{T_{bl\_start}} u_{jt}\ , t = 1,2,...,T_{bl\_start},\ j \in NBS_G,\ j \ne g \tag{5.30}$$

$$t - t_{j4}^{t} \le w_{j3}^{t} T_{bl\_start}\ ,\quad t = 1,2,...,T_{bl\_start},\ j \in NBS_G,\ j \ne g \tag{5.31}$$

$$w_{jh}^{t} \le w_{jh}^{t+1}\ , h = 1,2,3, t = 1,2,...,T_{bl\_start} - 1,\ j \in NBS_G,\ j \ne g \tag{5.32}$$

$$w_{i2}^{t} \le w_{i1}^{t}\ ,\quad t = 1,2,...,T_{bl\_start}, i \in ALL, i \ne g \tag{5.33}$$

$$t_{j1}^{t} \le t_{j1}^{t+1}\ ,\quad t = 1,2,...,T_{bl\_start} - 1,\ j \in NBS_G,\ j \ne g \tag{5.34}$$

$$t_{j3}^{t} \le t_{j3}^{t+1}\ ,\quad t = 1,2,...,T_{bl\_start} - 1,\ j \in NBS_G,\ j \ne g \tag{5.35}$$

where, *ALL* is the set including all generating units; P_{imax} is the maximum power capacity of the generating unit *i*; P_{jstart} is the cranking power needed by the generating unit *j*; t_{jstart} is the start-up time of the unit *j* (it is assumed to be zero for all B-S units); T_{jcmax} and T_{jcmin} are the critical maximum and minimum start-up time for the unit *j*; Rr_i is the ramp rate of the unit *i*; T_{bl_start} is the entire time duration of the B-S process; T_{lctp} is the cranking time for the unit *l*. The definition of t_{j1}^{t}, t_{j3}^{t}, t_{j4}^{t}, w_{j1}^{t}, w_{j2}^{t}, w_{j3}^{t}, u_{it} is illustrated in Figure 5.2 [117], where the generator output P_{gen} (left) and the cranking power P_{start} (right) during the start-up process are depicted.

The objective (5.17) aims at maximizing the total generation capacity during the B-S process. Note that the generation capacity of the B-S unit within T_{bl_start} is constant,

while the generation capacity of the NB-S unit can be expressed as the difference of the shaded area in the left and right charts in Fig.1, which is $S_{deqh}–S_{suzw}=S_{dkh}+S_{deqk}–S_{suzw}=S_{dkh}+S_{aeqf}–S_{bdkg}– S_{abgf}–(S_{ruzv}–S_{rswv})$. Since some of these areas are constant and independent of t_{jstart}, maximizing the area of $S_{deqh}–S_{suzw}$ can be transformed to minimizing the area of $S_{abgf}–S_{rswv}$, which leads to (5.17).

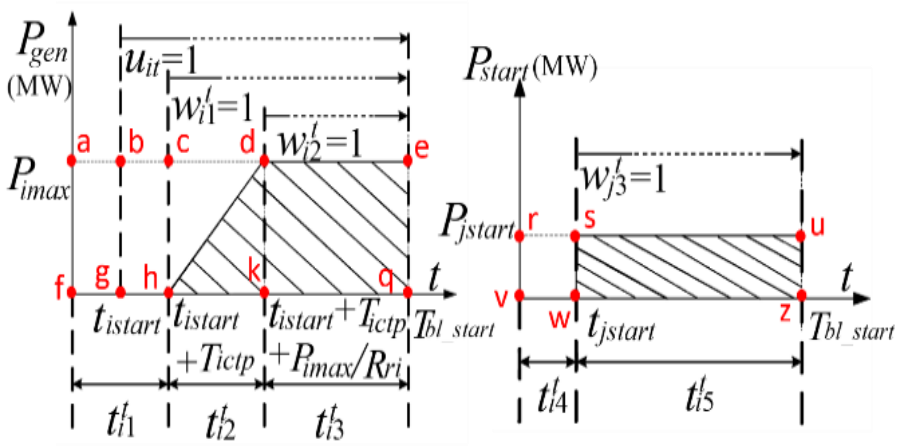

Figure 5.2: Illustration on the definition of some variables in the equation set (5.17) to (5.35) [117]

Equations (5.18) and (5.19) limit the start-up time of each NB-S units within their critical maximum and minimum start-up time accordingly; (5.20) formulates the power requirement during the B-S process, which implies that the power generated should be

greater than or equal to the total cranking power needed at each time moment; the boundaries of the time variable t^t_{i1} is set in (5.21) to (5.23), and also correlated with the status variable w^t_{i1}, which indicates that w^t_{i1} becomes 1 after T_{lctp} (for B-S units) or $t_{jstart}+T_{lctp}$ (for NB-S units); equation (5.24) set the boundary of the time duration $t^t_{i2}=t-t^t_{i1}-t^t_{i3}$ and its correlation with the status variables w^t_{i1} and w^t_{i2}, which denotes that t^t_{i2} should be 0 before w^t_{i1} becomes 1 and reaches it maximum after w^t_{i2} gets to 1; the boundary of the time variable t^t_{i3} and its correlation with the status variable w^t_{i2} is formulated from (5.25) to (5.27), indicating that w^t_{i2} becomes 1 and t^t_{i3} starts to be non-zero after the unit reaches its maximum generation capacity; the limitation and correlation between t^t_{j4} with w^t_{j3} for NB-S units are modeled in (5.28) and (5.29), , reflecting that t^t_{j4} reaches its maximum after w^t_{j3} turns to 1; (5.30) and (5.31) describe the correlation between the time $t^t_{j5}=t-t^t_{j4}$ and the status variable w^t_{j3}, indicating that t^t_{j5} will be non-zero after w^t_{j3} turns to 1, and should be within T_{bl_start}; and (5.32) to (5.35) constrain the status variables according to the operation status.

Finally, with the start-up time of each NB-S unit calculated, the energy to be picked up during the B-S process with no participation of the NB-S unit g is calculated in (5.36).

$$E^g_{bl-start}=\left\{\begin{array}{l}\sum\limits_{i\in ALL,i\neq g}\left[\left(P_{i\max}\right)^2/2Rr_i+P_{i\max}\left(T-T_{ictp}-P_{i\max}/Rr_i\right)\right]\\ -\sum\limits_{\substack{j\in NBS_G,\\ j\neq g}}P_{jstart}T_{bl\_start}-\left(\sum\limits_{i\in ALL,i\neq g}P_{i\max}t_{istart}-\sum\limits_{j\in NBS_G,j\neq g}P_{j\max}t_{jstart}\right)\end{array}\right\} \quad (5.36)$$

5.2.4 Optimal Allocation of Fixed BES and PV Generation

Improving the capacity accessibility for both the electricity demand and the NB-S units can improve the capacity adequacy during the extreme events, which is one of the many factors that contribute to the system resilience, resulting in more accessible capacities to deal with the unexpected situations. Improving the capacity accessibility during the planning of the allocation of the fixed BES and the PV generation can help enhance the system resilience.

5.2.4.1 Objectives

To improve our proposed accessibility for both demand and NB-S units while taking into account other important planning factors, multi-objective optimization is adopted to simultaneously consider: 1) the investment and operational cost; 2) capacity accessibility for the electricity demand; 3) capacity accessibility for the NB-S units; and 4) other factors.

Our aim is to determine the optimal power and energy capacity of the fixed BES together with the optimal power capacity of the PV generation at each bus, denoted as B_{pow}, B_{en}, and B_{pv}, respectively. During our planning, it is assumed that both the conventional generators and the fixed BES are enabled to participate in the ramp market, introduced in Section 4.2.

The first objective is formulated in (5.37), which includes both the investment cost on the fixed BES devices and PV generation, and the operational cost of the system. The stochastic optimization technique is adopted to consider the uncertainties of PV generation

intermittency, where various scenarios regarding to different PV generation patterns and load profiles are considered (characterized by the uncertainty set Ω and the probability P^j_{rob} of each scenario in Ω).

$$\text{obj1.}\quad Min\ \sum_{k\in K}\left[f_{cr}C^{energy}_{B\_in}B^k_{en} + f_{cr}C^{power}_{B\_in}B^k_{pow} + f_{cr}C_{pv\_in}B^k_{pv}\right] + \sum_{j\in\Omega}P^j_{rob}\sum_{t=t_0}^{t_n}\left\{\begin{array}{l}\sum_{i\in G}\left(C_{Gi}p^j_{Gi,t} + C_{FRUi}FRU^j_{i,t} + C_{FRDi}FRD^j_{i,t}\right)\\ +\sum_{k\in K}\left[\begin{array}{l}C_{BG,k}p^j_{Bdis,kt} + C_{BFRU,k}FRU^j_{B,kt}\\ +C_{BFRD,k}FRD^j_{B,kt} + \xi_{B,k}\left(p^j_{Bdis,kt} + p^j_{Bch,kt}\right)\end{array}\right]\end{array}\right\} \tag{5.37}$$

$$f_{cr} = r(1+r)^{L_p}\Big/\left[(1+r)^{L_p}-1\right] \tag{5.38}$$

where G is the generator set including all the conventional generating units; f_{cr} is the capital recovery factor, calculated in (5.38), which is utilized to converts the total investment into a stream of annual payments; L_p is the longevity of how long the capital can last; $C^{energy}_{B\_in}$, $C^{power}_{B\_in}$, and C_{pv_in} are the unit capacity investment cost of the battery energy, battery power and PV generation power, respectively; t_0 and t_n are the starting and ending time moment of the simulation; C_{Gi}, C_{FRUi}, C_{FRDi} are the marginal cost for generating unit i to provide energy service, ramp-up and ramp-down service, respectively (The marginal cost of PV generation is assumed to be very low, and here we assume it to be 0.); $p^j_{Gi,t}$, $FRU^j_{i,t}$, $FRD^j_{i,t}$ are the power generation, ramp-up and ramp down services of unit i at time t in scenario j; $C_{BG,k}$, $C_{BFRU,k}$, $C_{BFRD,k}$ are cost of the fixed BES at bus k for providing the energy service, ramp-up and ramp-down service; $p^j_{Bdis,kt}$, $p^j_{Bch,kt}$ are the discharging and charging power of the fixed BES at bus k and time t in scenario j; $FRU^j_{B,kt}$, $FRD^j_{B,kt}$ are the ramp-up

and ramp-down service provided by the fixed BES at bus *k* and time *t* in scenario *j*; $\xi_{B,k}$ is the coefficient for modeling the battery degradation cost.

The second objective, presented in (5.39), models the impact of the placement of the fixed BES and PV on the system-wide capacity accessibility to the electricity demand.

$$\text{obj}2.\quad \max \quad \text{PCA\_load}^{s} \times T_{lasting} + \sum_{j \in \Omega} P_{rob}^{j} \times \text{ECA\_load}^{s,j} \tag{5.39}$$

where the contribution of the conventional generating units are neglected, since our focus is on the allocation of the fixed BES and the PV generation; the coefficient $T_{lasting}$ is added here to combine the PCA_load and ECA_load together, which denotes approximately how long the power form the fixed BES and PV generation can last, and therefore converts the power into energy.

Similarly, the third objective is defined in (5.40) to reflect the contribution of the fixed BES and the PV generation on the system-wide capacity accessibility for the NB-S generating units.

$$\text{obj}3.\quad \max \quad \text{PCA\_Gen}^{s} \times T_{lasting} + \sum_{j \in \Omega} P_{rob}^{j} \times \text{ECA\_Gen}^{s,j} \tag{5.40}$$

The fourth objective, as presented in (5.41), targets at improving the system reliability and represents the extensibility of modeling and incorporating additional factors in such a planning study. The expected energy not supplied (EENS), as an example, is selected here to reflect the system reliability performance.

$$\text{obj}4.\quad \min \quad \text{EENS} = \sum_{z \in \Lambda} \sum_{k \in K} \left(IL_{k}^{z} \cdot \tau^{z} \cdot P_{rob}^{z} \right) \tag{5.41}$$

where IL_k^z is the interrupted load at bus k in contingency z; P^z_{rob} denotes the occurrence probability of the contingency z; Λ is the set of all contingencies; τ^z is the time duration of contingency z. The model is generic and this objective can be also adjusted to consider other factors such as risk, congestion management, etc. [118, 119].

5.2.4.2 Constraints

The constraints of this optimization problem are modeled as follows from (5.42) to (5.65).

$$0 \le p^j_{Bdis,kt} \le x^j_{Bdis,kt} B^k_{pow}, \quad j \in \Omega, k \in K, t = t_0, t_1, ..., t_n \tag{5.42}$$

$$0 \le p^j_{Bch,kt} \le x^j_{Bch,kt} B^k_{pow}, \quad j \in \Omega, k \in K, t = t_0, t_1, ..., t_n \tag{5.43}$$

$$x^j_{Bdis,kt} + x^j_{Bch,kt} \le 1, \quad j \in \Omega, k \in K, t = t_0, t_1, ..., t_n \tag{5.44}$$

$$x^j_{Bdis,kt}, x^j_{Bch,kt} = 0 \text{ or } 1, \quad j \in \Omega, k \in K, t = t_0, t_1, ..., t_n \tag{5.45}$$

$$0 \le p^j_{pv,kt} \le B^k_{pv} \alpha^j_{pv,kt}, \quad j \in \Omega, k \in K, t = t_0, t_1, ..., t_n \tag{5.46}$$

$$\sum_{i \in \{G\}} p^j_{Gi,t} + \sum_{k \in \{K\}} \left(p^j_{Bdis,kt} + p^j_{pv,kt} \right) = \sum_{k \in \{K\}} p^j_{Bch,kt} + \sum_{l \in \{L\}} D^j_{l,t}, \quad j \in \Omega, t = t_0, t_1, ..., t_n \tag{5.47}$$

$$B^k_{pow} \le B^k_{en} \beta, \quad k \in K \tag{5.48}$$

$$p^{\min}_{Gi} \le p^j_{Gi,t} \le p^{\max}_{Gi}, \quad j \in \Omega, k \in K, t = t_0, t_1, ..., t_n \tag{5.49}$$

$$0 \le FRU^j_{i,t} \le Rr_i \cdot \Delta t, \quad j \in \Omega, k \in K, t = t_0, t_1, ..., t_n \tag{5.50}$$

$$0 \le FRD^j_{i,t} \le Rr_i \cdot \Delta t, \quad j \in \Omega, k \in K, t = t_0, t_1, ..., t_n \tag{5.51}$$

$$p^j_{Gi,t} + FRU^j_{i,t} \le p^{\max}_{Gi}, \quad j \in \Omega, k \in K, t = t_0, t_1, ..., t_n \tag{5.52}$$

$$p_{Gi,t}^{j} - FRD_{i,t}^{j} \geq p_{Gi}^{\min}, \quad j \in \Omega, k \in K, t = t_0, t_1, ..., t_n \tag{5.53}$$

$$p_{Gi,t}^{j} - p_{Gi,t-1}^{j} \leq Rr_i \cdot \Delta t, \quad j \in \Omega, k \in K, t = t_0, t_1, ..., t_n \tag{5.54}$$

$$p_{Gi,t-1}^{j} - p_{Gi,t}^{j} \leq Rr_i \cdot \Delta t, \quad j \in \Omega, k \in K, t = t_0, t_1, ..., t_n \tag{5.55}$$

$$\sum_{i \in G} FRU_{i,t}^{j} + \sum_{k \in K} FRU_{B,kt}^{j} \geq D_{FRU,t}^{j}, \quad j \in \Omega, \ t = t_0, t_1, ..., t_n \tag{5.56}$$

$$\sum_{i \in G} FRD_{i,t}^{j} + \sum_{k \in K} FRD_{B,kt}^{j} \geq D_{FRD,t}^{j}, \quad j \in \Omega, \ t = t_0, t_1, ..., t_n \tag{5.57}$$

$$S_{k,t-1}^{j} - S_{k,t}^{j} = \left(p_{Bdis,kt}^{j} / \eta^{+} - \eta^{-} p_{Bch,kt}^{j} \right) \cdot \Delta t, \ j \in \Omega, k \in K, t = t_0, t_1, ..., t_n \tag{5.58}$$

$$S_k^j \Big|_{t=t_n} \geq S_{0,k}^{j} B_{en}^{k}, \quad j \in \Omega, k \in K \tag{5.59}$$

$$S_k^{\min} B_{en}^{k} \leq S_{k,t}^{j} \leq S_k^{\max} B_{en}^{k}, \quad j \in \Omega, k \in K, t = t_0, t_1, ..., t_n \tag{5.60}$$

$$p_{Bdis.kt}^{j} - p_{Bch,kt}^{j} + FRU_{B,kt}^{j} \leq B_{pow}^{k}, \ j \in \Omega, k \in K, t = t_0, t_1, ..., t_n \tag{5.61}$$

$$p_{Bdis.kt}^{j} - p_{Bch,kt}^{j} - FRD_{B,kt}^{j} \geq -B_{pow}^{k}, \ j \in \Omega, k \in K, t = t_0, t_1, ..., t_n \tag{5.62}$$

$$0 \leq FRU_{B,kt}^{j} \leq B_{pow}^{k}, \quad j \in \Omega, k \in K, t = t_0, t_1, ..., t_n \tag{5.63}$$

$$0 \leq FRD_{B,kt}^{j} \leq B_{pow}^{k}, \quad j \in \Omega, k \in K, t = t_0, t_1, ..., t_n \tag{5.64}$$

$$\mathbf{F}_{\min} \leq \mathbf{F}_t^j = \mathbf{HP} \leq \mathbf{F}_{\max}, \quad j \in \Omega, t = t_0, t_1, ..., t_n \tag{5.65}$$

where the status variables $x^j_{Bdis,kt}$ and $x^j_{Bch,kt}$ denote whether the fixed BES on bus k at time t is discharging/charging in scenario j; $D^j_{l,t}$ is the electricity demand at bus l and time t in scenario j; $p^j_{pv,kt}$ is the PV power at bus k and time t in scenario j; $\alpha^j_{pv,kt}$ is the PV prediction coefficient, i.e. the percentage of the maximum output, at bus k and time t in scenario j; p_{Gi}^{min} and p_{Gi}^{max} are the minimum and maximum power of the generating unit i; Δt is the

unit time interval; $D^j_{FRU,t}$ and $D^j_{FRD,t}$ are the system requirement for ramp-up and ramp-down services at time t in scenario j; η^+ and η^- are the discharging and charging efficiencies respectively; $S^j_{0,k}$ is the initial SOC of the fixed BES at bus k in scenario j; S_k^{min} and S_k^{max} are the minimum and maximum allowed SOC of the fixed BES at bus k; $\mathbf{F}_t^j$ is the vector of the line flow on different transmission lines at time t in scenario j; $\mathbf{F}_{\min}$ and $\mathbf{F}_{\max}$ are the vectors of the minimum and maximum transmission line capacity of different transmission lines.

Equations (5.42) to (5.45) constrain the fixed BES from simultaneously charging and discharging; equations (5.46) and (5.47) model the power balance considering the potential curtailment of the PV generation; the coefficient β in (5.48) sets the limitation between the power capacity and energy capacity of the fixed BES, and makes sure that the battery power can last for a period of time; the constraints on the operation of the conventional generators are set in (5.49) to (5.55): (5.49) regulates the unit generation within its upper and lower limits; (5.50) and (5.51) set limits on the ramp service provided by the unit; (5.52) and (5.53) constrain the sum of the generation and the ramp service within the generation capacity limits; (5.54) and (5.55) models the ramping limits. Equations (5.56) and (5.57) formulate the system requirement for the ramp-up and ramp-down services at each time step; the battery dynamic equation is presented in (5.58); the limitation on the energy requirement of the fixed BES is set in (5.59); equation (5.60) set the constraints on the battery energy at each time step; equations (5.61) to (5.64) formulate the battery operational limitation: (5.61) and (5.62) set the charging/discharging power of the battery storage as well as its ramp service within its charging/discharging limits; (5.63)

and (5.64) regulate the battery ramp service within its capacity limits. And equation set (5.65) formulates the power flow and the constraints on the transmission line flow. The extended distribution factor matrix **H** models the relationship between the branch flow and nodal power injections. It can include not only the regular transmission constraints but also N-1 contingencies and security constraints.

5.2.4.3 Consideration on the Unknowable Nature of the Extreme Event

In this proposed multi-objective optimization placement scheme, the demand reachability ($Reach^{k,s}_{load}$) and generating unit reachability ($Reach^{k,s}_{gen}$) of each bus, especially the sequences of $Reach^{k,s}_{load}$ and $Reach^{k,s}_{gen}$ on each bus, are playing an important role in maximizing the second and third objectives regarding to the capacity accessibility. That is because larger capacity accessibility can be achieved if the same amount of capacity is placed on the bus with higher $Reach^{k,s}_{load}$ or $Reach^{k,s}_{gen}$. However, the demand and generating unit reachability and the corresponding sequence of the buses are changing with the different severity levels of the extreme events, and thus leading to different allocation schemes accordingly.

Due to the unknowable nature of the extreme event, it is almost impossible to predict the severity level and the occurrence probability of the extreme event. In order to tackle that, the idea is to first calculate the optimal sizing and siting scheme under different severity levels, and then average them to obtain the final placement scheme. The detailed steps are: (1) calculate $Reach^{k,s}_{load}$ and $Reach^{k,s}_{gen}$ of each bus under extreme events of different severity levels, which can be simulated by altering $A_{event,s}$ within a certain range;

(2) obtain the optimal sizing and siting scheme under each set of $Reach^{k,s}_{load}$ and $Reach^{k,s}_{gen}$; (3) average the attained optimal schemes to find the final placement scheme, as in (5.66).

$$\overline{B^{k}_{en/\,pow/\,pv}} = \frac{\sum_{s\in S} B^{k}_{en/\,pow/\,pv}\left(A_{event,s}\right)}{N_S} \tag{5.66}$$

where the set S includes different levels of extreme event; N_S is number of severity levels that is considered in the set S; $B^{k}_{en/pow/pv}(A_{event,s})$ is the allocation scheme (battery energy, battery power or PV generation, respectively) at bus k under the extreme event of a particular severity level $A_{event,s}$; and $\overline{B^{k}_{en/\,pow/\,pv}}$ is the final optimal allocation scheme (battery energy, battery power or PV generation, respectively) at bus k.

5.3 Numerical Experiments and Analysis

We conduct the simulation on a modified IEEE-RTS 24-bus test system to validate the effectiveness of our proposed optimal sizing and siting scheme. The detailed configuration of the test system can be found in [99]. Besides, the load profile is obtained from [100], and the solar data are collected from [82].

5.3.1 Prioritizing the NB-S Generating Units

We assume that the hydro units, which are located on the bus 22, are B-S units during the B-S process; and the rest of the units are assumed to be NB-S generating units. The start-up parameters of all units are tabulated in Table 5.1.

Figure 5.3 illustrates the starting time of each NB-S generating unit under the scenario that all the units participate in the B-S process. Besides, the figure also shows the

priority of each NB-S unit, calculated using (5.16). It can be observed from this figure that the priority of the NB-S units depends on several factors other than the power capacity of the generating units, including: 1) starting time of the unit: early start-up of the unit leads to higher priority (No. 21 vs. 22); 2) the value of T_{ctp}: larger T_{ctp} results in lower priority (No.1, 2 vs. No. 5, 6, and No. 3, 4 vs. No. 7, 8); 3) the value of P_{start}: larger P_{start} causes lower priority; and 4) ramp rate: higher ramp rate brings about higher priority. The reason for 3) and 4) is that the NB-S unit with lower P_{start} and higher ramp rate tends to start up earlier, with the constraints on T_{cmin} and T_{cmax} satisfied.

Table 5.1: Start-up Parameters of Different Units

Gen ID	Bus ID	Unit Type	Tctp (hr)	Tcmin (hr)	Tcmax (hr)	Rr (MW/min)	Pstart (MW)
1, 2	1	U20	0	0:15	N/A	3	0
3, 4	1	U76	0	0:15	N/A	2	0
5, 6	2	U20	0:30	0	4:00	3	0.7
7, 8	2	U76	0:30	0	4:00	2	2.6
9-11	7	U100	2:00	0	3:30	7	3
12-14	13	U197	2:40	0:20	N/A	3	0.9
15	14	SC*	2:40	0:20	N/A	30	9
16-20	15	U12	2:00	0	N/A	1	0.7
21	15	U155	2:00	0	N/A	3	9
22	16	U155	1:40	0	N/A	3	3.1
23	18	U400	0:30	0	N/A	20	8
24	21	U400	0:30	0	N/A	20	8.8
25-30	22	U50	0	0	N/A	5	0
31-32	23	U155	1:40	0	2:50	3	3.1
33	23	U350	1:40	0	2:50	4	7

* Synchronous Condenser

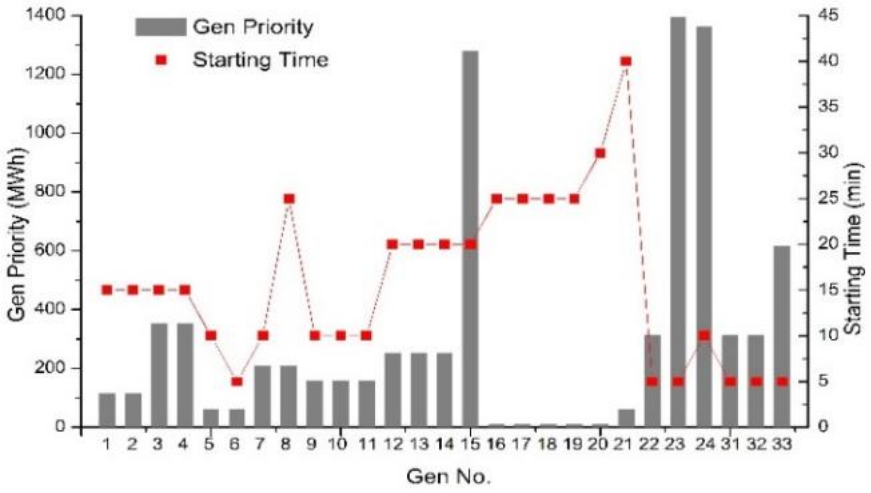

Figure 5.3: Illustration on the priority and starting time of each unit

5.3.2 Calculation on the Demand Reachability and Generating Unit Reachability

The demand reachability $Reach^{k}_{load}$ and generating unit reachability $Reach^{k}_{gen}$ of each bus under extreme events of different severity levels are calculated and depicted in Figure 5.4 and Figure 5.5, respectively. During the calculation, the load is prioritized based on their sizes, and the NB-S units are prioritized through (5.16) and calculated in Section 5.2.3. To illustrate the events of different levels (from light to extremely severe), $A_{event,s}$ is varied from 0.01 to 0.9, with the interval of 0.05. To simplify the problem, the adjusting coefficient ζ is assumed to be 1. One can easily observe that the reachability is decreasing with $A_{event,s}$ decreasing (extreme event more severe). And the reachability becomes 1 for all buses (no islands) when $A_{event,s}$ becomes larger than 0.9 (that is why the upper limit for $A_{event,s}$ is selected to be 0.9).

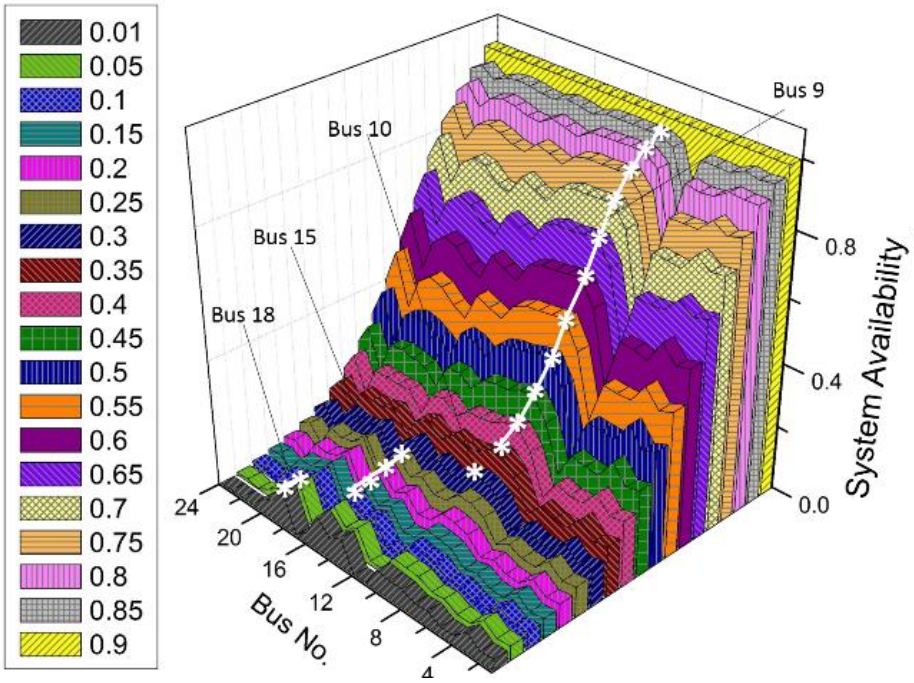

Figure 5.4: Illustration on the demand reachability $Reach^{k}_{load}$ of each bus under extreme events of different intensity levels

In Figure 5.4 and Figure 5.5, the white stars denote the bus with the highest reachability under each severity level, and the stars connected with white lines reflect that the highest reachability is achieved on the same bus. It can be observed in these two figures that the highest reachability might be achieved on different buses under extreme events of different severity levels. The extreme events of various levels need to be considered when determining the final sizing and siting scheme. Besides, the bus with the highest demand reachability $Reach^{k}_{load}$ may not be the one with the highest generating unit reachability $Reach^{k}_{gen}$, which confirms the necessity to adopt the multi-objective optimization

technique. The buses with the highest reachability levels remain the same when $A_{event,s}$ changes within a certain range, and therefore, the selection of the 0.05 interval for $A_{event,s}$ would not miss any important buses. The lower bound of $A_{event,s}$ is determined to be 0.01, as the important buses remain the same when $A_{event,s}$ is lower.

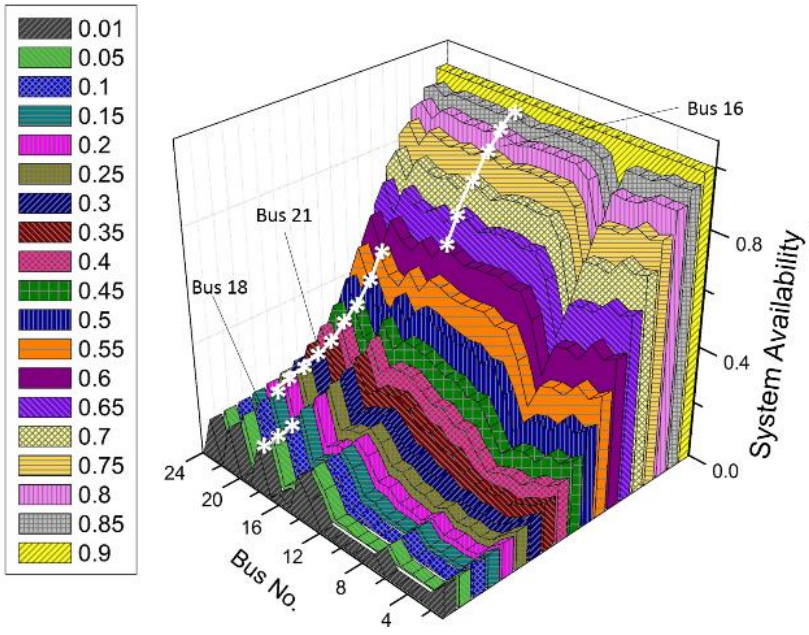

Figure 5.5: Illustration on the generating unit reachability $Reach^{k}_{gen}$ of each bus under extreme events of different intensity levels

5.3.3 Optimal Sizing and Siting of Fixed BES and PV Generation

To obtain the optimal sizing and siting scheme with the unknowable nature of the extreme event considered, the system available index $A_{event,s}$ is altered from 0.01 to 0.85, with 0.05 interval. The costs related to the generators are listed in Table 5.2, in which the generation cost is calculated from [99]. r and L_p in (5.38) are assumed to be 0.25 and 10, respectively. C_{BG} is selected to be 50; C_{BFRU} and C_{BFRD} are considered to be 5.44 [120]. $C^{energy}_{B\_in}$, $C^{power}_{B\_in}$ and C_{pv_in} are calculated from [121]. The proposed formulation is a mixed integer linear optimization model and is solved by CPLEX V12.5 in MATLAB (R2011a) environment on an Intel i5 1.6-GHz processor (8 GB of memory), with the computation time of about 23 min per case. The scaling of the problem by increasing the number of buses of the system can cause a rapid increase in the computation burden. One of the methods to alleviate the burden is through parallel computing by optimizing the sizing and siting schemes under the extreme event of different levels simultaneously and then combining the obtained results together. As a simplified example, 18 different levels of extreme events are considered in our numerical example here. If we have 18 processors, the total computation time for one case can be reduced to around 23min/18≈1.28 min. While the reduction in the computational time may not be linear, it is a good chance that parallel computation will bring the processing speed significantly down.

The Pareto Front of the proposed scheme is depicted in Figure 5.6, which illustrates the trade-off between the economic cost and the resilience. The value of lost load is assumed to be $3500/MWh [93], and is utilized to convert the second and third resilience-oriented objectives into monetary values. Besides, these two objectives are transformed

into minimization problems through their additive inverse, and therefore in negative numbers in Figure 5.6.

Table 5.2 List of Generation Cost and Ramp Cost

Unit Type	CG ($/MWh)	CFRU, CFRD ($/MWh)
U12	85	15
U20	90	15
U50	7	20
U76	31	15
U100	75	15
U155	27	20
U197	70	17
U350	25	15
U400	15	16

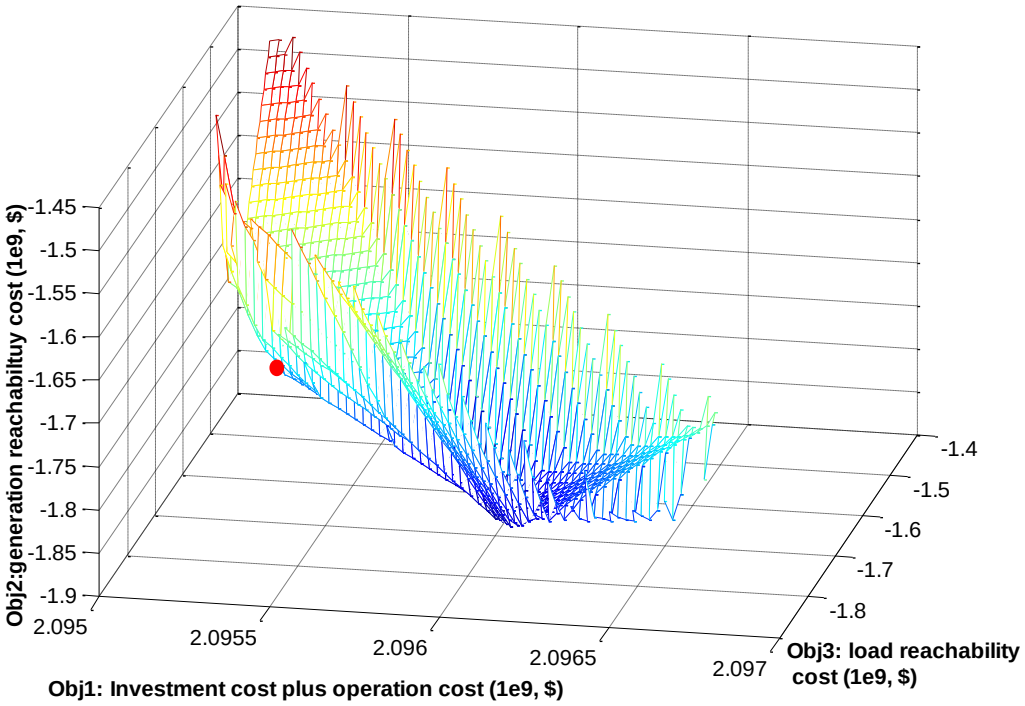

Figure 5.6: Illustration on the Pareto Front of the proposed scheme

To explore the relationship between the reliability and the capacity accessibility, we conduct the N-1 and N-2 reliability analysis (failure of any one or two elements in the system) on some of the optimal solutions in Figure 5.6. The index of Loss of Load Probability (LOLP) is utilized to evaluate the system reliability performance by reflecting the probability that the load interruption occurs in the system. It is calculated in (5.67), where Π is the set of single-order and second-order contingencies; y_z is a binary variable indicating whether the system experiences any load interruption (0: no load interruption; 1: load interruption); the contingency probability P^z_{rob} is calculated using the equipment failure probabilities.

$$\text{LOLP} = \sum_{z \in \Pi} y_z \cdot P_{rob}^z \tag{5.67}$$

Accordingly, Figure 5.7 shows the result of the LOLP indices as well as the system-wide capacity accessibility for both the electricity demand and the NB-S generating units (obj2 & obj3). The system LOLP is 0.82 in the base case without the installation of any fixed BES or PV generation. One can observe from Figure 5.7 that: 1) the integration of the fixed BES and the PV generation can help improve the system reliability, since the updated LOLP becomes lower than that of the base case; and 2) there is no distinct correlation between the LOLP and the capacity accessibility, which shows that: a) the proposed concept of capacity accessibility is different from the reliability; and b) the improvement on the reliability cannot guarantee the improvement on the capacity accessibility and system resilience, resulting in the necessity to additional consider the capacity accessibility during the planning study.

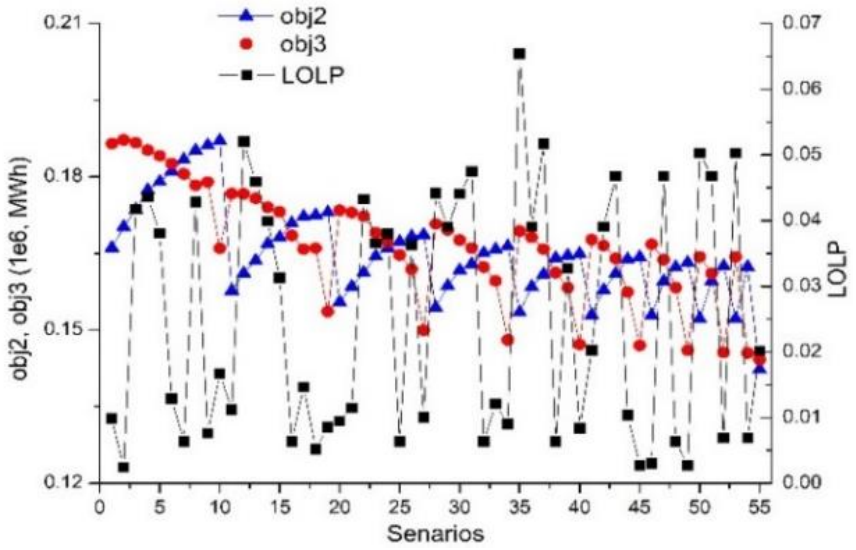

Figure 5.7 Illustration on the LOLP and the capacity accessibility

Figure 5.8 illustrates the detailed placement solution of the fixed BES and the PV generation on different buses for the result denoted in the red dot in Figure 5.6, together with the detailed allocation scheme for the conventional case that just consider the economic factors modeled in the first objective (5.37). It can be observed that the resources tend more to be placed on the buses with the highest $Reach^{k}_{load}$ or $Reach^{k}_{gen}$ under extreme events of different severity levels in the proposed scheme compared with that in the conventional placement case. Bus 11 is an exception, since the resource is placed on that bus in order to facilitate the operation at the same time.

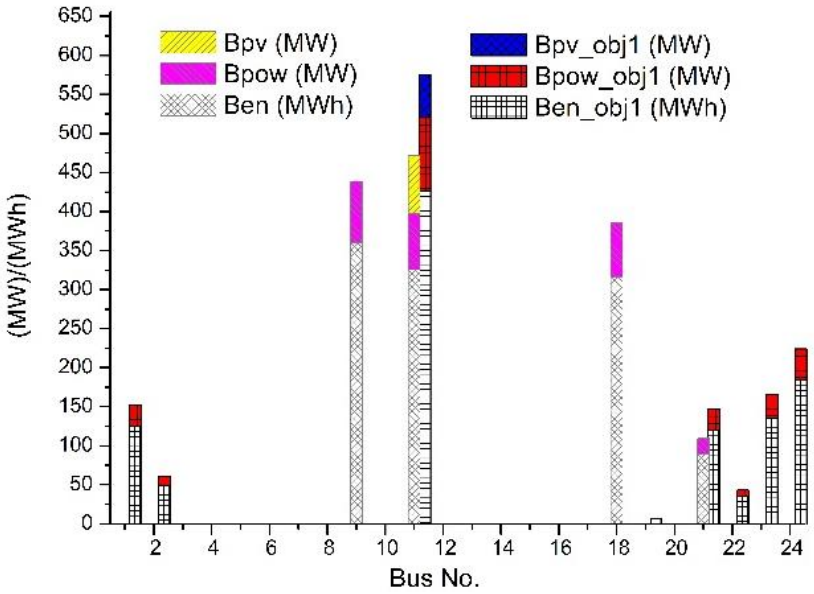

Figure 5.8: Illustration on the detailed placement solution

To further illustrate the impact of the sizing and siting of the fixed BES and the PV generation on the system resilience, especially on the load pick-up during the unexpected situation, several contingencies are simulated and the corresponding reaction of the system is studied. The detailed information of different contingencies is tabulated in Table 5.3 in the order from light to severe contingencies. The contingencies are assumed to occur on a certain day at hour 11 and last for 2 hours.

Table 5.3: List of the Studied Contingency Information

ID	Gen. in fault	Lines in fault	Gen. start-up
1	U23, U24	None	U13
2	U23, U24	None	None
3	U23, U24, U33	2, 3, 6	None
4	U23, U24, U33	2,3,6,10	None
5	U3, U4, U23, U24, U33	2, 3, 6, 10, 15, 16	None
6	U3, U4, U23, U24, U33	2,3,6,10,15,16,18,19,25,26,31	None

Figure 5.9 illustrates the ENS under different studied contingencies regarding to our proposed placement scheme as well as the situation with no fixed BES or PV generation. Meanwhile, Figure 5.10 illustrates the differences in ENS (compared with the ENS regarding to the proposed placement solution) under different studied contingencies regarding to other placement schemes. Also, the MAE of the differences in ENS under each contingency scenario is calculated and shown in the Figure 5.10. The placement case obj1 is the conventional case that just consider the economic factors modeled in the first objective alone (see Figure 5.8). The placement case *i* in Figure 5.10 denotes that the resources obtained by the proposed method are all placed on the bus *i*.

It can be observed from Figure 5.9 and Figure 5.10 that: 1) the installation of the fixed BES and the PV generation does help reducing the ENS during contingencies; 2) the proposed placement scheme gradually shows its obvious advantage over the other placement cases with the contingency becoming more extreme. The variations and the MAEs are increasing when the contingency is more severe.

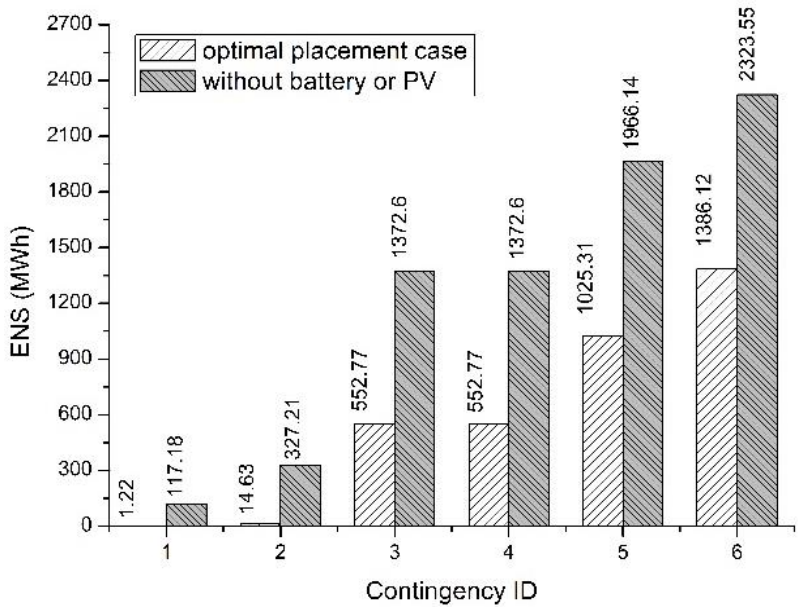

Figure 5.9: Illustration on the ENS under different contingencies

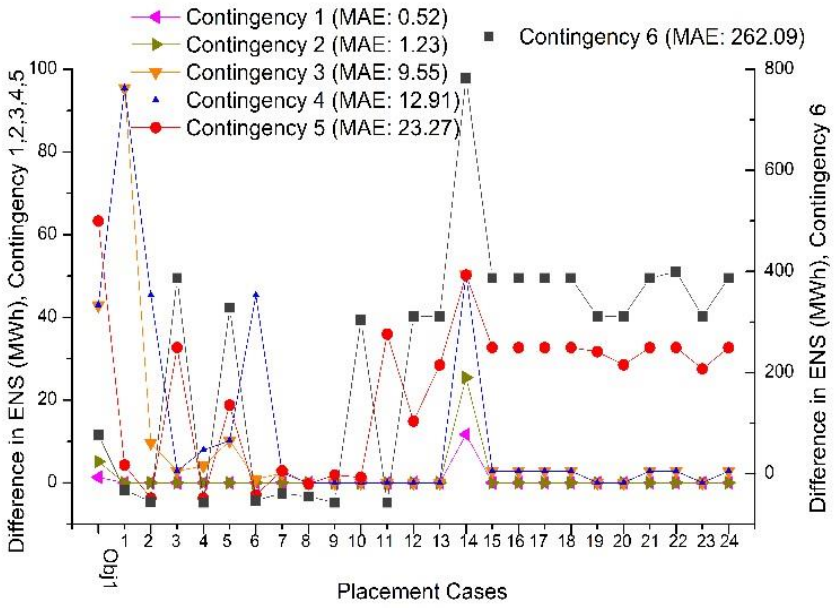

Figure 5.10: Differences in ENS under different placement cases

Table 5.4 lists the detailed results of the ENS of the conventional placement case depicted in Figure 5.8, and also the ENS without the PV generation (in the case of "No PV generation", the PV generation is removed from the proposed optimal placement scheme). The "Difference" in Table 5.4 is the difference compared to the ENS of the proposed placement scheme. The detailed results demonstrate that the PV generation, although not in a large scale compared to the installation of the fixed BES, is also playing an important role in mitigating the ENS during the contingencies, especially when the contingence tends to be more severe.

Table 5.4: List of the Detailed Difference in ENS

ID	Obj1		No PV generation	
	ENS(MWh)	Difference(MWh)	ENS(MWh)	Difference(MWh)
1	2.54	1.32	4.92	3.71
2	19.77	5.14	33.68	19.04
3	595.71	42.94	683.33	130.55
4	595.71	42.94	683.33	130.55
5	1088.62	63.31	1196.76	171.45
6	1463.37	77.26	1578.28	192.16

Last but not least, the impact of the placement of the fixed BES and the PV generation on another important aspect of the system resilience, which is the B-S process, is illustrated in Figure 5.11 in terms of the pick-up energy during the B-S process. It can

be observed that: 1) the installation of the fixed BES and the PV generation does help increase the pick-up energy during the B-S process (the pick-up energy is the least in the case of no PV or battery); 2) more energy can be restored in the proposed sizing and siting scheme than that of the conventional placement case, which just considers the cost in obj1; and 3) the pick-up energy of our proposed placement case is more than that of the most of the other placement cases, although it is not the highest.

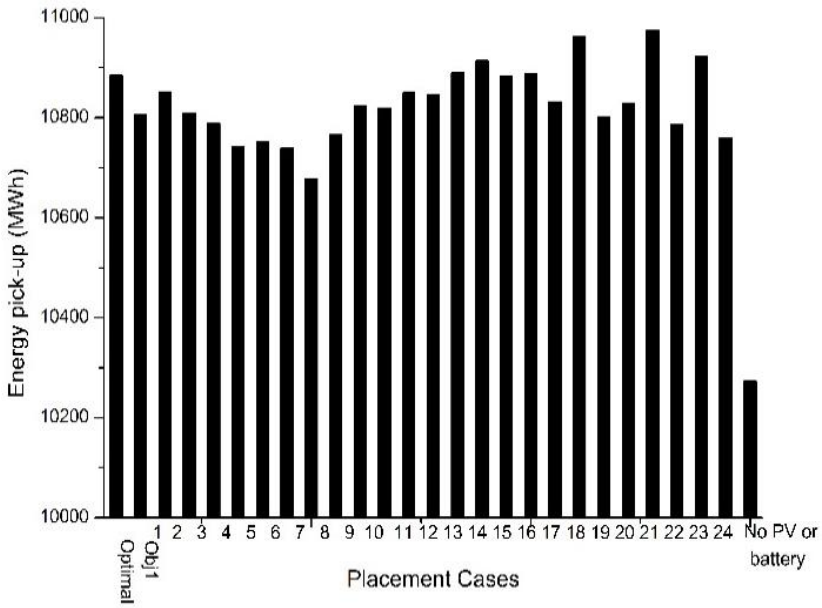

Figure 5.11: Illustration on the pick-up energy during the B-S process under different placement cases

5.4 Summary

This section addresses an optimal allocation scheme for the fixed BES and the PV generation aiming at enhancing the system resilience in face of the extreme events. The concept of capacity accessibility for both electricity demand and NB-S generating units is proposed to evaluate the reachability to the power and energy capacity during extreme events, taking into account the priority of the NB-S generators, characterized by their different importance during the B-S process. The unknowable nature of the extreme event is captured, and modeled through a multi-objective optimization problem to balance three main objectives: 1) the investment and operation costs; 2) the capacity accessibility for electricity demand; and 3) the capacity accessibility for NB-S generating units. The numerical experiments are conducted to verify the effectiveness of the proposed placement scheme. It is found in the numerical experiments that some buses are quite more critical than others, since resources placed on those buses can be more reachable by the loads or NB-S units during extreme events of different intensity levels. Following the proposed optimal sizing and siting scheme, the system has better performance in terms of load pick-up and the B-S process expedition during extreme events, compared with other placement schemes. The difference becomes more obvious when the contingency tends to be more extreme.

6. CONCLUSIONS*

The integration of the mobile (EV) BES, PV generation and fixed BES into the power gird is introducing new opportunities as well as new challenges. This dissertation presents a framework to not only utilize those opportunities but also carefully deal with some of the challenges, so as to enhance the system predictability, flexibility and resilience.

Firstly, in order to handle the new uncertainty caused by the widespread of EV BES and PV generation, forecast technologies based on the Markov model and GCRF method are introduced in Sections 2 and 3, respectively. The aggregated power capacity from EV BES is estimated in Section 2 in a probabilistic way considering several practical factors, such as mobility, drivers' behavior, battery degradation limit, etc. In the PV generation forecast in Section 3, both the temporal and spatial correlations are modeled. From the numerical experiments, one can observe that the uncertainties are better modeled in our

* This section is in part a reprint of the material in the following papers: (1) Reprinted with permission from B. Zhang, M. Kezunovic, "Impact of Available Electric Vehicle Battery Power Capacity on Power System Reliability," *IEEE Power and Energy Society General Meeting*, Vancouver, Canada, July, 2013. Copyright 2013, IEEE. (2) Reprinted with permission from B. Zhang, P. Dehghanian, M. Kezunovic, "Spatial-Temporal Solar Power Forecast through Use of Gaussian Conditional Random Fields," *IEEE Power and Energy Society General Meeting*, Boston, MA, July 2016. Copyright 2016, IEEE. (3) Reprinted with permission from B. Zhang, M. Kezunovic, "Impact on Power System Flexibility by Electric Vehicle Participation in Ramp Market," *IEEE Transactions on Smart Grid*, Vol. 7, No. 3, pp. 1285-1294, May 2016. Copyright 2016, IEEE. (4) Reprinted with permission from B. Zhang, P. Dehghanian, M. Kezunovic, "Optimal Allocation of PV Generation and Battery Storage for Enhanced Resilience", *IEEE Transactions on Smart Grid*, accepted. (5) Reprinted with permission from M. Kezunovic, Z. Obradovic, T. Dokic, B. Zhang, J. Stojanovic, P. Dehghanian, and P. -C. Chen, "Predicating Spatiotemporal Impacts of Weather on Power Systems using Big Data Science," Springer Verlag, Data Science and Big Data: An Environment of Computational Intelligence, Pedrycz, Witold, Chen, Shyi-Ming (Eds.), ISBN 978-3-319-53474-9, 2017.

proposed forecast methods, and thus leading to an improved system predictability, which can also benefit the system operation and planning.

Sections 4 and 5 mainly focus on utilizing the opportunities brought by the integration of the EV BES, PV generation and fixed BES. Considering their advantages and disadvantages (see Table 1.1), Section 4 proposes to integrate the EV and fixed BES into the ramp market, so that their fast ramping capability can get rewarded while their limitation on the energy capacity can be avoided to some extent. Besides, EV and fixed BES do not have to charge and discharge very frequently while providing the ramp service. By integrating the EV and fixed BES into the ramp market, the short term net-load uncertainty and variation can be better balanced, and therefore, the system operation flexibility is greatly enhanced.

Another opportunity arising from the integration of the fixed BES and the PV generation is their potential in the extreme events. Their being more scattered makes their energy more accessible during the extreme events. Section 5 aims at utilizing that opportunity to improve the system resilience. An optimal allocation scheme of the fixed BES and the PV generation is addressed in Section 5 taking into account the unknowable nature of the extreme event, so as to improve the capacity accessibility to both the electricity demand and NB-S generating units during the extreme event, as well as to facilitate the system operation.

6.1 Contribution

The main contributions of this Ph.D. research are summarized as follows:

1) Analytical estimation of the aggregated charging/discharging power capacity from EV BES is proposed by taking into account factors such as stochastic EV mobility and drivers' behavior, etc.;

2) Novel solar power generation forecast considering both the spatial and temporal correlations among different solar stations is developed by using the GCRF model;

3) Models to involve EV BES into the ramp market are proposed, for both the direct participation and cooperation with generators;

4) New indices are introduced to evaluate the power system flexibility under certain market clearing results;

5) The concept of capacity accessibility during the extreme event is proposed to help evaluate system resilience;

6) A sizing and siting scheme of the fixed BES and the PV generation, aiming at enhancing the system resilience, is proposed considering the unknowable nature of the extreme event.

6.2 Future Work

As to the estimation on the aggregated power capacity from EV BES, the future work lies in the more accurate estimation on EVs' availability, which is the first step to estimate the final aggregated power capacity. The improvement might be achieved by further considering the transition process as well as adopting a time-inhomogeneous Markov model.

For the PV generation forecast by GCRF model, the future work can be focused on: 1) further improvement on the modeling of the correlations: new graphs can be added to the current modeling to consider more factors and correlations, e.g., temperature, wind, etc.; 2) improvement on the modeling of the forecast error; 3) conduct more real-time forecast through the using of GCRF model when more real-time data becomes available; and 4) further verify the consistency of the results by adopting various techniques for forecast verification methods.

The possible extensions related to integrating EV and fixed BES into the ramp market would be: 1) improve the market model by integrating other ancillary services; 2) economically evaluate the cost of fixed BES and mobile (EV) BES to provide the ramp product; 3) study the incentive scheme for fixed BES and mobile (EV) BES to participate in the ramp market.

Last but not least, regarding to the optimal allocation of fixed BES and PV generation to improve the system resilience, future effort could be focused on: 1) further extension on the fourth objective, as shown in (5.41), to consider other issues in the planning; 2) the more detailed modeling on the trade-off between the economic cost and the system resilience; and 3) the reduction on the computational burden through parallel computing.

REFERENCES

[1] Solar Energy Industries Association, "U.S. Solar Market Insight", Sep. 12th, 2016. [Online]. Available: http://www.seia.org/research-resources/us-solar-market-insight. [Accessed: Sep. 29th, 2016].

[2] International Energy Agency, "Global EV Outlook2016", May, 2016. [Online]. Available: https://www.iea.org/publications/freepublications/publication/Global_EV_Outlook_2016.pdf. [Accessed: Sep. 29th, 2016].

[3] J. Fluhr, K. H. Ahlert, and C. Weinhardt, "A stochastic model for simulating the availability of electric vehicles for services to the power grid," in *Proc. IEEE Hawaii International Conference on System Science.*, pp. 1–10, Jan.5-8, 2010, Honolulu, Hawaii, USA.

[4] C. Sandels, U. Franke, N. Ingvar, L. Nordstrom, and R. Hamren "Vehicle to Grid: Monte Carlo simulations for optimal Aggregator strategies," in *2010 International Conference on Power System Technology (POWERCON),* pp. 1-8, Oct. 24-28, 2010, Zhengjiang, China.

[5] M. Guojian, Z. Xiangbo, and X. Zongchang, "Risk decision-making of vehicle availability based on fuzzy VPRS model," in *8th International Conference on Reliability, Maintainability and Safety, ICRMS*, pp. 164-166, Jul 20-24, Chengdu, China.

[6] J. Rolink, and C. Rehtanz, "Estimation of the availability of grid connected electric vehicles by non-homogeneous semi-Markov processes," in *2011 IEEE Trondheim, PowerTech*, pp. 1-7, Jun 19-23, 2011, Trondheim, Norway.

[7] U. C. Chukwu, and S. M. Mahajan, "V2G electric power capacity estimation and ancillary service market evaluation," in *2011 IEEE Power and Energy Society General Meeting*, pp. 1-8, Jul. 24-29, Detroit, Michigan, USA.

[8] H. Sekyung, H. Soohee, and K. Sezaki, "Estimation of achievable power capacity from plug-in electric vehicles for V2G frequency regulation: Case studies for market participation," *IEEE Trans. Smart Grid*, vol.2, no. 4, pp. 632–641, Dec. 2011.

[9] S. Jafarzadeh, M. S. Fadali, and C. Y. Evrenosoglu, "Solar power prediction using interval type-2 TSK modeling," *IEEE Trans. Sustainable Energy*, vol. 4, no. 2, pp. 333-339, Apr. 2013.

[10] E. Lorenz, J. Hurka, D. Heinemann, and H. G. Beyer, "Irradiance forecasting for the power prediction of grid-connected photovoltaic systems," *IEEE Journal of Selected Topics in Applied Earth Observations and Remote Sensing*, vol. 2, no. 1, pp. 2-10, Mar. 2009.

[11] W. Ji, and K. C. Chee, "Prediction of hourly solar radiation using a novel hybrid model of ARMA and TDNN," *Solar Energy*, vol. 85, no. 5, pp. 808-817, May. 2011.

[12] L. A. Fernandez-Jimenez, A. Muñoz-Jimenez, A. Falces, M. Mendoza-Villena, E. Garcia-Garrido, et al., "Short-term power forecasting system for photovoltaic plants," *Renewable Energy*, vol. 44, pp. 311-317, Aug. 2012.

[13] C. Yang, A. Thatte, and L. Xie, "Multitime-scale data-driven spatiotemporal forecast of photovoltaic generation," *IEEE Trans. Sustainable Energy*, vol. 6, no. 1, pp. 104-112, Jan. 2015.

[14] A. Sfetsos, and A. H. Coonick, "Univariate and multivariate forecasting of hourly solar radiation with artificial intelligence techniques," *Solar Energy*, vol. 68, no. 2, pp. 169-178, Feb. 2000.

[15] H. Long, Z. Zhang, and Y. Su, "Analysis of Daily Solar Power Prediction with Data-driven Approaches," *Applied Energy*, vol. 126, pp. 29-37, Aug. 2014.

[16] E. Izgi, A. Öztopal, B. Yerli, M. K. Kaymak, A. D. Dahin, "Short–mid-term solar power prediction by using artificial neural networks," *Solar Energy*, vol. 86, no. 2, pp. 725-733, Feb. 2012.

[17] J. Shi, W. J. Lee, Y. Liu, Y. Yang, and P. Wang, "Forecasting power output of photovoltaic systems based on weather classification and support vector machines," *IEEE Trans. Industry Applications*, vol. 48, no. 3, pp. 1064-1069, May. 2012.

[18] M. Lave, J. Kleissl, and J. S. Stein, "A wavelet-based variability model (WVM) for solar PV power plants," *IEEE Trans. Sustainable Energy*, vol. 4, no. 2, pp. 501-509, Apr. 2013.

[19] C. Yang, and L. Xie, "A novel ARX-based multi-scale spatio-temporal solar power forecast model," in *2012 North American Power Symposium*, pp. 1-8, Sep. 9–11, 2012, Urbana-Champaign, Illinois, USA.

[20] R. J. Bessa, A. Trindade, and V. Miranda, "Spatial-temporal solar power forecasting for smart Grids," *IEEE Trans. Industrial Informatics*, vol. 11, no. 1, pp. 232-241, Feb. 2015.

[21] C. Chen, S. Duan, T. Cai, and B. Liu, "Online 24-h solar power forecasting based on weather type classification using artificial neural network," *Solar Energy*, vol. 85, no. 11, pp. 2856-2870, Nov. 2011.

[22] H. T. Yang, C. M. Huang, Y. C. Huang, and Y. S. Pai, "A weather based hybrid method for 1-day ahead hourly forecasting of PV power output," *IEEE Trans. Sustainable Energy*, vol. 5, no. 3, pp. 917-926, Jul. 2014.

[23] G. Capizzi, C. Napoli, and F. Bonanno, "Innovative second-generation wavelets construction with recurrent neural networks for solar radiation forecasting," *IEEE Trans. Neural Networks and Learning Systems*, vol. 23, no. 11, pp. 1805-1815, Nov. 2012.

[24] C. Tao, D. Shanxu, and C. Changsong, "Forecasting power output for grid-connected photovoltaic power system without using solar radiation measurement," In *2010 2nd IEEE International Symposium on Power Electronics for Distributed Generation Systems (PEDG)*, pp. 773-777, Jun. 16-18, 2010, Hefei, China.

[25] P. Bacher, H. Madsen, and H. A. Nielsen, "Online short-term solar power forecasting," *Solar Energy*, vol. 83, no.10, pp.1772-1783, Oct. 2009.

[26] M. G. Kratzenberg, S. Colle, and H. G. Beyer, "Solar radiation prediction based on the combination of a numerical weather prediction model and a time series prediction

model," in *Proc. 1st International Congess Heat Cool Build*, pp. 1–12, Oct. 7–10, 2008, Lisbon, Portugal.

[27] M. F. Shaaban and E. F. El-Saadany, "Accommodating High Penetrations of PEVs and Renewable DG Considering Uncertainties in Distribution Systems," *IEEE Trans. Power Systems*, vol. 29, pp. 259-270, Jan. 2014.

[28] S. J. Gunter, K. K. Afridi, and D. J. Perreault, "Optimal Design of Grid-Connected PEV Charging Systems With Integrated Distributed Resources," *IEEE Trans. Smart Grid*, vol. 4, pp. 956-967, Jun. 2013.

[29] M. Lu, C. Chang, W. Lee, and L. Wang, "Combining the wind power generation system with energy storage equipment," *IEEE Trans. Industry Applications*, vol. 45, no. 6, pp. 2109–2115, Nov. 2009

[30] W. Su, J. Wang, and J. Roh, "Stochastic Energy Scheduling in Microgrids With Intermittent Renewable Energy Resources," *IEEE Trans. Smart Grid*, vol. 5, pp. 1876-1883, Jul. 2014.

[31] S. J. Gunter, K. K. Afridi, and D. J. Perreault, "Optimal Design of Grid-Connected PEV Charging Systems With Integrated Distributed Resources," *IEEE Trans. Smart Grid*, vol. 4, pp. 956-967, Jun. 2013.

[32] T. Zhang, W. Chen, Z. Han, and Z. Cao, "Charging Scheduling of Electric Vehicles With Local Renewable Energy Under Uncertain Electric Vehicle Arrival and Grid Power Price," *IEEE Trans. Vehicular Technology*, vol. 63, pp. 2600-2612, Jul. 2014.

[33] A. Y. Saber and G. K. Venayagamoorthy, "Efficient Utilization of Renewable Energy Sources by Gridable Vehicles in Cyber-Physical Energy Systems," *Systems Journal, IEEE,* vol. 4, pp. 285-294, Sep. 2010.

[34] A. Y. Saber and G. K. Venayagamoorthy, "Resource Scheduling Under Uncertainty in a Smart Grid With Renewables and Plug-in Vehicles," *Systems Journal, IEEE,* vol. 6, pp. 103-109, Mar. 2012.

[35] M. E. Khodayar, W. Lei, and M. Shahidehpour, "Hourly Coordination of Electric Vehicle Operation and Volatile Wind Power Generation in SCUC," *IEEE Trans. Smart Grid,* vol. 3, pp. 1271-1279, Sep. 2012.

[36] W. Su, J. Wang, and J. Roh, "Stochastic Energy Scheduling in Microgrids With Intermittent Renewable Energy Resources," *IEEE Trans. Smart Grid,* vol. 5, pp. 1876-1883, July. 2014.

[37] C. Goebel and D. S. Callaway, "Using ICT-Controlled Plug-in Electric Vehicles to Supply Grid Regulation in California at Different Renewable Integration Levels," *IEEE Trans. Smart Grid,* vol. 4, pp. 729-740, Jun. 2013.

[38] H. Sekyung, H. Soohee, and K. Sezaki, "Development of an Optimal Vehicle-to-Grid Aggregator for Frequency Regulation," *IEEE Trans. Smart Grid,* vol. 1, pp. 65-72, Jun. 2010.

[39] D. Dallinger, D. Krampe, and M. Wietschel, "Vehicle-to-Grid Regulation Reserves Based on a Dynamic Simulation of Mobility Behavior," *IEEE Trans. Smart Grid,* vol. 2, pp. 302-313, Jun. 2011.

[40] Y. Mu, J. Wu, J. Ekanayake, N. Jenkins, and H. Jia, "Primary Frequency Response From Electric Vehicles in the Great Britain Power System," *IEEE Trans. Smart Grid*, vol. 4, no.2, pp. 1142-1150, Jun. 2013.

[41] E. Sortomme and M. A. El-Sharkawi, "Optimal Charging Strategies for Unidirectional Vehicle-to-Grid," *IEEE Trans. Smart Grid*, vol. 2, pp. 131-138, Mar. 2011.

[42] N. Rotering and M. Ilic, "Optimal Charge Control of Plug-In Hybrid Electric Vehicles in Deregulated Electricity Markets," *IEEE Trans. Power Systems*, vol. 26, pp. 1021-1029, Aug. 2011.

[43] H. Sekyung, H. Soohee, and K. Sezaki, "Estimation of Achievable Power Capacity From Plug-in Electric Vehicles for V2G Frequency Regulation: Case Studies for Market Participation," *IEEE Trans. Smart Grid*, vol. 2, pp. 632-641, Aug. 2011.

[44] T. Masuta and A. Yokoyama, "Supplementary Load Frequency Control by Use of a Number of Both Electric Vehicles and Heat Pump Water Heaters," *IEEE Trans. Smart Grid*, vol. 3, pp. 1253-1262, Sep. 2012.

[45] A. Y. Saber and G. K. Venayagamoorthy, "Unit commitment with vehicle-to-Grid using particle swarm optimization," presented at *the 2009 IEEE Bucharest PowerTech*, pp. 1-8, Jun. 28 – Jul. 2, 2009, Bucharest, Romania.

[46] A. Y. Saber and G. K. Venayagamoorthy, "Intelligent unit commitment with vehicle-to-grid —A cost-emission optimization," *Journal of Power Sources*, vol. 195, pp. 898-911, Feb. 2010.

[47] R. J. Bessa, M. A. Matos, F. J. Soares, and J. A. P. Lopes, "Optimized Bidding of a EV Aggregation Agent in the Electricity Market," *IEEE Trans. Smart Grid*, vol. 3, pp. 443-452, Mar. 2012.

[48] M. A. Ortega-Vazquez, F. Bouffard, and V. Silva, "Electric Vehicle Aggregator/System Operator Coordination for Charging Scheduling and Services Procurement," *IEEE Trans. Power Systems*, vol. 28, pp. 1806-1815, May 2013.

[49] Y. Ota, H. Taniguchi, T. Nakajima, K. M. Liyanage, J. Baba, and A. Yokoyama, "Autonomous Distributed V2G (Vehicle-to-Grid) Satisfying Scheduled Charging," *IEEE Trans. Smart Grid*, vol. 3, pp. 559-564, Mar. 2012.

[50] E. Sortomme and M. A. El-Sharkawi, "Optimal Scheduling of Vehicle-to-Grid Energy and Ancillary Services," *IEEE Trans. Smart Grid*, vol. 3, pp. 351-359, Mar. 2012.

[51] R. J. Bessa and M. A. Matos, "Optimization Models for EV Aggregator Participation in a Manual Reserve Market," *IEEE Trans. Power Systems*, vol. 28, pp. 3085-3095, Aug. 2013.

[52] U. C. Chukwu and S. M. Mahajan, "V2G electric power capacity estimation and ancillary service market evaluation," in *2011 IEEE Power and Energy Society General Meeting*, pp.1-8, Jul 24-29, 2011, Detroit, Michigan, USA.

[53] E. Sortomme and M. A. El-Sharkawi, "Optimal Combined Bidding of Vehicle-to-Grid Ancillary Services," *IEEE Trans. Smart Grid*, vol. 3, pp. 70-79, Mar. 2012.

[54] C. Guille and G. Gross, "A conceptual framework for the vehicle-to-grid (V2G) implementation," *Energy Policy*, vol. 37, pp. 4379-4390, Nov. 2009.

[55] Y. Zheng, Z. Y. Dong, F. J. Luo, K. Meng, J. Qiu, and K. P. Wong, "Optimal allocation of energy storage system for risk mitigation of DISCOs with high renewable penetrations," *IEEE Trans. Power Systems*, vol.29, no.1, pp. 212-220, Jan. 2014.

[56] R. Ebrahimpourain, and M. Kazemi, "Multi-Objective Placement of Multiple Distributed Energy Resources in Distribution System Using Imperialist Competitive Algorithm (ICA)," *International Journal on Technical and Physical Problems of Engineering (IJTPE)*, issue. 18, vol. 6, no. 1, pp. 89-95, Mar. 2014.

[57] M. A. Darfoun, and M. E. El-Hawary, "Multi-objective optimization approach for optimal distributed generation sizing and placement*," Electric Power Components and Systems*, vol.43, no.7, pp. 828-836, Apr. 2015.

[58] G. Ribeiro, A. José, P. N. Luís, and A. Martins, "Multiobjective assessment of distributed energy storage location in electricity networks," *International Journal of Sustainable Energy*, DOI: 10.1080/14786451.2015.1066787.

[59] A. S. Awad, T. H. El-Fouly, and M. M. Salama, "Optimal ESS allocation and load shedding for improving distribution system reliability," *IEEE Trans. Smart Grid*, vol. 5, no. 5, pp. 2339-2349, Sep. 2014.

[60] C. Bussar, M. Moos, R. Alvarez, P. Wolf, T. Thien, et al., "Optimal allocation and capacity of energy storage systems in a future European power system with 100% renewable energy generation," *Energy Procedia*, vol. 46, pp. 40-47, 2014.

[61] R. Viveka, S. Kalyani, and P. M. Devie, "Optimal Planning of Energy Storage Systems in Transmission Networks using Evolutionary Algorithm," *International Journal*, vol. 3, no. 5, pp. 83-97, May. 2015.

[62] M. Ghofrani, A. Arabali, M. Etezadi-Amoli, and M. S. Fadali, "A framework for optimal placement of energy storage units within a power system with high wind penetration," *IEEE Trans. Sustainable Energy*, vol. 4, no. 2, pp. 434-442, Apr. 2013.

[63] M. Ghofrani, A. Arabali, M. Etezadi-Amoli, and M. S. Fadali, "Energy storage application for performance enhancement of wind integration," *IEEE Trans. Power Systems*, vol. 28, no. 4, pp. 4803-4811, Nov. 2013.

[64] L. Zheng, W. Hu, Q. Lu, and Y. Min, "Optimal energy storage system allocation and operation for improving wind power penetration," *IET Generation, Transmission & Distribution*, vol. 9, no. 16, pp. 2672-2678, Dec. 2015.

[65] C. Thrampoulidis, S. Bose, and B. Hassibi, "Optimal placement of distributed energy storage in power networks," *IEEE Trans. Automatic Control*, vol. 61, no. 2, pp. 416-429. Feb. 2016.

[66] H. Pandžić, Y. Wang, T. Qiu, Y. Dvorkin, and D. S. Kirschen, "Near-optimal method for siting and sizing of distributed storage in a transmission network," *IEEE Trans. Power Systems*, vol. 30, no. 5, pp. 2288-2300, Sep. 2015.

[67] S. Wogrin and D. F. Gayme, "Optimizing storage siting, sizing, and technology portfolios in transmission-constrained networks," *IEEE Trans. Power Systems*, vol. 30, no. 6, pp. 3304-3313. Nov. 2015.

[68] V. Krishnan and T. Das, "Optimal allocation of energy storage in a co-optimized electricity market: Benefits assessment and deriving indicators for economic storage ventures," *Energy*, vol. 81, pp. 175-188., Mar. 2015.

[69] M. Motalleb, E. Reihani, and R. Ghorbani, "Optimal placement and sizing of the storage supporting transmission and distribution networks," *Renewable Energy*, vol. 94, pp. 651-659, Aug. 2016.

[70] C. Velásquez, D. Watts, H. Rudnick, and C. Bustos, "A Framework for Transmission Expansion Planning: A Complex Problem Clouded by Uncertainty," *IEEE Power and Energy Magazine*, vol. 14, no. 4, pp. 20-29, Jul-Aug 2016.

[71] V. Radosavljevic, S. Vucetic, and Z. Obradovic, "Neural Gaussian Conditional Random Fields" In *Machine Learning and Knowledge Discovery in Databases*, Springer Berlin Heidelberg, pp.614-629, 2014.

[72] M. Panteli and P. Mancarella, "The grid: stronger, bigger, smarter?: Presenting a conceptual framework of power system resilience," *IEEE Power and Energy Magazine*, vol. 13, no. 3, pp. 58-66, May./Jun. 2015.

[73] M. Kezunovic, S. T. Waller, and I. Damnjanovic, "Framework for Studying Emerging Policy Issues Associated with PHEVs in Managing Coupled Power and Transportation Systems," in *IEEE Green Technologies Conference*, 2010, pp. 1-8, Apr. 15-16, 2010, Grapevine, Texas, USA.

[74] C. Pang, P. Dutta, and M. Kezunovic, "BEVs/PHEVs as Dispersed Energy Storage for V2B Uses in the Smart Grid," *IEEE Trans. Smart Grid*, vol. 3, no. 1, pp. 473-482, Mar. 2012.

[75] W. Kempton, and J. Tomić, "Vehicle-to-grid power fundamentals: Calculating capacity and net revenue," *Journal of Power Sources*, vol. 144, no. 1, pp. 268-279, Jun. 2005.

[76] L. Xia, and Y. Shao, "Modelling of traffic flow and air pollution emission with application to Hong Kong Island," *Environmental Modelling & Software*, vol. 20, no. 9, pp. 1175-1188, Sep. 2005.

[77] N. M. A.Santos, H. Y. Nakamoto, D. Gray, and S. Liss, "SUMMARY OF TRAVEL TRENDS: 2009 National Hose hold Travel Survey", FHWA-PL-11-022, U.S. Department of Transportation, June, 2011.

[78] S. Rezaee, E. Farjah, and B. Khorramdel, "Probabilistic analysis of plug-in electric vehicles impact on electrical grid through homes and parking lots," *IEEE Trans. Sustainable Energy*, vol. 4, no. 4, pp. 1024-1033, Oct. 2013.

[79] J. Widen, "Correlations between large-scale solar and wind power in a future scenario for Sweden," *IEEE Trans. Sustain. Energy*, vol. 2, no. 2, pp. 177–184, Apr. 2011.

[80] J. Stojanovic, M. Jovanovic, Dj. Gligorijevic, and Z. Obradovic, "Semi-supervised learning for structured regression on partially observed attributed graphs" *in Proc. the 2015 SIAM International Conference on Data Mining*, Vancouver, Canada, April 30 - May 02, 2015.

[81] V. Radosavljevic, "Gaussian conditional random fields for regression in remote sensing," Ph.D. dissertation, Department of Computer and Information Sciences, Temple University, Philadelphia, Pennsylvania, USA, 2012.

[82] California Irrigation Management Information System (CIMIS), [Online]. Available: http://www.cimis.water.ca.gov/, [Accessed: Sep. 20th, 2015].

[83] M. Nicolosi, "Wind power integration and power system flexibility–An empirical analysis of extreme events in Germany under the new negative price regime," *Energy Policy,* vol. 38, pp. 7257-7268, Nov. 2010.

[84] H. Holttinen, A. Tuohy, M. Milligan, E. Lannoye, V. Silva, S. Muller, et al., "The Flexibility Workout: Managing Variable Resources and Assessing the Need for Power System Modification," *Power and Energy Magazine, IEEE,* vol. 11, pp. 53-62, Nov./Dec. 2013.

[85] N. Navid, G. Rosenwald, and D. Chatterjee, "Ramp Capability for Load Following in the MISO Markets," Midwest Independent System Operator, July 15, 2011.

[86] California ISO, "Flexible Ramping Products: Revised Draft Final Proposal," Dec. 17, 2015. [Online]. Available: https://www.caiso.com/Documents/RevisedDraftFinal Proposal-FlexibleRampingProduct-2015.pdf [Accessed: May. 12th, 2016].

[87] N. Navid and G. Rosenwald, "Ramp Capability Product Design for MISO Markets," Midwest Independent System Operator, July 10th, 2013.

[88] K. H. Abdul-Rahman, H. Alarian, M. Rothleder, P. Ristanovic, B. Vesovic, and L. Bo, "Enhanced system reliability using flexible ramp constraint in CAISO market," in *Proc. 2012 IEEE Power and Energy Society General Meeting*, pp. 1-6, Jul 22-26, 2012, San Diego, California, USA.

[89] N. Navid and G. Rosenwald, "Market Solutions for Managing Ramp Flexibility With High Penetration of Renewable Resource," *IEEE Trans. Sustainable Energy*, vol. 3, pp. 784-790, Oct. 2012.

[90] C. Yonghong, P. R. Gribik, Z. Li, R. Merring, J. Gardner, K. Sperry, et al., "Real time ramp model in midwest iso co-optimized energy and ancillary service market design," in *Proc. 2009 IEEE Power and Energy Society General Meeting*, pp. 1-8, Jul 26-30, 2009, Calgary, Canada.

[91] A. Cornelius, "Assessing the Impact of Flexible Ramp Capacity Products in the Midcontinent," Ph.D. dissertation, Dept. ECE., Duke University, Durham, North Carolina, 2014.

[92] W. Congcong, P. B. Luh, and N. Navid, "Requirement design for a reliable and efficient ramp capability product," in *Proc. 2013 IEEE Power and Energy Society General Meeting*, pp. 1-5, Jul. 21-25, 2013, Vancouver, Canada.

[93] A. A. Thatte, X. A. Sun, and X. Le, "Robust Optimization Based Economic Dispatch for Managing System Ramp Requirement," in *Proc. 2014 IEEE Hawaii International Conf. System Sciences*, pp. 2344-2352, Jan 6-9, Waikoloa, Hawaii, USA.

[94] B. Wang and B. F. Hobbs, "A flexible ramping product: Can it help real-time dispatch markets approach the stochastic dispatch ideal?," *Electric Power Systems Research*, vol. 109, pp. 128-140, Apr. 2014.

[95] W. Kempton and J. Tomić, "Vehicle-to-grid power implementation: From stabilizing the grid to supporting large-scale renewable energy," *Journal of Power Sources*, vol. 144, pp. 280-294, Apr. 2005.

[96] E. Lannoye, D. Flynn, and M. O'Malley, "Evaluation of Power System Flexibility," *IEEE Trans. Power Systems,* vol. 27, pp. 922-931, May. 2012.

[97] N. Menemenlis, M. Huneault, and A. Robitaille, "Thoughts on power system flexibility quantification for the short-term horizon," in *Proc. 2011 IEEE Power and Energy Society General Meeting*, pp. 1-8, Jul 24-29, 2011, Detroit, Michigan, USA.

[98] F. Bouffard and M. Ortega-Vazquez, "The value of operational flexibility in power systems with significant wind power generation," in *Proc. 2011 IEEE Power and Energy Society General Meeting*, pp. 1-5, Jul 24-29, 2011, Detroit, Michigan, USA.

[99] C. Grigg, P. Wong, P. Albrecht, R. Allan, M. Bhavaraju, et al., "The IEEE Reliability Test System-1996. A report prepared by the Reliability Test System Task Force of the Application of Probability Methods Subcommittee," *IEEE Trans. Power System*, vol. 14, no. 3, pp. 1010-1020, Aug. 1999.

[100] ERCOT Balancing Energy Services Daily Reports Archives, "2008 balancing energy services daily reports", Jan, 2009 [Online]. Available: http: //www.ercot.com/mktinfo/services/bal/2008/index [Accessed: Oct. 10th, 2012].

[101] B. Zhang, and M. Kezunovic, "Impact of Available Electric Vehicle Battery Power Capacity on Power System Reliability," in *Proc. 2013 IEEE Power and Energy Society General Meeting*, pp. 1-5, Jul. 21-25, 2013, Vancouver, Canada.

[102] S. Frueh, "Improving Power System Resilience in the 21st Century," Resilient America Roundtable. Jul. 24-25, 2014. [Online]. Available: http://sites.nationalacademies.org/cs/groups/pgasite/documents/webpage/pga_153420.pdf. [Accessed: Jan, 21st, 2017].

[103] NERC, "2015 Risk Element: Extreme Physical Events," Industrial Webinar, Oct. 15, 2015. [Online]. Available: http://www.nerc.com/pa/comp/Documents/2015%20Extreme%20Physical%20Events%20v1.08.pdf. [Accessed: Jan, 21st, 2017].

[104] M. Panteli, and P. Mancarella, "Modeling and evaluating the resilience of critical electrical power infrastructure to extreme weather events", *IEEE System Journal*, Feb. 2015. [Online]. Available: http://ieeexplore.ieee.org/stamp/stamp.jsp?arnumber=7036086. [Accessed: Jan, 21st, 2017].

[105] M. Panteli, and P. Mancarella, "Operational resilience assessment of power systems under extreme weather and loading conditions", in *Proc. IEEE Power & Energy Society General Meeting*, pp. 1-5, Jul. 26-30, 2015, Denver, Colorado, USA.

[106] D. Barus, "Implementation of Free Governor Action in Power Plant to Increase System Resilience of Jawa Bali Power System Network", in *Proc. 46th International Universities' Power Engineering Conference (UPEC)*, pp. 1-5, Sep. 5-8 ,2011, Soest, Germany.

[107] Y. Liu, Q. H. Wu, and X. X. Zhou, "Co-Ordinated Multiloop Switching Control of DFIG for Resilience Enhancement of Wind Power Penetrated Power Systems", *IEEE Trans. Sustainable Energy*, vol. 7, no. 3, pp. 1089-1099, Jul. 2016.

[108] K. Eshghi, B. K. Johnson, and C. G. Rieger, "Power system protection and resilient metrics", in *Proc. IEEE Resilience Week*, pp. 1-8, Aug. 18-20, 2015, Philadelphia, Pennsylvania, USA.

[109] T. C. Ly, J. N. Moura, and G. Velummylum, "Assessing the Bulk Power System's resource resilience to future extreme winter weather events", in *IEEE Power & Energy Society General Meeting*, pp. 1-4, 2015, Denver, Colorado, USA.

[110] Y. Sun, Z. Li, M. Shahidehpour, and B. Ai, "Battery-based energy storage transportation for enhancing power system economics and security", *IEEE Trans. Smart Grid*, vol. 6, no. 5, pp. 2395-2402, Sep. 2015.

[111] N. Kadel, W. Sun, and Q. Zhou, "On battery storage system for load pickup in power system restoration", in *2014 IEEE Power and Energy Society General Meeting*, pp. 1-5, 2014, Washington DC, USA.

[112] W. Liu, L. Sun, Z. Lin, F. Wen, and Y. Xue, "Multi-objective restoration optimisation of power systems with battery energy storage systems," *IET Generation, Transmission & Distribution*, vol. 10, no. 7, pp. 1749-1757, Feb. 2016.

[113] R. Fernández-Blanco, Y. Dvorkin, B. Xu, Y. Wang, and D. S. Kirschen. "Energy Storage Siting and Sizing in the WECC Area and the CAISO System" Jun. 2016. [Online]. Available: https://www2.ee.washington.edu/research/real/Library/Reports/storage_siting_and_sizing.pdf.

[114] H. Yu, J. Pan, and A. Xiang, "A multi-function grid-connected PV system with reactive power compensation for the grid," *Solar Energy*, vol. 79, no. 1, pp. 101-106, Jul. 2005.

[115] S. Adhikari and F. Li, "Coordinated Vf and PQ control of solar photovoltaic generators with MPPT and battery storage in microgrids", *IEEE Trans. Smart Grid*, no.5, vol.3, pp.1270-1281, May 2014.

[116] L. Jiang, and Q. Yang, "Intelligent power supply restoration in power distribution networks with distributed generation," in *IEEE 2016 China International Conference on Electricity Distribution (CICED)*, pp. 1-6, Aug. 2016

[117] W. Sun, C. C. Liu, and L. Zhang, "Optimal generator start-up strategy for bulk power system restoration", *IEEE Trans. Power System*, vol. 26, no. 3, pp. 1357-1366, Aug. 2011.

[118] M. Moeini-Aghtaie, A. Abbaspour, and M. Fotuhi-Firuzabad, "Incorporating large-scale distant wind farms in probabilistic transmission expansion planning—Part I: Theory and algorithm," *IEEE Trans. Power Systems*, vol. 27, no. 3, pp. 1585-1593, Aug. 2012.

[119] A. Arabali, M. Ghofrani, M. Etezadi-Amoli, M. D. Fadali, and M. Moeini-Aghtaie, "A multi-objective transmission expansion planning framework in deregulated power systems with wind generation," *IEEE Trans Power Systems*, vol. 29, no. 6, pp. 3003-3011, Nov. 2014.

[120] B. Zhang, and M. Kezunovic, "Impact on power system flexibility by electric vehicle participation in ramp market", *IEEE Trans. Smart Grid*, vol. 7, no. 3, pp. 1285-1294, May. 2016.

[121] L. Xu, X. Ruan, C. Mao, B. Zhang, and Y. Luo, "An improved optimal sizing method for wind-solar-battery hybrid power system," *IEEE Trans. Sustainable Energy*, vol. 4, no.3, pp. 774-785, Jul. 2013

APPENDIX A

PUBLISHED PAPERS AND REPORTS

My publications are listed as follows:

Book Chapter:

1. M. Kezunovic, Z. Obradovic, T. Dokic, **B. Zhang**, J. Stojanovic, P. Dehghanian, and P. -C. Chen, "Predicating Spatiotemporal Impacts of Weather on Power Systems using Big Data Science," Springer Verlag, Data Science and Big Data: An Environment of Computational Intelligence, Pedrycz, Witold, Chen, Shyi-Ming (Eds.), ISBN 978-3-319-53474-9, 2017.

Journal Papers:

1. **B. Zhang**, P. Dehghanian, M. Kezunovic, "Optimal Allocation of PV Generation and Battery Storage for Enhanced Resilience", *IEEE Transactions on Smart Grid*, accepted.
2. **B. Zhang**, M. Kezunovic, "Impact on Power System Flexibility by Electric Vehicle Participation in Ramp Market," IEEE Transactions on Smart Grid, Vol. 7, No. 3, pp. 1285-1294, May 2016.

Conference Papers:

1. Q. Yan, C. Qian, **B. Zhang**, M. Kezunovic, "Statistical Analysis and Modeling of Plug-in Electric Vehicle Charging Demand in Distribution Systems", to be presented in International Conference on Intelligent Systems Applications to Power (ISAP), San Antonio, Texas, USA, September 17-21, 2017.

2. **B. Zhang**, Q. Yan, M. Kezunovic, “Placement of EV charging stations integrated with PV generation and battery storage,” 2017 Twelfth International Conference on Ecological Vehicles and Renewable Energies (EVER), Monaco, April 11-13, 2017.
3. **B. Zhang**, P. Dehghanian, M. Kezunovic, “Spatial-Temporal Solar Power Forecast through Use of Gaussian Conditional Random Fields, “ IEEE Power and Energy Society General Meeting, Boston, MA, July 2016.
4. Q. Yan, **B. Zhang**, M. Kezunovic, "The Demand Response Support Under Weather Impacts Using PV Generation and EV Energy Storage", EEEIC, Florence, Italy, June, 2016.
5. **B. Zhang**, P. Dehghanian, M. Kezunovic, “Simulation of Weather Impacts on the Wholesale Electricity Market”, DEMSEE, Budapest, Hungary, September, 2015.
6. Q. Yan, **B. Zhang**, M. Kezunovic, “Optimization of Electric Vehicle Movement for Efficient Energy Consumption,” The 46th North American Power Symposium (NAPS), Pullman, Washington, USA, September 2014.
7. **B. Zhang**, M. Kezunovic, “Impact of Available Electric Vehicle Battery Power Capacity on Power System Reliability,” IEEE Power and Energy Society General Meeting, Vancouver, Canada, July, 2013.

Technical Reports:

1. M. Kezunovic, S. Meliopoulos, R. Baldick, T. Alquthami, Q. Yan, **B. Zhang**, “The Electricity and Transportation Infrastructure Convergence Using Electrical Vehicles”, PSerc Report #14-08, September 2014.

2. M. Kezunovic, C. Pang, Q. Yan, **B. Zhang**, "The Role of PHEV/BEV in Outage/Asset and Demand Side Management", EV-TEC Report #1, April 2013.

APPENDIX B

EQUIVALENT DISTRIBUTION FOR THE SUM OF SEVERAL POISSON DISTRIBUTIONS

In order to prove that the equivalent distribution for the sum of several Poisson distributions are still a Poisson distribution, we first examine the equivalent distribution for two Poisson distributions with parameters λ_1 and λ_2, this means that $P_1(x_1 = k) = \frac{\lambda_1^k e^{-\lambda_1}}{k!}$ and $P_2(x_2 = k) = \frac{\lambda_2^k e^{-\lambda_2}}{k!}$

Therefore, the equivalent distribution will be

$$P_{1\&2}(x_1 + x_2 = k) = \frac{\lambda_1^0 e^{-\lambda_1}}{0!} \cdot \frac{\lambda_2^k e^{-\lambda_2}}{k!} + \frac{\lambda_1^1 e^{-\lambda_1}}{1!} \cdot \frac{\lambda_2^{k-1} e^{-\lambda_2}}{(k-1)!} + \cdots + \frac{\lambda_1^k e^{-\lambda_1}}{k!} \cdot \frac{\lambda_2^0 e^{-\lambda_2}}{0!}$$

$$= e^{-(\lambda_1+\lambda_2)} \cdot \left(\frac{\lambda_1^0}{0!} \cdot \frac{\lambda_2^k}{k!} + \frac{\lambda_1^1}{1!} \cdot \frac{\lambda_2^{k-1}}{(k-1)!} + \cdots + \frac{\lambda_1^k}{k!} \cdot \frac{\lambda_2^0}{0!} \right)$$

Since: 1) $\frac{(\lambda_1 + \lambda_2)^k}{k!} = \frac{C_k^0 \lambda_1^0 \lambda_2^k + C_k^1 \lambda_1^1 \lambda_2^{k-1} + \cdots + C_k^k \lambda_1^k \lambda_2^0}{k!}$

2) $\frac{C_k^i}{k!} = \frac{\frac{k!}{i!(k-i)!}}{k!} = \frac{1}{i!(k-i)!}$

Hence, $P_{1\&2}(x_1 + x_2 = k) = e^{-(\lambda_1+\lambda_2)} \cdot \frac{(\lambda_1 + \lambda_2)^k}{k!}$

We can see that the combined $P_{1\&2}$ is still a Poisson distribution with the parameter $(\lambda_1 + \lambda_2)$. We can conclude that the equivalent distribution of several Poisson distribution would still be a Poisson distribution with parameter $(\lambda_1 + \lambda_2 + \cdots + \lambda_m + \lambda_n)$.